Molecular Structure of Water at Interfaces: Wetting at the Nanometer Scale

A. Verdaguer,[†] G. M. Sacha,[†] H. Bluhm,[‡] and M. Salmeron*[,†]

Materials Sciences Division and Chemical Sciences Division, Lawrence Berkeley National Laboratory, University of California, Berkeley, California 94720

Received June 30, 2005

Contents

1. Introduction

The structure of water at the interface with other materials is thought to determine their wetting properties and underlies the vast array of phenomena known under the names of hydrophobicity and hydrophillicity, which describe the interaction between objects in aqueous media. These phenomena are crucial in biology and in materials sciences. It is therefore not surprising that the study of interfacial water structure continues to be a subject of great interest and that numerous studies are devoted to it. Several excellent reviews exist that cover extensively the large body of literature published prior to 2002.[1,2] Updates and extensions of these reviews are found in this issue of Chemical Reviews, which contains papers covering various aspects of water interfaces with vacuum, air, or other materials. In this chapter, we review recent studies on the structure and growth of water films at interfaces, covering approximately a period of 5 years. When necessary, we also report on older studies that have particular relevance to the topics being discussed, at the price of an unavoidable overlap with previous reviews. With a few exceptions, we limit this review to studies on well-defined surfaces, mostly single crystalline interfaces were the microscopic mechanism of water adsorption could be more easily modeled. We concentrate in particular on studies dealing with the structure of the first few layers of water because it is these layers that probably determine most of the interfacial properties. We use the word "probably" deliberately, to indicate that it is not yet well-understood what is the role of the second, third, and subsequent layers in determining and modifying the structure of the first one. Such a strong influence of the layers beyond the first is perhaps not surprising when one considers that the water−water interaction through H-bonds is quite strong, comparable, or greater than that of the water−substrate interaction. Unfortunately, molecular scale studies encompassing more than just one or two layers are not abundant. Studies using scanning probe methods have the promise of changing this, and for this reason, we devote particular attention to them.

We will also mention studies using other surface sensitive techniques, including core level spectroscopies such as X-ray photoelectron spectroscopy (XPS), X-ray absorption spectroscopy (XAS), and X-ray emission spectroscopy (XES). Vibrational spectroscopies such as infrared reflection absorption spectroscopy (IRAS), Raman, and sum frequency generation (SFG) have also provided a very substantial amount of information. Among the crystallographic techniques, we mention low energy electron diffraction (LEED), X-ray grazing diffraction, and a few others. We defer, however, the more detailed accounts using these techniques to other articles published in this special issue.

We start by reviewing studies of isolated water molecules on metals at low temperature, in particular, their diffusion and aggregation to form clusters, monolayers, and multilayers. In contrast to the situation of monolayer films, there is much less structural and spectroscopic information available for multilayer films. We will then focus on studies under ambient conditions, on materials such as mica, alkali halides, and a few others. Finally, we will review the phenomena occurring when water condenses in narrow gaps between surfaces, where capillary effects are very important.

* Corresponding author. Phone: (510) 486-6230; fax: (510) 486-6044; e-mail: salmeron@stm.lbl.gov.
[†] Materials Sciences Division.
[‡] Chemical Sciences Division.

10.1021/cr040376l CCC: $59.00
Published on Web 03/30/2006

Albert Verdaguer was born in 1971 in Vic, Catalunya, Spain. He studied physics at the University of Barcelona. He received his Ph.D. in physics in 2001 after completing his thesis work in computer simulation of liquids under the direction of Prof. Joan-Àngel Padró at the University of Barcelona. He spent two years at the Nanometric Techniques Unit of the Scientific-Technical Services of the University of Barcelona using scanning force microscopy techniques in a wide range of different studies. Currently, he is a postdoctoral research fellow in the laboratory of Dr. M. Salmeron at the Lawrence Berkeley National Laboratory sponsored by a NANOS fellowship of the Generalitat de Catalunya. His current research interests include the interaction of water with surfaces under ambient conditions and the interaction of atmospheric gases with salt crystal surfaces. He has been recently awarded with a grant from the Spanish Government to continue his research at the Institut Català de Nanotecnologia in Barcelona.

Hendrik Bluhm is a staff scientist in the Chemical Sciences Division at Lawrence Berkeley National Laboratory. He obtained his M.S. in crystallography from the University of Leipzig (Germany) in 1992 and his Ph.D. in physics from the University of Hamburg, Germany (under research supervisor R. Wiesendanger). He then spent several years in a postdoctoral position in the group of Dr. M. Salmeron, where he used scanning force microscopy to study molecularly thin water and ice films on oxide surfaces and participated in the development of synchrotron-based ambient pressure photoemission spectroscopy for studies of surfaces at pressures of several Torr, a work that he continued during his subsequent stay at the Fritz Haber Institute of the Max Planck Society in Berlin. His current research interests include the study of water adsorption on environmentally relevant surfaces under ambient conditions, as well as the interaction of atmospheric trace gases with ice surfaces.

Sacha Gomez was born in 1976 in Madrid. He studied psychology at the Universidad Nacional de Educación a Distancia and physics at the Universidad Autónoma de Madrid, where he received his Ph.D. with Prof. Juan José Sáenz in 2003. Then, he moved to the Lawrence Berkeley National Laboratory to join the research group of Dr. M. Salmeron in the Materials Science Division. He collaborates with the MoLE group and Laboratorio de Nuevas Microscopias in Spain. His research centers on wetting processes, surface science, and electrostatic interactions at the nanoscale. He is interested in the development of simulations and theoretical approximations for different scanning probe microscopies, being one of the main developers of the Generalized Image Charge Method.

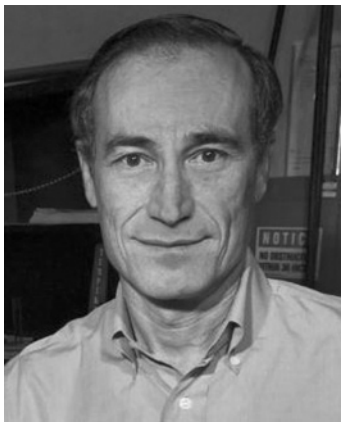

Miquel Salmeron is a Senior Staff Scientist and Principal Investigator in the Materials Sciences Division of the Lawrence Berkeley National Laboratory. He graduated from the University of Barcelona in 1967. He obtained a Master's degree in solid-state physics from the Université Paul Sabatier, Toulouse, France in 1970 and a Ph.D. in physics at the Universidad Autonoma de Madrid, Spain in 1975. After spending 2 years as a postdoctoral fellow in Berkeley studying reactive scattering of molecular beams of hydrogen molecules on platinum, he returned to Spain in 1977. There, he was an investigator in the Spanish Research Council (CSIC) and Professor of Physics at the Universidad Autonoma de Madrid. In 1984, he assumed his current position where he has since developed STM and AFM techniques and applied them to studies of surface structure, chemisorption, semiconductors, and tribology. He has been recently elected to a fellowship in the American Physical Society and received the awards for Sustained Outstanding Research in 1996 and for Outstanding Scientific Accomplishment in 1995 in the Materials Chemistry Category as part of the U.S. Department of Energy Materials Science Research Competition. He serves on the Editorial Advisory Board of Tribology Letters. He has taught at the University of Barcelona in Spain, at the Universidad Autonoma de Madrid in Spain, and at the University of California at Berkeley.

2. Structure of Water Films at Cryogenic Temperatures

2.1. Water Layers on Metals

2.1.1. From Single Molecules to Clusters

Studies of the adsorption of single water molecules require low temperature and low coverage. This is necessary to limit the aggregation of the molecules into clusters as a result of the high diffusivity of single molecules. Once water molecules collide with each other, they can form strong H-bonds, which are comparable in strength to the water−substrate bonds.

Monomers and small clusters, from dimers to hexamers, have been proposed to exist on metal surfaces, based on results of experiments using vibrational spectroscopies.[2] Although these techniques are in general capable of identify-

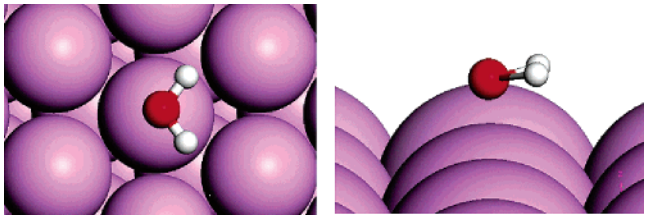

Figure 1. Most favorable adsorption configuration of a water molecule on an on-top position. The molecular plane lays nearly parallel to the surface for Pd{111}, Pt{111}, Ru{0001}, Rh{111}, Ni{111}, Cu{111}, Ag{111}, Au{111}, and Al{111}. (Reprinted with permission from ref 3 (http://link.aps.org/abstract/PRL/v90/p216102). Copyright 2003 by the American Physical Society.)

ing the presence of monomeric water and small water clusters, it is difficult from such data alone to conclusively deduce the aggregation state of the molecules because these techniques average over large areas of the surface, which are likely to contain a variety of cluster sizes as well as surface steps and defects that strongly determine the adsorption properties. It was not until the advent of scanning tunneling microscopy (STM) that water monomers and their diffusion and aggregation could be reliably studied on metal surfaces.

The energetics of adsorption of water monomers on different (111) metal surfaces has been studied theoretically by Michaelides et al.[3] using density functional theory (DFT). The authors found that, in general, the favored adsorption site of the monomer is on top of the metal atoms, where the O lone pair orbital hybridizes with metal orbitals to form a covalent bond. The optimal geometry is one where the plane of the water molecule lays nearly parallel to the surface, as shown in Figure 1. The adsorption energies were found to vary from 0.1 to 0.4 eV, which is on the order of the energy of a hydrogen bond (~0.25 eV). The adsorption energy depends on the metal and was found to be ranked in the order Au < Ag < Cu < Pd < Pt < Ru < Rh, which reflects the strength of the oxygen−metal bond. The intramolecular bond angles and bond lengths of the water molecule were found to be only slightly perturbed as compared to the gas-phase values by the interaction with the surface. Similar results have been obtained by Meng et al.[4] in their DFT studies of monomers and clusters on metal surfaces. Michaelides et al. also found that, when the water molecule is laterally displaced from the top site by up to ~0.3 Å on Ru, Pt, and Ag, the binding energy changes only by ~0.02 eV. This can explain the stability of small clusters observed by STM on Pd, Ag, and Cu despite apparent mismatches between substrate lattice constants and O−O separation in the H-bonded molecules. Changes in azimuthal orientation of the molecule gave similar small adsorption energy differences of ~0.02 eV, suggesting that adsorbed water will be randomly oriented on the surface at temperatures above a few degrees Kelvin. The weak dependence of the binding energy on these two parameters implies that monomers in adjacent top sites can easily reorient to form dimers. In this manner, even if an orientation may not be energetically the most favorable for each monomer separately, it might still lead to a stable cluster because of the gain from H-bond formation.

K. Morgenstern and Rieder[5,6] were first to image water monomers adsorbed on Cu(111) using STM. Their experiments were performed at a temperature of 16 K. They found that the monomers were easily perturbed by the tip, causing them to move and form clusters. The smallest of the newly formed structures were dimers, cyclic trimers, and cyclic hexamers. The diffusion and clustering of monomers was induced by the excitation of vibrational modes of the molecule by the tunneling electrons.[7] Single water molecules on Pd(111) were studied by Mitsui et al.[8] between 40 and 52 K. The molecules showed up as protrusions in the STM images with heights varying from 0.5 to 1.0 Å, depending on tunneling conditions and tip structure. Because of the very low energy barrier for rotation around the O-atom (~0.02 eV), even at 40 K the protrusion due to the water molecule in the STM image appears symmetric. The determination of the binding site is not trivial due to the strong interaction between the tip and the molecule under the tunneling conditions needed to resolve the Pd atoms. Despite this, by alternating low gap and high gap tunneling conditions, the authors could image the Pd lattice around a molecule in one single image. They concluded that the adsorption site is over a Pd atom, as predicted theoretically.[3]

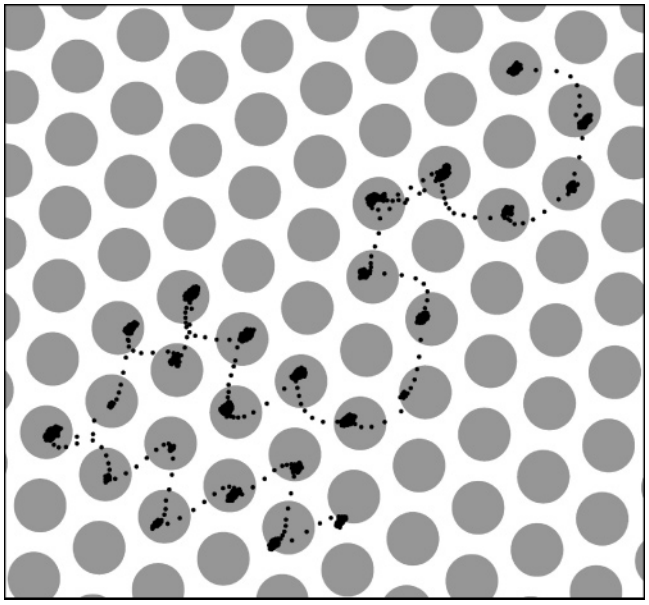

Figure 2. Trajectory of the STM tip as it tracks a water molecule in its random walk on Pd(111) at 52 K. A model of the Pd lattice is shown for reference. (Reprinted with permission from *Science* (http://www.aaas.org), ref 8. Copyright 2002 AAAS.)

The diffusion of single water molecules on Pd(111) was studied by Mitsui et al.[8] by analyzing movies made of consecutive STM images. The authors also used a tracking method where the position of the tip was recorded as it followed a diffusing molecule. In this manner, the random walk path of the molecules was captured and shown to proceed via single jumps to nearest neighbor sites of the Pd-(111) substrate, as illustrated in Figure 2. The movie method was used in the lower range of temperatures studied, where the diffusion was slow, while the tracking method was used in the higher temperature range, when the molecular hopping rate was too high for imaging. By performing experiments at different temperatures and by plotting the molecular hopping frequency versus $1/T$, the diffusion parameters were determined. The activation energy was found to be 126 meV and the frequency factor $10^{2.0\pm0.6}$ Hz. In addition to thermally excited diffusion, it is possible to excite translational motions of the molecules by excitation of specific internal modes, similar to the observations mentioned previously for Cu-(111). Fomin et al.[9] showed that when the tunneling electrons have an energy equal to or above that of the quantum of bending mode (200 meV for H_2O), the diffusion rate of water

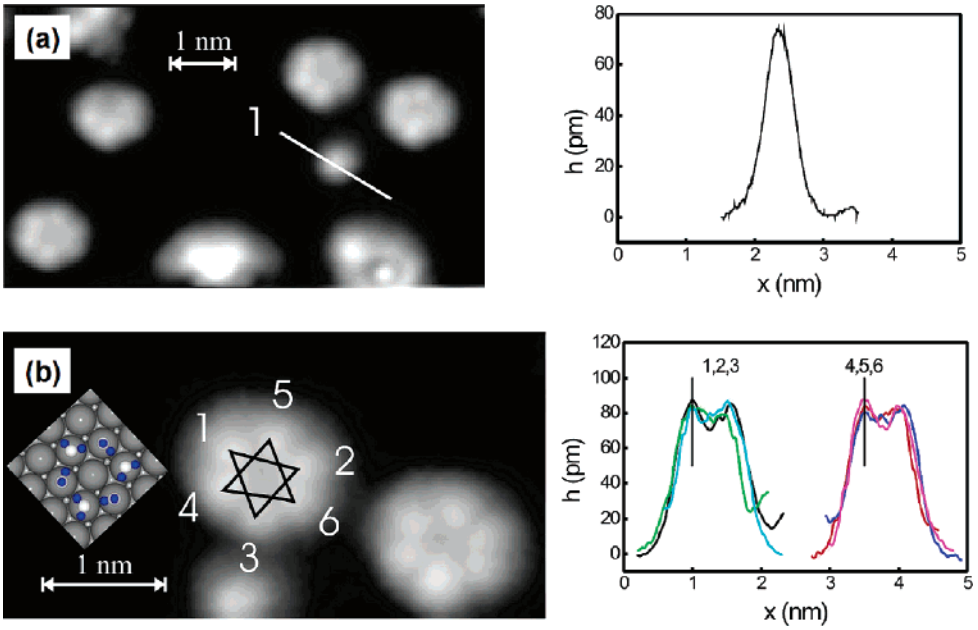

Figure 3. STM images of water molecules and clusters on Cu(111). A line scan is shown on the right for the monomer in (a). A hexamer cluster is shown in (b). Line scans through the marked points are shown on the right. The inset shows the Cu lattice with a symmetric cyclic hexamer in on-top adsorption sites. Hydrogen atoms are black, and oxygen atoms are white; molecules 4−6 are hydrogen bonded to molecules 1−3. (Reprinted with permission from ref 5. Copyright 2002 American Institute of Physics.)

on Pd(111) increases substantially. For D_2O, the threshold energy of the tunneling electron to promote molecular hops shifted to 150 meV, as expected from the isotope effect. The authors proposed a model where the near horizontal geometry of the molecular plane favors coupling of the bending and horizontal motions of the molecule, effectively lowering the barrier for thermal excitation of the frustrated translation mode.

A widely used spectroscopic technique to study water adsorption on metals is IRAS. In these studies, several features of the spectra of water on metals at low temperature and low coverage are associated to vibrational modes in different cluster configurations. Ito and co-workers have used IRAS to study D_2O on Pt(111),[10] Ru(0001),[11,12] Ni(111),[13] and Cu(111).[14] The spectrum on Pt(111) at 20 K was associated to water dimers at a coverage of 0.01 ML. When the coverage was increased to 0.2 ML, the spectral features changed and were associated to water tetramers. Annealing converted the dimers and tetramers formed at 20 K into hexamers, until finally, at 130 K, an ice monolayer was formed. These results are in line with recent studies of the initial stages of water adsorption on Pt(111) by Daschbach et al. using He scattering.[15] By monitoring the evolution of the specular peak intensity, they observed changes at 60 K that were interpreted as a transition from isolated molecules to islands.

On Ru(0001), the features of the spectra at 20 K and at low coverage (<0.4 ML) were interpreted as due to monomers, dimers, and tetramers, with a dominance of monomers. The dominance of the monomeric species was attributed to a large barrier for diffusion. The authors found that the molecules began to dissociate into OH and O at temperatures above 170 K, a subject that we review in more detail below. In more recent work, Nakamura et al. reexamined the spectra measured on Pt(111), Ni(111), and Ru(0001), comparing them to the spectra on Cu(111) and to DFT calculations.[14] They found that for similar conditions, 25 K and ~0.3 ML coverage, four adsorption bands in the OD stretching region were observed that could be assigned to modes of the dimers and hexamers. On Ru(0001), monomers were also found to be present. In contrast, Ogasawara et al.[16] found that on Pt(111) at 25 K, the spectra showed features that were associated to vibrational modes of monomeric water and dimers. When the surface was annealed to 40 K, the spectra showed an increase in the amount of monomers and a decrease in that of dimers, indicating that a certain number of dimers dissociate to monomers. Yamamoto et al.[17] used IRAS to study water adsorption on Rh(111). At 20 K, they found that at 0.03 ML coverage, water molecules existed as monomers, as dimers around 0.13 ML, and as small clusters of unspecified numbers of molecules at 0.3 ML. Upon heating the surface with 0.13 ML, the monomers and dimers migrated and aggregated to form larger clusters and 2-D islands. From the temperature dependence of the OD stretching peaks, the authors could distinguish between water molecules inside 2-D islands and those at the edge of the islands. They concluded that at 20 K, the number of water molecules at the edge of the 2-D islands is comparable to that of those inside the 2-D islands. By comparing their results with those of Nakamura et al., they found that the relative number of water molecules at the edge as compared to those in the interior of the islands was larger on Ru(0001) and Rh(111) than on Ni(111) and Pt(111), which indicates that the average cluster size on Ni(111) and Pt(111) is larger than on Ru(0001) and Rh(111). The authors concluded from this finding that on Ru(0001) and Rh(111), water migration is hindered as compared to that on Pt(111) and Ni(111). These spectroscopic results illustrate the general finding that some cluster sizes occur in higher proportions than others, an indication that their structures are particularly stable.

Using STM some cluster structures have been observed. For example, K. Morgenstern and Rieder[5] have studied water clustering on Cu(111). Figure 3 shows several water aggregates: monomers in (a) and other clusters in (a) and (b).

The aggregation of water molecules into clusters on Pd(111) was studied by Mitsui et al.[8] The authors found that

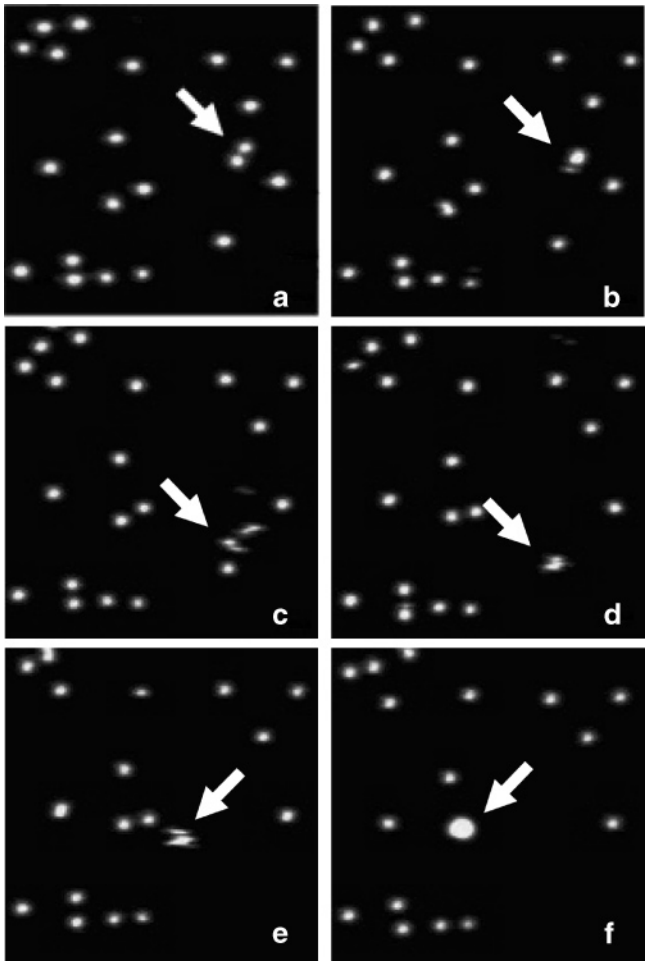

Figure 4. Sequence of images showing water molecules adsorbed on Pd(111) at 40 K. Two monomers in panel (a) join to form a dimer (b). The dimer diffuses faster than the scanning speed so that the tip scans over the molecule for one line before moving to a neighboring site and produces the streak in panel (c). The dimer encounters a third monomer and forms a trimer (d), which diffuses approaching a pair of nearby monomers (e). A pentamer is formed by the collision in panel f. (Reprinted with permission from *Science* (http://www.aaas.org), ref 8. Copyright 2002 AAAS.)

dimers, trimers, tetramers, and larger clusters were formed by the successive addition of colliding molecules (Figure 4). An unexpected result of these studies was that the mobility of the dimers, trimers, and tetramers was higher than that of the monomers by several orders of magnitude. The cluster mobility decreased again to a value similar or smaller than that of the monomer when the clusters reached a size of five or more molecules. During these experiments, carried out at temperatures below 60 K, no dissociation of the molecules was observed. The authors proposed that the large mobility of the small clusters is due to the strong H-bonding between molecules and to the mismatch between the O−O distance in dimers and the lattice constant of Pd(111). In this model, the mismatch would prevent both molecules from forming bonds to the substrate in optimal geometries, thus reducing the diffusion barrier of the pair. Asscher et al.[18] studied monomer and dimer diffusion on Ru(0001) using molecular dynamics (MD) simulations. Their simulations indicated a faster diffusion for dimers than monomers, similar to the findings of Mitsui et al. for Pd(111). To study the effect of the mismatch between the substrate lattice constant and the O−O distance on the diffusion of dimers, they compared the results with that of a hypothetical system where the Ru lattice constant was shortened by 7% without changing the interaction strength between water molecules and Ru atoms. This hypothetical system has a larger mismatch between O−O distances in the dimer and the lattice of the metal surface. They found a reduction of the activation energy and an increase of the hopping rate of dimers when the lattice was shortened. Although in line with the interpretation of Mitsui et al., this interpretation is at odds with the theoretical findings of Michaelides et al., described previously, where only small changes in the binding energy were found from small geometrical deviations in adsorption site or bond angles. This group[19] proposed a different mechanism for dimer diffusion on Pd(111). They used density functional theory to determine the geometry of the dimer, which was found to be asymmetric, with a surface bound donor molecule (via the O lone pair orbital) and an acceptor molecule adsorbed 0.5 Å farther away from the surface, so that it forms no direct bonds with the surface. This geometry allows the dimer to rotate nearly freely around the axis centered at the donor molecule as shown in Figure 5. The calculations show that if the pair moves as a rigid entity, with the donor molecule hopping from site to site, the activation energy is similar to that of the monomer, which is contrary to the observations. That led to the proposal of a mechanism where the dimer changes its structure by thermal activation to one where both molecules bind to neighboring Pd atoms for a short time. In this intermediate position, the water molecules can exchange the roles of donor and acceptor by a rotation involving quantum tunneling of the H-atoms, as illustrated schematically in Figure 5. After this exchange, the dimer resumes its stable structure, with the donor molecule bound to the Pd atom and the acceptor farther away from the surface. This leads to a net translation of the dimer by one lattice spacing. Depending on the barrier height, the tunneling mechanism can be much faster than mere thermal diffusion when the temperature is sufficiently low. Clearly, more experiments are required to test this interesting idea.

Adsorption of water monomers on Al(100) has been theoretically studied by Michaelides et al.[20] They found that the favored adsorption site is the top site with a binding energy of ∼350 meV. Water molecules were found to bind very weakly to bridge sites (∼60 meV) and did not adsorb on the 4-fold hollow sites. They examined the potential energy surface of a water molecule diffusing between top sites through a bridge site. The energy barrier was in the range of 307−327 meV, depending on the orientation of the molecule. It had been widely assumed that the diffusion barrier of an adsorbate can be predicted from the difference in adsorption energies in the most stable and the next more stable high symmetry adsorption sites. The calculated value, however, was larger than expected from this assumption and approached the binding energy value for the on-top site. A barrier close to the binding energy will effectively suppress the diffusion of water molecules on the surface.

On the (111) and (100) metal surfaces discussed above, monomers were only observed at low temperature and low coverage. In contrast, on the (110) surface of some fcc metals (Cu, Pd, Ni), monomers are actually favored over clustering for coverages below a monolayer.[2] For these surfaces, a c(2 × 2) LEED structure was found and attributed to a water bilayer.[1,2] Spitzer and Lüth[21] observed a c(2 × 2) pattern on Cu(110) at 90 K at 0.5 ML. On the basis of ultraviolet

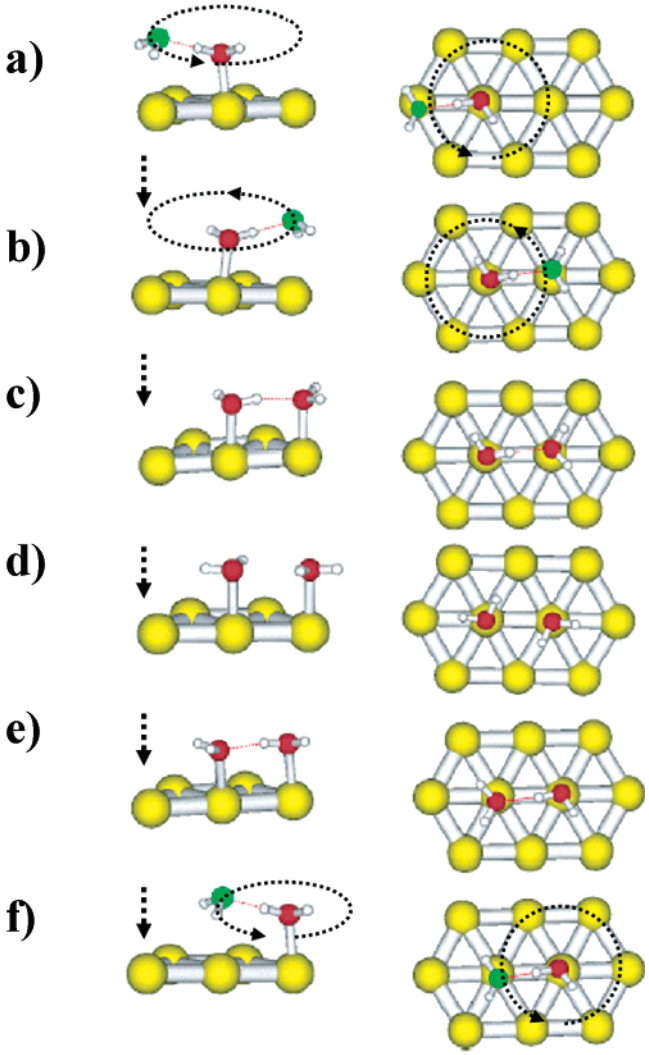

Figure 5. Proposed mechanism for the diffusion of water dimers on Pd(111). Only the donor molecule forms a strong bond with the Pd atoms. The acceptor molecule is bound to the donor through a H-bond. Panels a and b illustrate the nearly free rotation of the acceptor molecule; panel c corresponds to the intermediate state where a wagging motion brings the acceptor down so that both water molecules are at a similar height above the surface. In this configuration, they undergo a donor−acceptor rotation by H-tunneling (d and e). After this, the roles of donor and acceptor are exchanged. From panels e to f, the dimer restores its equilibrium geometry with the acceptor lifted above the substrate, which results in a net translation by one lattice spacing. (Reprinted with permission from ref 19 (http://link.aps.org/abstract/PRL/v92/p136104). Copyright 2004 by the American Physical Society.)

photoelectron spectroscopy (UPS) data, they concluded that there was no H-bonding between water molecules on the surface. Water clusters on Pd(110) have been recently investigated by Komeda et al. using STM. At 4.7 K and low coverage, clusters of three different sizes were observed.[22] The smallest size was attributed to monomers, although dimers could not be excluded since the protrusion in the images was elongated in the [110] direction. As the amount of water on the surface was increased, larger clusters were found forming local c(2 × 2) structures. These ordered structures were identical to the previously reported structure of water on Pd(110) based on LEED[23] and HREELS.[24] Komeda et al. therefore concluded that the largest clusters correspond to water tetramers. No diffusion of the clusters was observed at this temperature.

As mentioned previously, a particularly stable cluster is the cyclic hexamer, which is the basic structure in hexagonal ice I_h. Hexamers were indeed found to be very stable on metal surfaces and constitute the basic motif of the first water layer. The structure of isolated hexamers, however, might differ appreciably from that in ice I_h, depending on the strength of the water−substrate interaction and on the mismatch between the substrate lattice constant and the water molecule oxygen distances. STM has been used by K. Morgenstern and Nieminen to study water hexamers on Ag(111) at 70 K.[25−27] At this temperature, the molecules are found to be sufficiently mobile to form large clusters on terraces. The smallest structure found was the cyclic hexamer with the molecules adsorbed on the top positions. The Ag(111) lattice constant is 2.89 Å as compared to the 2.75 Å O−O distance in crystalline ice I_h at 90 K (i.e., a lattice mismatch of ∼5%). Despite this, the hexamers showed a perfect accommodation to the silver lattice constant, indicating considerable stretching of the H-bonds as compared to hydrogen bonds in ice I_h. The same group also observed a cyclic hexamer on Cu(111) at 16 K.[5] Since the distance between Cu atoms is 2.54 Å, the water hexamers have a larger mismatch here, leading to an ∼8% compression (as compared to the O−O distances in I_h) if they would fit exactly to the copper lattice. The hexamers deviate considerably from a high symmetry hexagon and show different H-bond lengths within the hexamer. In addition, the apparent height of the molecules within the hexamer is not alternating as in the ice bilayer (see Figure 3). In the competition between ideal hydrogen-bond lengths and favorable on-top positions, it appears that none of them clearly dominates. This leads to the formation of hexagons where not all molecules are adsorbed in identical positions, explaining the variety of apparent heights that are observed with STM. Another result of the experiments on Ag(111) and Cu(111) is that stretching H-bonds in the hexamer is apparently easier than compressing them.

A recent study by Mitsui et al.[8] has produced results that shed more light on the growth of water structures on Pd-(111). The authors found that at coverages below one monolayer and temperatures below 130 K, the aggregation of water leads to the formation of hexagonal honeycomb structures in registry with the Pd(111) substrate. Interestingly, the lateral growth of these clusters is limited to a few unit cells, as shown in Figure 6. The addition of more water to the surface either leads to the nucleation of more clusters with similar sizes or produced second layer structures. The STM images indicate a constant tunneling probability on each corner of the hexagonal cell where water is located, except at the periphery of the islands. This observation was interpreted as indicating that the water molecules are in the same chemical and geometrical state inside the cluster, in agreement with the IRAS results on the (111) surfaces of Pt, Rh, Ni, and Ru[17] that showed just two different kinds of water molecules for clusters on these surfaces, one inside and the other at the edge of the cluster. It excludes, therefore, any model where alternating molecules are at different heights over the Pd atoms or have a different H-bonding structure, except for those at the cluster periphery. On the basis of these results, Mitsui et al. proposed a model where the molecules are nearly coplanar and use all their H-atoms to form bonds with neighboring molecules, while bonding to the substrate through the lone pair orbitals. This model implies necessarily that the cluster size must be limited to a

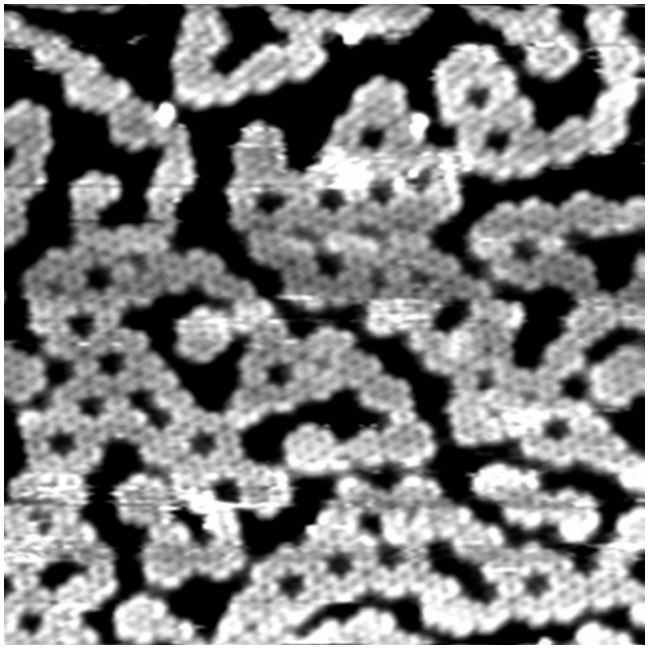

Figure 6. (175 Å × 175 Å) STM image of D_2O clusters on Pd(111) at 100 K. The growth of the hexagonal honeycomb clusters is limited to a few unit cells in one direction. (Reprinted with permission from ref 28 (http://link.aps.org/abstract/PRL/v93/p116101). Copyright 2004 by the American Physical Society.)

few cells since in two dimensions only a finite number of molecules can be fully H-bonded (double donors, single acceptor, and a fourth bond to the substrate). It is the peripheral molecules that contain the unsaturated bonds, either dangling H-atoms sticking out toward the vacuum, or directed to the Pd underneath, or perhaps with the H-bond broken to form OH. DFT calculations were carried out to determine which of these three possibilities is more stable.[28] Although the optimized geometries did all produce flat, undissociated, and fully H-bonded molecules inside the clusters, the energies for the three peripheral geometries (H-up, H-down, and OH) were too close in value to decide which model was most likely. The answer was found by a comparison of the calculated STM images for each configuration with the experimental one. As shown in Figure 7, only the model with peripheral molecules with a H-down configuration (Figure 7b) produced STM images that closely matched the experiments.

Mitsui et al. also found that the structures discussed previously are metastable: when the sample was heated to 130 K, the structure of the water layer changed considerably. Extended hexagonal networks were produced, which necessarily imply a different binding of water inside the clusters, with alternating molecules having dangling H-atoms pointing up, or down toward the Pd substrate (similar to the case of Pt(111), which we will discuss next), or perhaps dissociated to OH and H. In addition, water molecules were found to form second layer structures that were not observed for the clusters at lower temperatures.[29]

2.1.2. Structure of the Water Monolayer

As the water coverage on the surface increases, the clusters merge into extended structures, eventually forming a monolayer, followed by flat multilayers (wetting case), or by 3-D islands (nonwetting case). Whether the water will wet the surface depends on the relative strength of the water−water interaction in a layer and across layers. The structure of the first water layer has received considerable attention recently. It can be formed readily at low temperatures (<150 K) in ultrahigh vacuum and studied with a number of surface science techniques. In the case of multilayers, however, the insulating nature of water hinders the application of some surface science techniques (e.g., STM) to their study.

The first structural study of a water layer on a metal using STM was performed by M. Morgenstern et al.,[30,31] who investigated the growth of water on Pt(111) between 120

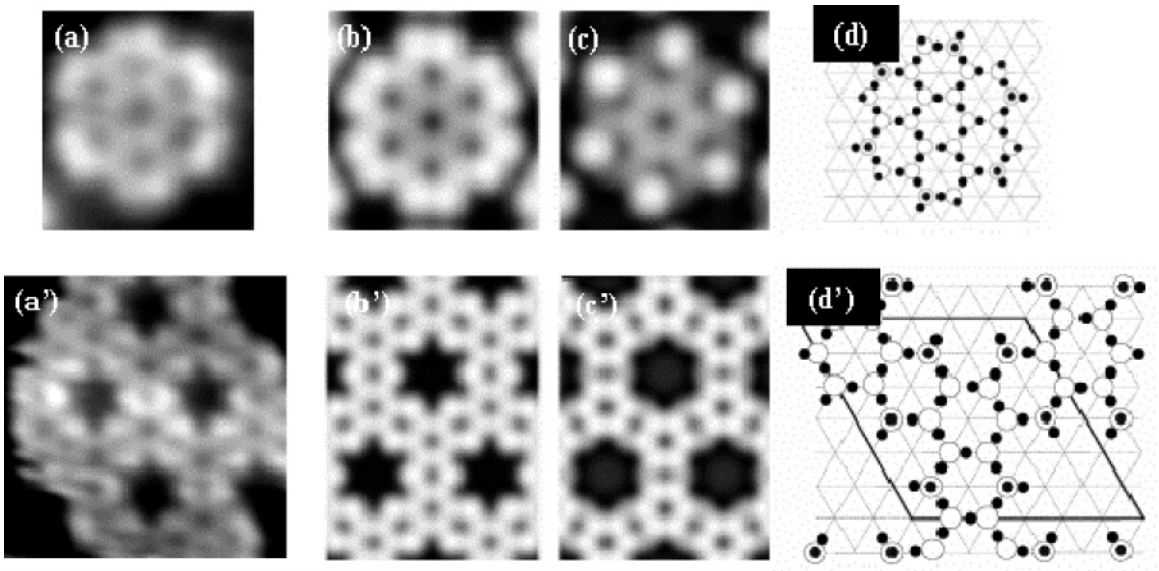

Figure 7. D_2O clusters on Pd(111) at 100 K. (a) Experimental STM images of a rosette structure made of seven hexagons. (b and c) STM topographic image simulations for two different DFT-optimized models of the rosette structure. In panel b, the edge water molecules have a H-down configuration. In panel c, alternating molecules are dissociated to OH (a similar simulated image was obtained from an H-up configuration). Clearly, panel b matches much better with the experimental image in panel a. (d) DFT optimized structure of panel b. White circles are O-atoms, and dark circles are H-atoms. Dark circles inside white circles are dangling H-atoms below the O-atoms (down configuration). Panels a′−d′ show the results for a larger structure. Again, the STM images can be reproduced only with edge molecules with dangling H-atoms pointing toward the surface. (Each part of Figure 7 is reprinted with permission from ref 28 (http://link.aps.org/abstract/PRL/v93/p116101). Copyright 2004 by the American Physical Society.)

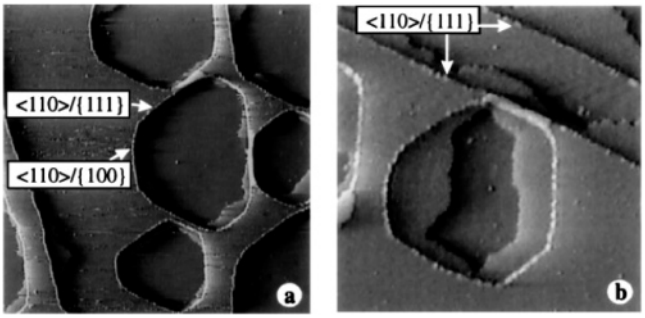

Figure 8. STM images of the Pt(111) surface after adsorption of water. The orientation of the monatomic steps of the hexagonal vacancy islands are labeled in panels a and b. A 2-D water layer can be observed growing at the lower terraces inside the hexagonal vacancy islands. Chain-like structures of adsorbed water molecules can also be observed at the upper side of the monatomic steps. (Reprinted with permission from ref 30 (http://link.aps.org/abstract/PRL/v77/p703). Copyright 1996 by the American Physical Society.)

and 145 K. They found that water adsorbs preferentially at the top and bottom of the step edges (Figure 8). At the lower side of the edges, 2-D ice-like patches were observed, while on the upper side, quasi-1-D chains were formed. The morphology of these chains was found to depend on the crystallographic orientation of the step edge: on {100} steps, continuous 1-D chains were found, while on {111}-oriented steps, such chains were only found near kink sites, with the chain lengths depending on the spacing between kinks along the steps. The authors explained these observations based on the Smoluchowski effect.[32] According to this effect, the finite Fermi screening length of conduction electrons rounds off the sharp geometry of the positive atomic cores in the steps and produces an electrical dipole with the positive end at the top edge and the negative pole at the base of the step. This leads to an enhancement of the water binding energy at the top of the steps relative to the terraces. The authors commented that the dipole due to the Smoluchowski effect was 20% greater on the {100} steps than on the {111} steps, except at the kinks, which explains the observed preferential adsorption. The 2-D water islands formed on the lower side of the steps grew and covered the entire surface when the coverage increased.

Depending on the preparation conditions (temperature and water vapor exposure), M. Morgenstern et al. found three different structures (which they named I, IIa, and IIb) for the water monolayer that differed in molecular density. STM images of the three phases are shown in Figure 9. The densest phase (Phase I) showed a hexagonal pattern with a period

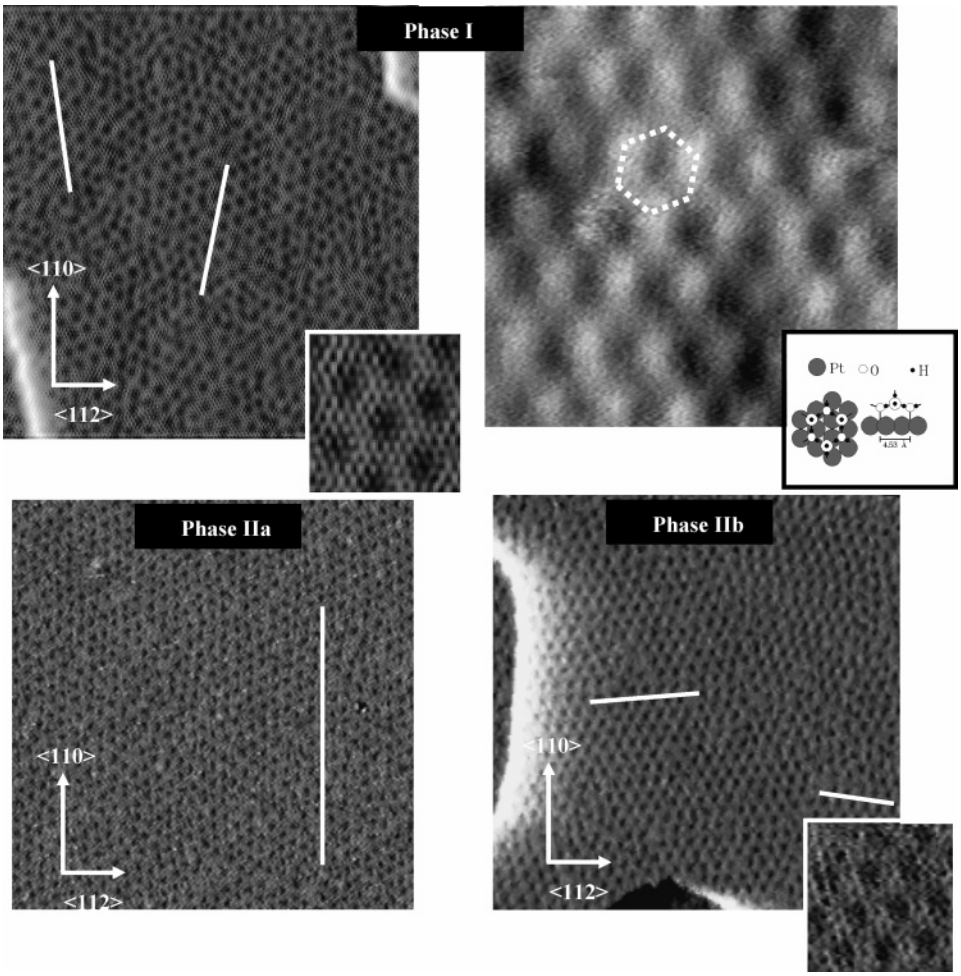

Figure 9. STM images showing different phases of the water layer on Pt(111). The white lines indicate the close packed directions of each domain in each phase. Phase I (top left): hexagonal superstructure. Two different orientations can be observed. Inset: Detail of the Moirée pattern. Phase I (top right): hexagonal ice rings. The hexagon drawn indicates one ice ring. The vertexes of the hexagon appear as bright and dark spots alternatively. This corresponds to the two different configurations of the water molecules in the ice ring. Phase IIa: only one orientation is observed. Phase IIb: two different orientations of the superstructure hexagonal domains. Note that they are different from those in Phase I. Inset: expanded images show molecular scale details. (Each part of Figure 9 is reprinted with permission from ref 31. Copyright 1997 Oldenbourg Wissenschuftsverlag.)

of 18.1 ± 0.2 Å. It was interpreted as a Moirée superstructure formed by an ice layer made of hexagonal rings with 4.56 ± 0.13 Å spacing over the Pt(111) lattice. The ice lattice is rotated by 7° relative to the ⟨112⟩ substrate direction (i.e., the $\sqrt{3}$ direction), and its unit cell is smaller than the 4.81 Å Pt(111) $\sqrt{3} \times \sqrt{3}$ unit cell. Two different domains of the hexagonal superstructure rotated by 14° with respect to each other were found in the images. The hexagonal ice rings contain only three protrusions in the STM images (instead of the expected six for a hexagonal ring), which indicate that alternating molecules in the ring have either different heights over the surface, as in the puckered bilayers of bulk ice, or a different structure than the other three. The second ice layer phase observed (IIb) was formed by heating phase I to 140 K in vacuum. According to the authors, this led to the desorption of some water from the surface. Phase IIb forms also a hexagonal superstructure, this time with a periodicity of 15.7 ± 0.5 Å. Higher resolution images showed that this superstructure consists of two different regions: hexagonal rings with side lengths of 4.8 Å oriented parallel to the Pt(111) $\sqrt{3} \times \sqrt{3}$ unit cell direction and other regions where no molecular ordering was visible. The third, Phase IIa, was formed by warming the IIb phase to 147 K while adding some water to the surface. Phase IIa shows also a superstructure with the same periodicity of 15.7 ± 0.5 Å as Phase IIb, but here, the sides of the hexagons are oriented parallel to the {110} direction. Only one domain was found for this phase. These ordered phases could be transformed into each other by changing temperature and water exposure to induce adsorption, desorption, and rearrangement of the adsorbed water molecules. The presence of a disordered region, interpreted as a 2-D liquid phase, was observed during the phase transitions.

Monolayer ice structures on Pt(111) were also observed by Glebov et al.[33] using He atom scattering. These authors found two different ice structures with different densities at 130 K during growth of the first monolayer. Initially, islands with $(\sqrt{37} \times \sqrt{37})$R25.3° periodicity formed at submonolayer coverage, followed by a $(\sqrt{39} \times \sqrt{39})$R16° structure after completion of the monolayer. The size of this unit cell is 17.5 Å, close but not equal to the size of the superstructure cell in Phase I of M. Morgenstern et al. discussed previously. In addition, the STM phases were rotated by 7° instead of 16° with respect to the ⟨112⟩ substrate direction. The origin of these differences is not clear. It is possible that water forms a variety of structures that differ slightly in density and orientation relative to the substrate and that small differences in temperature and preparation conditions give rise to different structures, all with similar energies, as already noted by Glebov et al. As we will discuss in more detail soon, large activation energies may kinetically lock some metastable structures. We will see more dramatic manifestations of these effects in the following sections.

The growth of water layers on Pt(111) was also studied by Haq et al.[34] at $T \geq 135$ K using LEED, RAIR, and TPD. In agreement with Glebov et al., they found that water formed first an ordered hexagonal layer with a $(\sqrt{39} \times \sqrt{39})$R16° LEED pattern with respect to the Pt(111) surface.

Until 2002, most experimental results of water layers on metals were interpreted according to a model where the water monolayer adopts the structure of the puckered honeycombs found in the basal plane of ice I_h. The monolayer was found to be in many cases in registry with the surface lattice of fcc(111) and hcp(0001) metals, based in part on low energy electron diffraction (LEED) observations of a $(\sqrt{3} \times \sqrt{3})$-R30° structure.[1,2,35,36] It had been commonly accepted that the hydrogen atoms that are not part of a H-bond were pointing up perpendicular to the surface, in what is called the H-up configuration. Figure 10a shows a schematic representation of this ice-like bilayer. The first STM studies of monolayers on Pt(111),[30] Ag(111),[25] and Cu(111)[5] were also interpreted following this model.

The ice bilayer model was challenged by experimental and theoretical work. Held and Menzel[35] found by analysis of LEED intensities that on Ru(0001), the O-atoms in D_2O are nearly coplanar, a conclusion recently corroborated by the same authors using a more refined analysis of the LEED intensities.[37] The result, at odds with the puckered ice bilayer model, motivated a theoretical analysis of the energetics of water adsorption by Feibelman.[38] He found that the binding energy of the undissociated monolayer was less than the energy formation of bulk ice, which means that the monolayer should not be stable and therefore de-wet the surface to form 3-D ice crystals. This led Feibelman to propose a different model where alternating water molecules (those not attached to the substrate in the original ice-like bilayer) dissociate into OH and H, with the O in the OH groups bonding covalently to the metal and forming a quasi-planar layer, as shown in Figure 10d. This model maximizes both hydrogen bonding and oxygen−metal interactions.

A different water monolayer model was proposed by Ogasawara et al.[39] based on experimental and theoretical XPS, NEXAFS, and XES studies of a water monolayer on Pt(111) that was annealed to 140 K. In this model, water also forms a hexagonal structure with two different molecular arrangements inside the unit cell. One molecule, with its plane nearly parallel to the surface, is a double H-donor and binds to the Pt-atoms through the O lone pair orbital. The other molecule is a single donor with its molecular plane roughly vertical and with a H-atom located between the O- and the Pt-atoms. As in the previous models, the puckering of the hexagon is much reduced as compared with that of the intact ice hexagon. This model is shown in Figure 10b.

Recently Meng[40] used ab initio molecular dynamics simulations at 130 K to analyze the structure of the monolayer on Pt(111), starting with the $(\sqrt{39} \times \sqrt{39})$R16° model of Glebov et al. In contrast to Ogasawara's results, he found a structure that is roughly similar to that of the puckered ice bilayer of the ice I_h basal plane. According to his calculations, the $(\sqrt{39} \times \sqrt{39})$R16° unit cell contains four different species: about 20% of the molecules are located in a nearly flat first layer, with the O-atoms 2.23 Å above the Pt-atoms. The largest fractions of water molecules, about 66%, are located in a second layer with the oxygen atoms at a distance of 3.27 Å above the surface. A smaller fraction of molecules (13.7%) are found even farther away from the surface at a distance of 4.5 Å. A small percentage (9%) was found to dissociate to OH and H_3O. No H-atoms were found between the O- and Pt-atoms of the first layer, which is in disagreement with Osagawara's results. Meng and Ogasawara et al. agree, however, that water does not dissociate on Pt(111), or does so in very small amounts.

Other DFT calculations were performed to examine the stability of intact layers with alternating molecules in the H-up and -down configurations, as well as of half dissociated water layers on the (111) surfaces of Ni, Cu, Rh, Pd, Pt, and Ag and on the (0001) face of Ru.[41] The results are shown in Table 1. The stability of the half dissociated layers varies

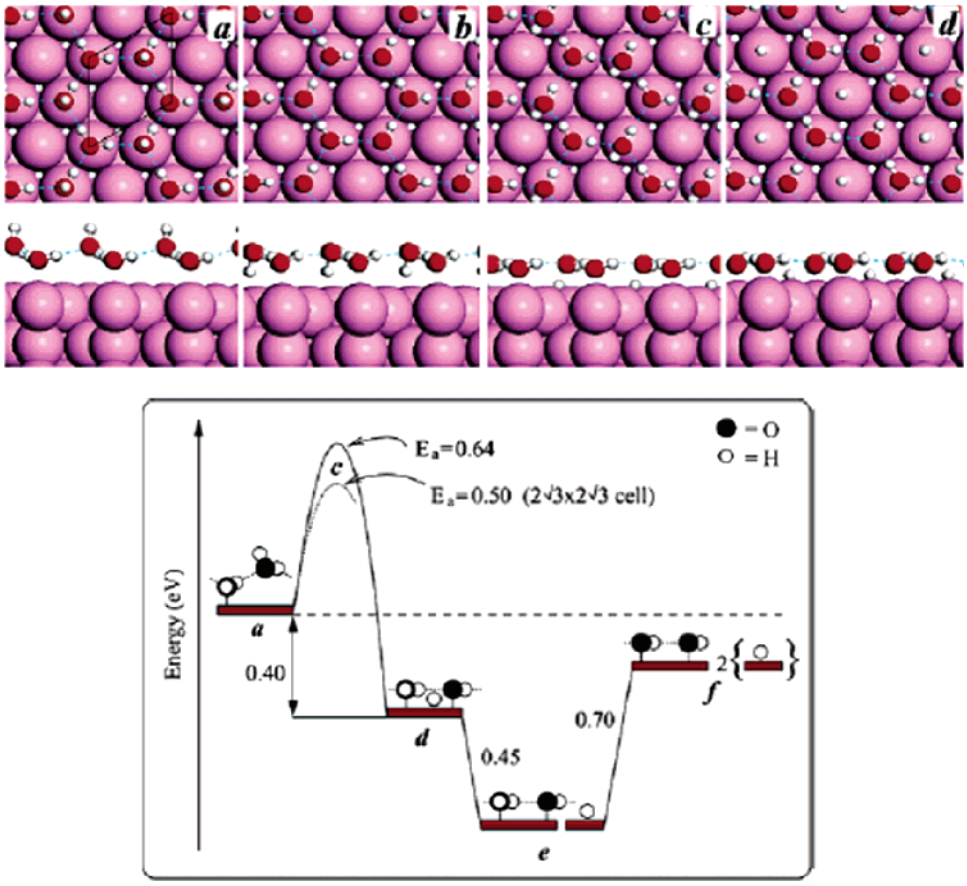

Figure 10. Top: top and side views of different configurations proposed for the water monolayer on Ru(0001). (a) H-up layer as in bulk ice, (b) H-down layer, (c) transition state for dissociation, and (d) partially dissociated OH − H_2O + H mixed layer. The ($\sqrt{3} \times \sqrt{3}$)R30° unit cell is shown in panel a by lines. Bottom: energy diagram (in eV) for H_2O adsorption and dissociation on Ru(0001). States a, c, and d correspond to the structures shown above. Stage e corresponds to a different dissociated overlayer with the H atom removed from the center of the hexagon into a separate area of the surface. Panel f is the pure OH fully dissociated layer. All energies, unless indicated otherwise, are for a ($\sqrt{3} \times \sqrt{3}$)R30° unit cell. (Each part of Figure 10 is reprinted with permission from ref 50. Copyright 2003 American Chemical Society.)

Table 1

$E_{ADS-TOT}^{(1)}$ (eV/H_2O)	H-up	H-down	H_2O−OH−H	H_2O−OH + H/M
Ni	−0.42	−0.37	−0.12	−0.62
Cu	−0.45	−0.43	−0.07	−0.4
Ru	−0.54	−0.50	−0.77	−1.00
Rh	−0.53	−0.55	−0.51	−0.78
Pd	−0.52	−0.56	−0.16	−0.56
Pt	−0.46	−0.49	−0.31	−0.38
Ag	−0.46	−0.48	+0.26	−0.05

considerably between substrates, whereas the stability of intact monolayers does not. A careful analysis of the various contributions to the total binding energy, separated into those arising from H-bonding inside the layer and those arising from bonding to the metal substrate, was performed to explain this interesting result. The analysis revealed that the largest contribution to the binding of the layer was due to the internal H-bonding, which accounts for 70−80% of the total energy, while the binding to the substrate (mainly due to the formation of bonds between the metal orbitals and the O lone pair orbital) contributes a smaller 30−20% of the total energy. Figure 11a, b shows the variation of these two contributions for the metals listed in Table 1, plotted as a function of their lattice constant. Despite the smaller oxygen−metal contribution to the total energy, the stability of partly dissociated overlayers can be traced back to the OH adsorption energy on each surface. Accordingly, Michaelides et al.[41] proposed that the strength of the OH-bond with the substrate is a useful guide to predict if wetting will take place in the form of intact layers or mixed dissociated layers. The graph in Figure 11c illustrates this result. Intact layers were found to be favored on Ag and Pt (H-down) and on Cu (H-up), in agreement with the experimental results. On Ru, Rh and Ni partially dissociated layers are preferred over intact ones. On Pd(111), the H-down and the partially dissociated layers are equally stable. The results are sensitive to the final location of the chemisorbed H-atom. If one assumes that the H-atoms from the dissociation into OH and H remain on the top sites inside the unit cell, then the partially dissociated layer is more stable than the intact one only on Ru(0001). Materzanini et al.,[42] using first principles studies, also found that for water on Ru(0001), the half-dissociated structures are more stable.

While there is a general agreement about the DFT results discussed previously, in the experimental area the situation is less clear, and a strong controversy exist on whether the experiments support one model or another. Denzler et al.[43] measured hydrogen desorption following thermal desorption of water to analyze the amount of atomic hydrogen remaining on the ruthenium surface as a function of initial water coverage. In these experiments, water was deposited at 140 K, and then the sample was annealed to 230 K, while the water desorption was measured. Hydrogen desorption was measured in the temperature range from 230 to 550 K. For

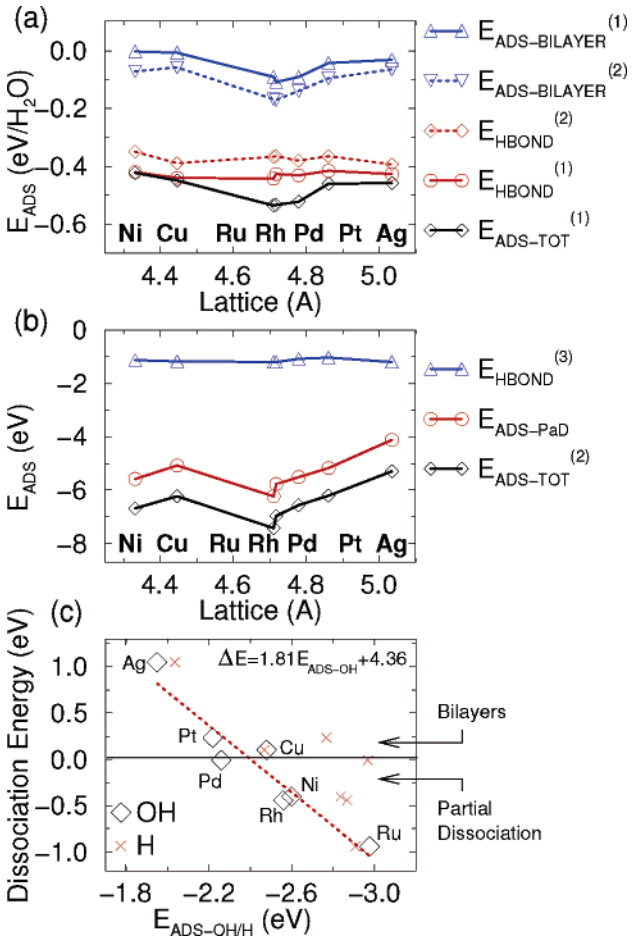

Figure 11. Total H_2O adsorption energy and its decomposition into adsorbate−substrate and H-bonding contributions as a function of the calculated substrate lattice constant for (a) H-up monolayer and (b) H_2O − OH + H/M monolayer. (c) Monolayer dissociation energy against OH adsorption at on-top site and H adsorption at 3-fold fcc sites on metal surfaces. The dotted line is a least-squares fit to the OH points, which are labeled as diamonds. (Reprinted with permission from ref 41 (http://link.aps.org/abstract/PRB/v69/p113404). Copyright 2004 by the American Physical Society.)

both H_2O and D_2O, atomic hydrogen was observed to remain on the surface after water desorption, indicating that dissociative adsorption is taking place at least to a small extent. The equivalent of 14% of a monolayer of H_2 was found to desorb after water desorption and 0.6% of a monolayer for D_2. The different amounts of H_2 and D_2 were associated to two possible effects: an incomplete recombination of an originally partially dissociated water structure during desorption, with the degree of recombination differing for H_2 and D_2, or a different degree of dissociation of water molecules for the two isotopes. While this picture is compatible with the proposed half dissociated layer structure for water on Ru(0001), one should be cautious in the interpretation. For example, the initial layer that is formed at a low temperature could be undissociated, with dissociation occurring only at higher temperatures during annealing. This would correspond to a situation where the undissociated layer was not equilibrated to the stable half dissociated layer. A spectroscopic analysis of the initial layer could therefore show a different structure as the one deduced from the H_2 TPD experiments. Another potential pitfall in the TPD experiments is the possibility of adventitious adsorption of H from the background on the metal surface that would then show up in the TPD spectrum.

Partly dissociated water on Ru(0001) was also found in XPS studies that were performed at a substrate temperature of 105 K.[44] From the relative areas of the O1s peaks due to OH and H_2O, the layer of water was found to contain OH and H_2O in a roughly 3:5 proportion. Feibelman has explained this departure from the proposed 1:1 proportion of OH and H_2O [38] by taking into account relaxations of the water molecules from their exact on-top positions and by introducing Bjerrum defects.[45] The energy cost to produce these defects is much easier to accommodate in the adsorbed monolayer than in bulk ice because the relaxations possible in the monolayer produce a gain in energy that more than compensates for the defect formation energy.

The half-dissociated model for water on Ru(0001) was later disputed by Denzler et al.[46] On the basis of their SFG results, they proposed that alternating molecules in the hexagonal unit cell are not dissociated but have H-atoms pointing toward the metal substrate, thereby forming O−H− metal bonds, similar to the model proposed by Ogasawara et al. for water on Pt(111).[39] This finding has found additional support by recent XPS experiments from the same group[47] showing that water adsorbs nondissociatively on the surface of Ru(0001) below 150 K.

A TDP and RAIR study by Clay et al.[48] of water on Ru(0001) revealed that the spectra of ice layers grown below 145 K show OH stretch and H_2O bending modes that are characteristic of intact molecules, although some dissociation could not be excluded in these studies. Above 150 K, these modes disappear, and only out of plane bending modes remain. Both of these findings are consistent with the formation of an intact monolayer at temperatures below 150 K and a partially dissociated overlayer at $T > 150$ K.

In the preceding paragraphs, we have described a number of experimental and theoretical results that disagree about whether the water monolayer on Ru(0001) is partially dissociated or if it consists of intact water molecules. At the heart of this controversy is the contention by some authors[47,49] that many observations of dissociated water structures by LEED, XPS, and other techniques that use energetic probes are the result of dissociation induced by the incident electron or X-ray beam. Andersson et al.[47] showed that the energy pathway leading to thermal dissociation of the adsorbed water on Ru(0001) lies above the energetic barrier for thermal desorption. This is, we believe also, the key to the current conundrum. The existence of large energy barriers that separate metastable water structures often precludes reaching the thermodynamically stable state. This is exacerbated by the fact that most surface science experiments are performed at cryogenic temperatures, so that metastable structures can easily form and remain kinetically stable for long times. Glebov et al.[33] have shown that water ordering on Pt(111) is strongly influenced by temperature and deposition rate. Michaelides et al.[50] found also very substantial activation barriers of ∼0.5 eV for the dissociation of molecularly adsorbed water to the energetically favored mixed H_2O + OH layer on Ru(0001), as shown in the schematic of Figure 10. These energy barriers between stable and metastable structures turn out to be comparable to the binding energy of water molecules to either the substrate or to other molecules. Annealing the water films to attain thermodynamically stable structures easily results in the desorption of water from the surface. Energetic particles, electrons and photons, can provide the necessary energy to overcome barriers and to dissociate the molecules. We believe that a

satisfactory understanding of the structure of the first water layers must come from experiments performed under equilibrium conditions of water vapor pressure and temperature. There is good hope that soon this can be accomplished (e.g., by the use of newly developed ambient pressure photoelectron spectroscopy instruments that allow one to obtain XPS spectra at ambient temperatures and in equilibrium with the vapor (i.e., at Torr pressures)). Ambient pressure XPS has already shown its promise in the study of ionic segregation in water droplets.[51]

Before concluding this section, it is worth commenting on a paradoxical result that is apparent from Table 1. In all cases, the binding energy found in DFT simulations for the most stable water films on metals, whether H-up, H-down, or partially dissociated, is less than that of the sublimation of bulk ice, which is 0.75 eV per molecule for a proton ordered system. Thus, except for Ru(0001), 3-D ice clusters should form on any other metal surface in Table 1. This remains true even if a more extensive calculation is done using larger unit cells (a $(\sqrt{3} \times \sqrt{3})$R30° cell was used in the calculations giving the data in the table), where a gain of about 70 meV is obtained for the binding energy. As Michaelides et al.[41] explain in their paper, the paradox should not be overstated because, while the DFT is excellent at producing good energy values in different metals that can then be compared to each other, this is due in part to a cancellation of errors that works in the same way for each metal. Bulk ice, however, is an insulator, and the exchange-correlation contribution to the energies is very different in the two systems, so that comparison of energies in metals and insulators is not as reliable.

2.1.3. Thin Water Films

In the previous sections, we focused on studies of the structure of water on metals below one monolayer. These studies made use of powerful techniques such as LEED, STM, XPS, and IR that provided a wealth of fundamental information. The next natural step in the study of wetting is to expand these studies to the growth of multilayer films. In comparison with the monolayers, however, much less information exists on the molecular scale structure of thicker films. This is due primarily to experimental difficulties since few of the techniques that so successfully provided spectroscopic or microscopy data on monolayers can operate on thick water films except, as we shall see, after special modifications of the technique. Electron spectroscopies suffer from the insulating nature of bulk water, which leads to charging of the surface. STM cannot be performed on films beyond two or three layers again due to conductivity problems that cause the perturbation by the tip to become too large. Infrared spectroscopy provides information on the structure of the entire film, thereby averaging over the contributions from bulk and interfaces. A very valuable technique for interface studies is sum frequency generation because the signal is generated only in the water layers at the interface with either the substrate or with the gas phase. The extreme surface selectivity of this technique, however, is also a limitation because information on the structure of layers beyond the one at the interface is not obtainable.

Photoelectron spectroscopies can provide information on a few water layers beyond the first at the interface of water or ice, depending on the kinetic energy of the photoelectrons. It can even be used to probe the water/vapor interface at elevated pressure, above the water desorption temperature in vacuum of approximately 170−200 K (the equilibrium vapor pressure of water at the triple point is 4.58 Torr). This can be accomplished by differential pumping schemes, first introduced by H. Siegbahn et al. in the 1970s.[52] Recently, synchrotron-based ambient pressure XPS that can operate at pressures above 5 Torr has been developed and used to study the surface of ice, water, and ionic solutions in equilibrium with water vapor at temperatures close to and above the melting point, thus showing the potential of this technique for the study of multilayer water and ice films under ambient conditions.[51,53,54]

Starke et al.[55,56] used LEED to study nanometer thick water films on Pt(111) at 140 K. To avoid charging, they used very low incident beam currents of only a few picoamperes. The thickness of their films was estimated to be larger than 1 nm based on the extinction of the Pt substrate diffraction spots. Their results show the growth of a hexagonal ice film, exposing the basal plane of ice I_h. The LEED diffraction spots correspond to a $(\sqrt{3} \times \sqrt{3})$R30° periodicity with respect to the substrate unit cell. The diffraction spots were quite broad, indicating that the ice film was comprised of small domains. This is an interesting finding because it indicates that the influence of the Pt(111) substrate in nucleating crystallographically oriented films extends well beyond the monolayer. A similar result was found by Glebov et al.[33] The high background of the LEED pattern obtained by Starke et al. implies disorder as well as high thermally excited vibration amplitudes at the ice film surface. From the dependence of the diffracted intensities on energy, and from MD simulations and total energy calculations, the authors concluded that the last molecular layer vibrates with very high amplitude, such that the Debye−Waller factor obliterates their contribution to the diffracted beams. They interpreted this phenomenon as indicative of a surface melting of ice.[57]

In their LEED studies, Haq et al.[34] observed that the $(\sqrt{39} \times \sqrt{39})$R16° structure of the first water layer on Pt(111) persisted as growth proceeded to up to approximately five layers at 137 K, indicating that this denser structure was maintained in all the layers up to the fifth. Beyond that, further adsorption reorients the film to form an incommensurate hexagonal structure with the characteristics of bulk ice, which is aligned at 30° to the Pt(111) close packed directions, in agreement with the findings of Starke et al. and Glebov et al. Interestingly, they observed that the transition was irreversible so that desorption of the multilayers did not restore the $(\sqrt{39} \times \sqrt{39})$R16° LEED pattern.

M. Morgenstern et al.[31] studied the nucleation of a second ice layer on Pt(111) using STM. They found that water exposure at 140 K up to 8×10^{-9} mbar vapor pressure did not lead to nucleation of the second bilayer. Nucleation was only observed for temperatures below 135 K. As mentioned previously, depending on water exposure and temperature, three different phases were found for the first layer. On Phase I, further exposure to 5×10^{-9} mbar at 135 K induced the nucleation of the second bilayer. The second layer formed a regular pattern of clusters adsorbed on every second corner of the superstructure. The authors suggested that the corners in the first superstructure corresponded to water molecules adsorbed on hollow sites of the Pt(111) surface and that this adsorption site in the first layer increased the nucleation probability of the second layer. The growth of the second water layer was also examined on Phases IIa and IIb. In both phases, a regular array of clusters was formed, but only the

clusters on Phase IIb could be molecularly resolved. They consisted of five protrusions with a structure not compatible with I_h ice rings.

Su et al.[58] studied the growth of water multilayers on Pt(111) at temperatures between 120 and 137 K using SFG. The spectra showed characteristic OH stretch frequencies of tetrahedrally coordinated water, in addition to the frequency of free OH, with the H dangling in the vacuum. The selection rules for SFG require that the modes be noncentrosymmetric, a condition that is found in nonisotropic media lacking inversion symmetry, and at interfaces, where the surrounding of the molecules is asymmetric. Interestingly, the authors observed that the intensity of the OH stretch mode in the tetrahedral H-bonds continued to grow as the film became thicker, which indicates that the H-network is not random (i.e., isotropic) but exhibits a ferroelectric order (the term is used here to describe a net polar ordering of water molecules in the ice film[59]). Because SFG is a second-order process, a uniform order should produce a spectral intensity that increases as the film thickness is squared. Instead, they found the increase to be weaker, which was interpreted as due to the decay of polar order in successive layers. The decay length was found to be 30 monolayers. A similar conclusion regarding the formation of H-oriented growth induced by the first layer was proposed by Devlin et al.[60,61] According to these authors, if a water layer was formed on a metal surface with H-up termination, it could induce a structure where each successive bilayer was also in the same orientation. The water molecules in the upper half of the top bilayer would then also have dangling H-bonds pointing out of the surface. In other words, the proton order in the first layer would be transferred up through the film, in contrast to bulk ice, which is proton disordered. We will see later another example of the growth of dipole-oriented water films in the case of mica.

We have seen in the section dealing with the structure of the water monolayer that experimental evidence indicates that the monolayer on Pt(111) has no free OH or dangling H pointing into the vacuum.[39] Instead, in alternating molecules of the hexagonal rings, the H-atoms that do not participate in H-bonds point down towards the Pt substrate. The observation by Su et al. of a SFG peak characteristic of a free OH stretch at a coverage of 1.2 monolayers and above raises the interesting possibility that the structure of the first water layer on the Pt(111) substrate could be modified when the second layer grows on top. That the presence of multilayers changes the structure of the first layer is not surprising because, as we have seen, the binding energy of an entire water layer is a small fraction of the total stabilization energy, with the largest fraction coming from the H-bonding inside the layer. In addition, the water layer−metal binding energy per molecule is of the same order as the water−water binding energy.

The Pt(111) system was also studied by Iedema et al.[62] using the Kelvin probe method[63] to measure the surface potential of the growing ice film. They found that at 40 K, only a slight orientation of the water molecules takes place, about 0.2% of a net dipole per water molecule or −3 mV per monolayer, a result that was discussed as contrary to the conclusions of the SFG study of Su et al. They also found that the dipolar orientation decreases exponentially with deposition temperature. In addition, near 130, 140, and 150 K, sharp features related to water orientation were observed as the ice changed from an amorphous to a crystalline structure. By 150 K, the effect disappeared. The issue of ferroelectric ice has been examined by Witek and Buch[64] by means of molecular dynamic simulations. The authors assumed rigid first monolayers, either flat or puckered as in ice, with dangling bonds pointing to the vacuum. They found that ferroelectric order was lost rapidly in successive layers (up to four were studied), by flips of the dangling OH toward the interior and the formation of defects that left some of the downward pointing H dangling.

A large amount of information for water films with thicknesses beyond a few layers is derived from techniques based on desorption measurements. Films deposited on substrates at low temperatures (less than 130 K) have been shown to form an amorphous phase, named amorphous solid water (ASW) by Kay et al.[66] The absence of long-range order in such films is related to the limited surface mobility of the molecules at these temperatures. Although at the monolayer level ordered structures form on most metals, this order cannot be maintained indefinitely due to the accumulation of imperfections as the film grows thicker than a few nanometers. The ASW film morphology depends on the temperature and dosing conditions.[66] The amorphous water is metastable and crystallizes, forming ice I near 160 K, in a transition similar in nature to that between the supercooled liquid phase and crystalline ice.[67] The transition manifests itself in a change in desorption rate from a high to a smaller value in crystalline ice, which produces an inflection in the TPD spectra at around 160 K, as shown in Figure 12.[68]

Smith et al.[69] measured the water desorption rate of nanometer thin ice films (∼56 water layers) grown on Au(111) and Ru(0001). After deposition at 85 K, they increased the temperature to 160 K and measured the time evolution of the desorption rate. It was found that the transition from amorphous to crystalline ice was independent of the substrate. Interestingly, it was also observed that after crystallization, the desorption rate did depend on the substrate (i.e., Au(111) or Ru(0001), see Figure 13). According to the authors, this can be understood by considering the hydrophilic nature of Ru(0001) versus the hydrophobic nature of Au(111). The desorption rate measured on Ru(0001) would be consistent with a hydrophilic substrate that favors the growth of smooth and extended ice films, while the rate measured on Au(111) would be consistent with the formation of 3-D, spherical clusters of crystalline ice.

Ikemira and Gewirth[70] studied water adsorption on Au(111) at 100 K using STM. They observed an amorphous, two-dimensional first layer. Three-dimensional water clusters were observed on the amorphous film but not on the bare Au(111) surface. The authors speculated that the 3-D growth on Au(111), even if the interaction with the surface is weak, requires a 2-D wetting layer as a precursor for the formation of multilayers.

Löfgren et al.[71] studied the desorption of water from Pt(111), graphite, graphite pre-covered with Cs, and Pt(111) pre-covered with octane and with CO. They concluded that the desorption rate after crystallization depends on the wettability of the surface, in line with the previous observations. On the basis of these studies, they ranked the wettability of crystalline ice on bare and pre-covered metal surfaces in the order Pt(111) > CO/Pt(111) > Ru(0001) > Cs/graphite > graphite > octane/ Pt(111) ≥ Au(111). On the basis of these findings, Meng et al.[72] used ab initio density functional calculations of water on Pt(111) and Au(111) to study the hydrophilic and hydrophobic character of these

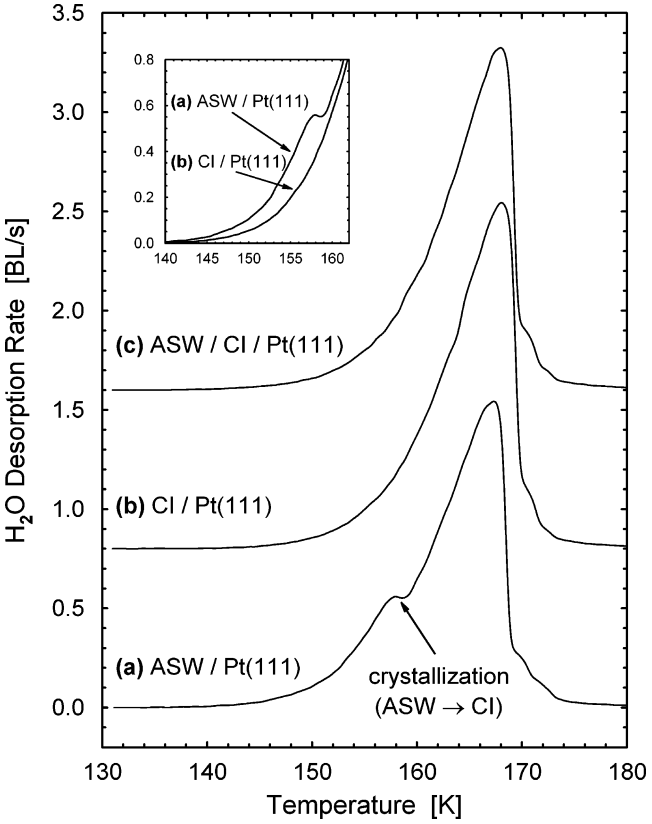

Figure 12. Thermal programmed desorption spectra of H_2O from films deposited on a Pt(111) substrate at different temperatures. (a) 25 layers deposited at 22 K. At this temperature, the amorphous solid water is formed (ASW); (b) 25 layers deposited at 140 K, a temperature where crystalline ice forms (CI); and (c) 15 layers deposited at 140 K followed by 10 layers deposited at 22 K. The spectra are offset for clarity. The inset shows a superposition of spectra a and b to indicate the higher desorption rate of ASW as compared to CI. (Reprinted with permission from ref 68. Copyright 1999 American Institute of Physics.)

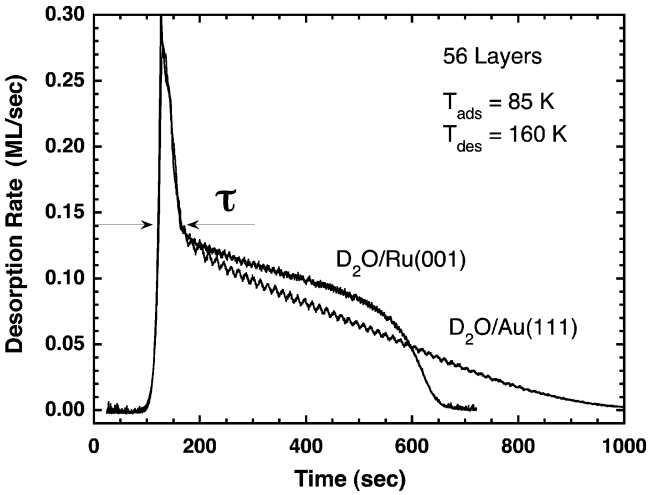

Figure 13. Isothermal desorption spectra from amorphous D_2O ice grown at 85 K on Ru(001) and Au(111). The initial spike corresponds to the conversion from amorphous to crystalline ice. The late-time difference in the desorption kinetics reflects the different morphologies of the ice films in the two substrates. (Reprinted with permission from ref 69. Copyright 1996 Elsevier.)

surfaces. They characterized the wettability of a surface from the ratio between the H-bond energy and the adsorption energy. Taking a value of 1 in the ratio as representing the borderline between hydrophobic and hydrophilic interactions, they found that for film thicknesses of up to 4 ML, this ratio was below or very close to 1 for Pt(111) and above 1 for Au(111). Dohnálek et al.[73] studied the crystallization kinetics of thin ASW films deposited on crystalline ice on Pt(111) using TPD. They found an acceleration of the crystallization rate for amorphous films on crystalline ice substrates. This acceleration is due to the absence of nucleation barriers on the crystalline ice substrate. In contrast, the crystallization rate on Pt(111) was constant, indicating bulk nucleation and 3-D growth. The authors found that the crystallization rate of thin films of ASW decreases rapidly as the film thickness increases.

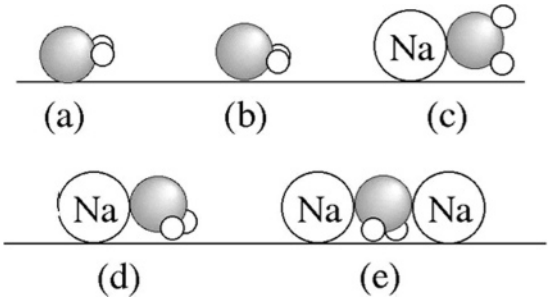

Figure 14. Schematic models of water coadsorbed with Na on Ru(0001). (a) Flat monomer in the absence of Na. (b) Bent monomer for a Na coverage of 0.04 ML. (c) Perpendicular monomer for 0.06 ML of Na. (d) Rotated monomer for 0.1 ML. (e) Sandwiched monomer for 0.16 ML. (Reprinted with permission from ref 74. Copyright 2002 Elsevier.)

2.1.4. Coadsorption with Other Adsorbates

Water adsorption in natural processes always occurs in the presence of other molecules that are coadsorbed on the substrate, competing with water for favorable adsorption sites, forming mixed structures with water, and possibly reacting with water and inducing dissociation. Water dissociation induced by the coadsorption with other molecules has been widely studied because of its importance in chemical reactions that take place on metal surfaces. We will not discuss this topic here but will focus instead on the effect of coadsorbed species on the structure of water layers. Four important coadsorbate species will be reviewed: alkali metal atoms, atomic oxygen, carbon monoxide, and halide atoms. Coadsorption with other adsorbates such as hydrogen, organic molecules, CO_2, O_2, nitrogen, and sulfur compunds, etc., are of great interest, but they have received less attention up to now.

2.1.4.1. Alkali Atoms. Water molecules interact strongly through electrostatic forces with coadsorbed alkali atoms. This interaction results in a change of the orientation of the water molecules as compared to the orientation that is present on a bare substrate. The structure of coadsorbed water is a result of the competition between water−alkali electrostatic interactions and water−water H-bonding interactions. The interaction of water with the metal surface is generally weaker or of the same order as H-bonding interactions, as we have discussed in previous sections. Nakamura and Ito[74] studied water coadsorption with Na on Ru(0001) using IRAS in the temperature range between 20 and 220 K. They suggested different models for the orientation of water molecules coadsorbed with Na, depending on Na coverage as shown in Figure 14. Some of these orientations were already proposed previously for different metals and alkali atoms.[75−79]

The strong orientational effects of water coadsorbed with alkalis can readily be detected in work function measurements. Bonzel and co-workers[79] studied the changes in work function of water coadsorbed with Na, K, and Cs on Pt(111) and Ru(0001) surfaces. They found that the tilt of the plane of the water molecule increases with the strength of the alkali−surface dipole (i.e., in the order Na < K < Cs). They also found that the tilt for a particular alkali is stronger for substrates with a weaker water−metal interaction. The slope of the work function as a function of water coverage is positive for low coverage but changes to a negative slope at a certain water coverage. This behavior of the work function can be explained in a two-step model for the adsorption of water on these surfaces: the adsorption of water starts at sites in the vicinity of the alkali atom where water molecules form a hydration-like complex, which in turn results in an increase in the work function. Clustering of water due to H-bonding interactions does not occur until all the hydration sites around the alkalis have been occupied. Once these sites are filled, adsorption takes place on sites that are not influenced by the alkali atoms, leading to the observed decrease of the work function. The authors point out that this sequential adsorption should only take place when the water alkali interaction is stronger than the water−substrate interaction. In contrast, when both are of similar strength, adsorption is more homogeneous, and the work function continually increases with water coverage.

2.1.4.2. Oxygen. It is know that oxygen reacts with water on some metal surfaces and can induce water dissociation. The dissociation creates OH structures that have been observed by LEED, He scattering, and STM. A very useful table of the different structures of OH from the reaction of water and oxygen on different metal surface can be found in Henderson's review[2] and will not be discussed here.

We focus here on the structure of undissociated water molecules. It has been observed by IRAS, TPD, and HREELS that low coverage (<1 ML) of preadsorbed oxygen on Ru(0001) inhibits the azimuthal ordering of water, thereby disrupting the bonding network between water molecules and suppressing the formation of water clusters.[80−82] On average, one oxygen atom can influence about five to eight water molecules in its vicinity.

Gibson et al.[83] studied water adsorption on an oxygen predosed Rh(111) surface using TPD and He atom scattering at 80 K. On clean Rh(111), water was found to form a $(\sqrt{3} \times \sqrt{3})$R30° structure. Preadsorption of small amounts of oxygen (<0.05 ML) improved the long-range order of the water layer, and the $(\sqrt{3} \times \sqrt{3})$R30° pattern was clearly visible for an ice thickness equivalent to 24 water layers. However, when half a monolayer of oxygen with a well-ordered (2 × 1)-O/Rh(111) was prepared, the diffraction pattern of the deposited water layers did not show any long-range order. In contrast, water adsorption on a full monolayer of oxygen with a (1 × 1) structure that was deposited on Rh(111) lead to a (1 × 1) diffraction pattern of the water molecules with a very long-range order. The He atom scattering did not show the expected $(\sqrt{3} \times \sqrt{3})$-R30° pattern for films up to 20 ML height. A new high-density model of ice, in registry with the oxygen monolayer, was proposed to explain this structure. This model consists of a p(2 × 1) structure formed by two interpenetrating lattices of water molecules with one H-bond at an angle with an adsorbed O and the other O−H bond parallel to the surface. Interference of the oxygen atoms with the long-range ordering of H_2O has also been been reported for Ni(111)[84] and Ru(0001).[80]

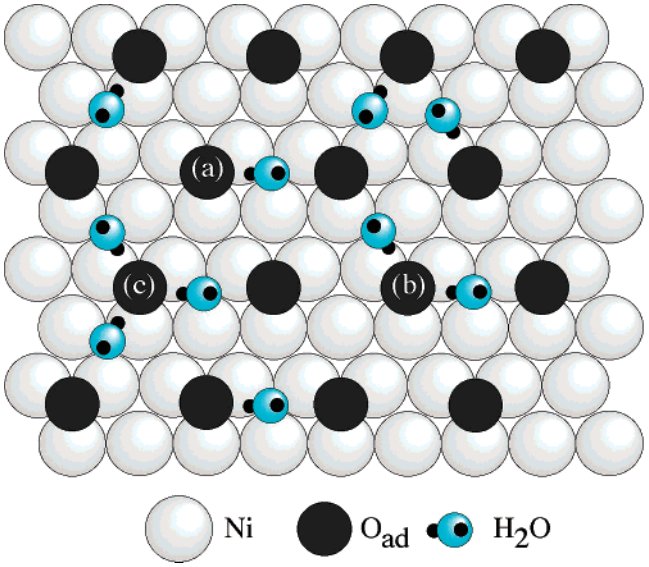

Figure 15. Schematic model of the H_2O adsorption on a Ni(111) surface with a preadsorbed *p*(2 × 2)-O layer at 25 K. Each O in the 2 × 2 structure can bind one (a), two (b), or three (c) water molecules. (Reprinted with permission from ref 90 (http://link.aps.org/abstract/PRL/v94/p35501). Copyright 2005 by the American Physical Society.)

Using different spectroscopy techniques, water has also been found to form periodic ordered structures on p(2 × 2) (i.e., 0.25 ML) oxygen structures on Ni(111),[84−86] Pt(111),[87,88] and Ru(0001)[89,80] at low temperatures. The model structures of water on these surfaces suggest that water forms hydrogen bonds to the oxygen atoms, with each oxygen atom accommodating two or three water molecules. Nakamura and Ito[90] studied water on a p(2 × 2)-Ni(111)-O surface at 25 and 140 K using surface X-ray diffraction and difference Fourier calculations. They found that at 25 K, the H_2O−O interaction is strong enough to prevent water cluster formation. The oxygen atoms were surrounded by one to three water molecules. The sites of adsorbed water on the (2 × 2) oxygen structure were found to be statistically disordered, with each atom accommodating one, two, or three water molecules, as shown in Figure 15. At 140 K, the water molecules were found to occupy top sites as in the clean surface.

2.1.4.3. Carbon Monoxide. CO generally bonds more strongly to metal surfaces than water. Coadsorption of CO can therefore lead to a blocking of the usual water adsorption sites by the CO molecules. This can force water molecules to occupy secondary adsorption sites or even prevent water from adsorbing at all, depending on the temperature. Blocking of water sites by CO has been observed on Pd(111),[91] Pt(111),[92] Rh(111),[93] and Cu(111).[94] Site blocking forces water to grow into 3-D clusters. Another effect that has been observed is that water on many metal surfaces is displaced when the surface is exposed to CO.[95] When the preadsorbed amount of water is higher than one layer, this effect is generally suppressed.[96,97]

Competition between water and CO for adsorption sites has been observed to lead sometimes to a site shift of the CO molecule. This shift can be detected by the changes in CO stretching frequency. The frequency shift can be used to determine the adsorption CO site. Shifts from top to bridge and hollow sites have been observed on Pt(111),[98,99] from top to 3-fold hollow sites on Rh(111),[100] from top to bridge

sites on Rh(100),[95] from top to 3-fold hollow sites on Ru(0001),[12] and from top to bridge and 4-fold hollow sites on Ni(100).[101] The shift of the CO adsorption site is due to the interaction between H_2O and CO molecules on the surface. This interaction can lead to the formation of mixed phases (complexing of water and CO) due to attractive forces between the molecules or to islanding (segregation of water and CO) as a result of repulsive forces. On the basis of TPD, IRAS, and HREELS measurements, attractive forces between CO and H_2O were suggested on Pt(111),[102] Al(111),[103] Ru(0001),[12] Ni(100),[104] and Rh(111)[100] and repulsive on Pt(111)[100] and Rh(100).[95] Recent studies of D_2O and CO coadsorption on Pt(100)[105] at 105 K using IRAS showed that the dynamics of the species on the surface can be very slow, on the order of minutes, involving a gradual rearrangement of the adsorbed species and suggesting a final solvated CO structure.[102]

2.1.4.4. Halogen Atoms. The structure of water coadsorbed with bromide, chloride, and fluoride has been studied on Ag(110),[106−111] with chloride and fluoride on Pt(111),[87,112,113] with chloride on Ag(100),[114] and with bromide on Cu(110),[115] Cu(111),[116] and Cu(100).[117] It has been shown that all three halides stabilize water via solvation-like interactions as seen in the shift of the water desorption peak to higher temperatures. The fraction of stabilized water reached its maximum at a halide atom coverage of around 0.25 ML and then decreased to almost zero for a saturation coverage of halide. LEED patterns of the coadsorbed halide/water layers showed long-range order, with a specific structure for each halide. The change in the LEED pattern of the preadsorbed halide as water adsorbed suggested that water induced a site shift of the halide atoms. The orientation of the water molecules coadsorbed with halides is not clear: some studies suggest a flat orientation, while others suggest the existence of O−H bonds pointing up toward the vacuum. Nakamura et al.[87] studied water coadsorbed with Cl on Pt(111) using IRAS and STM. At 20 K and at low coverage of Cl (0.05 ML) and water (<0.07 ML), the IRAS spectrum was found to be similar to that of pure water tetramers and hexamers. The authors were able to image water−chlorine clusters by STM. The clusters showed six water molecules surrounding a Cl atom located at the center of the water hexagon, sitting on a top position above a Pt-atom, as shown in Figure 16. After the surface was annealed to 160 K, a new sharp vibrational peak appeared at 3440 cm^{-1}, which is not found in the spectrum of water adsorbed on clean Pt(111). This peak was assigned to weak interactions between water and Cl. A (3 × 3)-Cl structure was created by first introducing HCl at 80 K followed by annealing to dissociate the HCl molecules. When water was adsorbed on this (3 × 3)-Cl, a new (4 × 2) structure was found that was assigned to Cl^- and H_3O^+ (Figure 16 bottom).

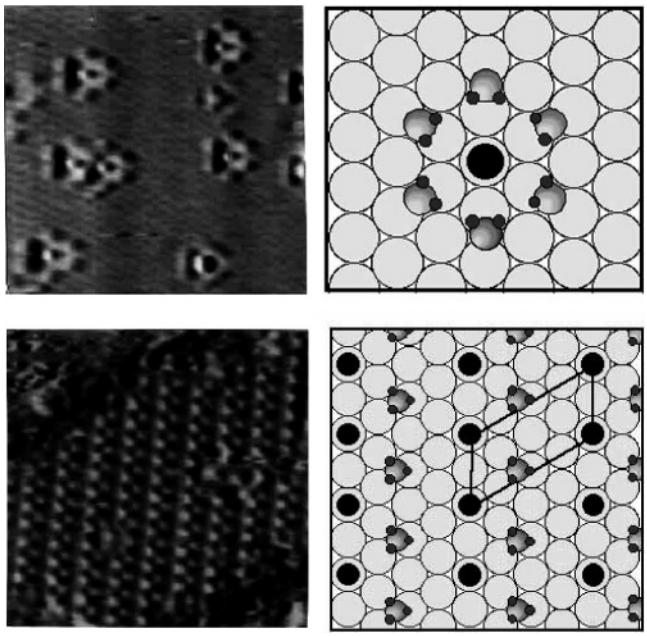

Figure 16. Top: water adsorbed on a HCl predosed Pt(111) surface for a Cl^- coverage of 0.05 ML. Left: 13 × 13 nm STM image. The white spot in the center of the hexagon is a chloride anion on a top site. The chloride ions are surrounded by six water molecules ranging in distance to the Cl atom from 4.3 to 4.5 Å. Right: schematic model. Bottom: water adsorbed on a HCl predosed Pt(111) surface for a Cl^- coverage of 0.44 ML. Left: 8.5 × 8.5 nm STM image. Bright and darker spots are attributed to Cl^- on top Pt sites and to H_3O^+ on 3-fold hollow sites, respectively. Right: possible model for the observed (4 × 2) structure. (Each part of Figure 16 is reprinted with permission from ref 87. Copyright 2000 Elsevier.)

2.2. Nonmetallic Surfaces

As shown in previous reviews,[2,118,119] the interaction of water with metal oxides has received considerable attention over the last few years. Most of the work has been focused on the ability of these surfaces to induce water dissociation and much less on the structure of the water layers itself. The reader is directed to the reviews mentioned previously for an overview of the large number of published works. SPM techniques have been used to detect water dissociation products, namely, on TiO_2 surfaces.[120−123] Another nonmetallic substrate that has also received considerable attention is silicon.[124−126] Most of the studies on silicon have focused on water dissociation at room temperature. In the following subsections, we will review studies where not only water dissociation but also the structure of the adsorbed water film was studied, focusing mainly on studies published after the Henderson review.

2.2.1. Metal Oxides

Tzvetkov et al.[127] have studied water adsorption at 100 K on thin Al_2O_3 films grown on NiAl(110) by TPD, work function measurements, UPS, and XPS. They observed water monomers during the initial adsorption stage. The authors proposed that oxygen lone pair orbitals interact weakly via polarization forces with the Al^{3+} cations located below the oxygen layer that terminates the surface. At higher water exposures, clustering of water occurred followed by growth of 3-D ice films. No indication of H_2O dissociation was observed.

Leist et al.[128] studied the adsorption of deuterated water on FeO(111) and Fe_3O_4(111) using IRAS and TPD in the temperature range from 110 to 320 K. They found that the initial adsorption of water as well as the subsequent growth of thick water layers and their crystallization depends on the termination of the iron oxide surfaces, which can be either oxygen (FeO(111)) or iron (Fe_3O_4(111)). Initial adsorption on epitaxial Fe_3O_4(111) was found to be dissociative, as deduced from the presence of two peaks in the TDP spectrum, which corresponded to dissociated and molecular water. The authors suggested that water adsorption produces initially monomers, followed by the formation of dimers, which then act as nucleation centers for the growth of 3-D

ice. The hydrogen-bonding structure that was observed in the infrared spectra indicated the formation of ice after an exposure to water vapor of 3 L. For exposures larger than 7 L, the surface is covered completely with a 3-D layer of water. The recrystalization of amorphous to crystalline ice was observed between 130 and 173 K. On the oxygen terminated FeO(111) surface, the interaction with the substrate was found to be weak. Hydrogen bonding is observed in the infrared spectrum at exposures as small as 0.2 L. With increasing coverage, characteristic amorphous 3-D ice spectra were observed. The formation of 3-D ice clusters at much lower exposures than on $Fe_3O_4(111)$ indicates that FeO(111) surfaces are wetted less by water than $Fe_3O_4(111)$ surfaces. In addition, in contrast to $Fe_3O_4(111)$, no recrystallization was observed on FeO(111) for exposures of up to 10 L. The authors attribute this to the lack of nucleation centers due to the weak water−surface interaction. Water on FeO(111) has also been studied by Daschbach et al.[129] using TDP and IRAS. They found different water growth modes at temperatures below and above 120 K. For 1 ML of D_2O deposited below 120 K, the resulting film showed voids and water clusters in the second layer. For water adsorbed above 120 K, ordered 2-D islands were formed, which completely wet the FeO(111) surface.

2.2.2. MgO(100)

MgO(100) is one of the most intensely studied oxide materials as a substrate for water adsorption. MgO has a rock salt structure and, like the alkali halides, is cleavable along the low energy, nonpolar (100) surface, which exposes equal numbers of Mg and O ions in a square checkerboard arrangement. The MgO(100) surface has the unusual property that water clustering and a wetting layer can coexist. This is due to the comparable strength of water−substrate and water−water interactions. Picaud et al.[130,131] proposed, based on potential energy calculations, that water is bound with its plane nearly parallel to the surface on top of the Mg ions and wets the MgO(100) surface by forming 2-D clusters through H-bonds with other molecules. Heidberg et al.[132] observed a two domain LEED pattern at 150 K for a 1 ML water coverage, corresponding to a $c(4 \times 2)$ and a $c(2 \times 4)$ structure. From IRAS spectra, they found indications of hydrogen bonding between water molecules in the monolayer and a predominately tilted orientation of the water plane with respect to the MgO(100) surface, in contrast to Picaud et al.'s calculations. Heidberg et al. suggested a model for the water monolayer structure on MgO(100) that reconciles theirs and Picaud et al.'s findings. In this model, the water molecule is slightly displaced from the Mg top sites so that the water−water distance in the overlayer is smaller and hydrogen-bonding between water molecules in the monolayer is possible. If the water molecules would indeed be located in the top sites above the Mg atoms, their O−O separation would be 2.98 Å, which is larger than the O−O distance in ice I_h and would be incompatible with hydrogen-bond interactions.

Xu and Goodman[133] studied water on MgO(100) using IRAS, LEED, and metastable impact electron spectroscopy (MIES). Their results are consistent with water adsorbing with the molecular plane parallel to the Mg(100) surface. In contrast to the results of Heidberg et al., they observed a $p(3 \times 2)/p(2 \times 3)$ LEED pattern. However, their observations were made after heating a multilayer-covered surface to 185 K. They concluded that water wets the MgO (100) surface during adsorption of the first 0.5 ML but forms 3-D clusters with increasing coverage beyond 0.5 ML. Ferry et al.[134−136] examined the apparent inconsistency between the LEED patterns by Xu and Goodman and Heidberg et al. using He atom diffraction and LEED. They observed the $c(4 \times 2)$ patterns for adsorption temperatures below 180 K and the $p(3 \times 2)$ for adsorption temperatures between 180 and 210 K, both at coverages above 0.4 ML. They found that below 0.3 ML, no $p(3 \times 2)$ pattern was detected. They also found a displacement of water molecules from the top position on the Mg ions in the MgO(100) surface. A $p(3 \times 2)$ structure was also observed by Demirdjian et al.[137] by neutron scattering at temperatures between 200 and 270 K.

There is a controversy in the literature about the dissociation of water on the MgO(100) surface. Earlier theoretical work predicted that dissociation can occur only on defect sites.[138−141] However, recent theoretical studies seem to agree that a mixed (H_2O + OH) monolayer is more stable than a pure molecular water layer on the ideal defect-free MgO(100) surface.[142−145] This seems to be confirmed by the recent experiments of Kim et al.[146] These authors studied D_2O adsorption on MgO(100) at 95 K using MIES, UPS, and TDP. A very flat film of MgO was deposited on a Mo(100) substrate. For submonolayer coverage, the MIES spectra showed a peak at 5.8 eV that could not be explained by a linear combination of the bare MgO(100) and the D_2O spectra, and the authors assigned this peak to the 1-π orbital of the OD group. The conclusion was that D_2O molecules adsorb both dissociatively and molecularly on the MgO(100) surface, forming a mixed (D_2O + OD) phase at submonolayer coverages and a layer-by-layer growth of D_2O on top of this phase at higher coverages. The authors explained previous results where no evidence for layer-by-layer growth was found by the difficulty to obtain a defect-free surface. On defective MgO(100) surfaces formation of 3D water islands would be more energetically favorable. Yu et al.[147] studied water adsorption on an ordered film of MgO(100) on Mo(100) at 100 K by HREELS and UPS and found results that were consistent with a partially dissociated water layer at low coverage.

Hawkins et al.[148] recently studied D_2O films deposited at 115 K on MgO(100) surfaces by TDP and Fourier transform infrared spectroscopy (FTIR). Their results were consistent with an essentially flat, hydrogen-bonded water network with no significant amounts of dangling OD. However, the presence of ionic species such as OH^- due to water dissociation was not excluded from these results.

2.2.3. NaCl(100)

Another important class of crystallographically well-defined surfaces where water adsorption has been widely studied are the cleavage faces of alkali halides, which like MgO are the nonpolar (100) faces. We will discuss the water interaction with these surfaces at ambient temperatures more extensively in a later section. However, some studies have also been carried out at low temperature. As in the case of MgO(100), these studies have already been discussed in previous reviews,[1,2] and therefore, only a summary will be given here. Water adsorption at 130 K on the (100) cleavage face of NaCl was studied by Heidberg and Häser using IRAS.[149] Their findings suggest that water forms 3-D clusters under these conditions. Other authors found that 2-D layers can be formed on NaCl(100) at temperatures between 140 and 160 K. On the basis of He diffraction experiments at

148 K, Bruch et al.[150] suggested that the 2-D phase has a (1 × 1) structure with the water molecules bound to the Na atoms and tilted in a {110} direction toward a water molecule adsorbed on the next Na site. Fölsch et al.[151] found a LEED pattern consisting of two c(4 × 2) domains at 135−155 K. They proposed that water forms a distorted ice bilayer phase on NaCl(100) at those temperatures. The structure was laterally compressed in one direction and expanded in the other direction when compared to the basal plane of ice I_h. The same LEED pattern was found by Malaske et al.[152] at 140 K. The system has been revisited recently by Toennies et al.[153] using He diffraction before and after a LEED experiment at 140 K. Their results show that initially a (1 × 1) structure is formed, which is transformed to a c(4 × 2) structure after the LEED experiment. After the c(4 × 2) water layer was desorbed from the surface at temperatures above 150 K, a freshly deposited water layer produced again a (1 × 1) structure. This result indicates that the transition from a (1 × 1) to a c(4 × 2) structure was induced by electrons impinging on the surface during the LEED experiment. These results illustrate once again the problem with metastable structures at low temperatures and how they can be strongly influenced by the probes used in the measurement.

2.2.4. Self-Assembled Monolayers (SAM)

Most studies of water adsorption on SAM at low temperatures were performed before 1995 and have been previously reviewed.[2] Dubois and co-workers[154,155] studied water adsorption on -CH_3 and -COOH terminated alkanethiol films on Au(111) at temperatures between 80 and 140 K using IRAS and TPD. They found a transition from an amorphous to a crystalline phase at 120 K for water coverages above one monolayer. When the -COOH termination H-bonded to water, a shift in the C═O stretching mode was observed. They found that below 130 K for coverages of one layer and above, mixed spectra of a perturbed and unperturbed C═O stretching mode were observed. According to the authors, these findings suggest that water does not wet the surface. The authors explained this by the mismatch between the lattice constant in the ice I_h lattice and the distances of the -COOH groups on the surface. Engquist et al.[156−158] studied water adsorption on -CH_3 and -OH terminated alkanetyhiol films on Au(111) and also on a series of mixed solutions of the two terminations. The different mixtures showed a wide wettability range with water contact angles varying from 0 to 112°. Using IRAS, they found that on all surfaces, D_2O formed amorphous layers when deposited below 100 K. The transition temperature from the amorphous to the crystalline phase depended on the termination of the alkanethiol films for a coverage of two to three monolayers. On the -CH_3 terminated surface, the transition started at about 110 K and was completed before desorption began. In contrast, on the -OH terminated films, the phase transition started at about 150 K and did not complete before desorption. IRAS measurements at 140 K showed that on the -CH_3 terminated surface, the ice overlayer was crystalline for thicknesses up to about 50 monolayers. Above that, the spectra changed and showed features associated with amorphous ice. On the -OH terminated films, this effect was found to be limited to coverages below five monolayers. The authors attributed this to the formation of 2-D clusters on the -OH terminated SAM, in contrast with the 3-D cluster structure of water on the -CH_3 terminated SAM.

3. Structure of Water Films at Ambient Conditions

In the previous sections, we reviewed studies of the structure of water in the first layer and in multilayer films grown at cryogenic temperatures. These studies benefited from the application of powerful microscopy and spectroscopy techniques that provided data that can be compared with modern ab initio calculations and dynamic simulations (ab initio, molecular dynamics, Monte Carlo). Since water plays such an essential role in environmental processes, it is very important to investigate thin water layers under environmentally relevant conditions, even if the number of techniques available to accomplish this task is not as extensive as for the traditional UHV surface science studies. There are more fundamental reasons why such studies should be carried out. We have already seen that cryogenic temperatures can easily lead to situations where thermodynamic equilibrium is not reached, so that the results might not be transferable to ambient conditions.

It is the high vapor pressure of water at ambient temperatures (4.6 Torr at 273 K) that makes the investigation of water films under ambient conditions challenging because many powerful surface science techniques require high vacuum conditions. And yet, it is in equilibrium with other phases of water (vapor, liquid, and solid) that the most relevant phenomena that involve water interfaces take place.

Optical techniques are arguably the most versatile for investigations under ambient conditions since photons are much less scattered in the gas phase than electrons or ions. Among them, IR and nonlinear techniques such as SHG and SFG have provided important results. Because their application to the study of thin water films is reviewed in this issue,[159] we will not cover these exciting results except in a few cases.

Among the microscopy tools with nanoscale resolution that can operate under ambient conditions, AFM is one of the most versatile. A large number of publications report AFM studies of the effect of water on surface properties such as adhesion, friction, dissolution, oxidation, and hydroxylation.[2] In many cases, the AFM tip is directly in contact with the surface, which strongly perturbs the liquid film. Because the emphasis of the present review is on the molecular level structure of water films, we will not include oxidation and electrochemical studies that were carried out under water or in aqueous solutions.

Different noncontact AFM methods have been used to study liquid films and droplets. For liquids of low viscosity, it is easy, even when using noncontact methods, to perturb the film. In many AFM methods, the cantilever is set to oscillate with an amplitude that causes the tip to either briefly contact (tapping), or to come very close to the surface.[160−162] While this eliminates the friction and dragging effects that occur in contact mode, the brief interaction between tip and liquid surface can still result in perturbations that need to be considered.[163] Scanning polarization force microscopy (SPFM), developed in 1994, overcomes many of these problems and provides, in addition to surface topography, information on other surface properties, such as local variations in the surface potential and ionic mobility.[164−166] SPFM is based on electrostatic forces between the tip and the surface and can be applied to both conductive and nonconductive substrates. The principle of operation is shown in Figure 17. A bias voltage on the order of a few volts is applied to a conductive tip. Opposite charges at the tip and the surface arising from

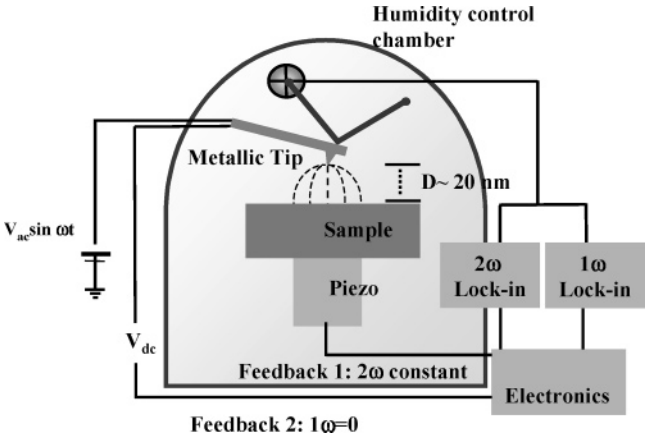

Figure 17. Illustration of the principle of operation of scanning polarization force microscopy (SPFM). A voltage of a few volts is applied to a conductive cantilever and the tip of the atomic force microscope. Induced charges at the tip and surface create attractive electrostatic forces that bend the tip toward the surface. An ac voltage $V = V_{dc} + V_{ac}\sin(\omega t)$ is applied to the metallic tip. Using lock-in amplifiers, the second and first harmonics of the modulation frequency are measured separately in the electrostatic force. To separate the contributions of topography and the contact potential distribution at the surface, two feedback loops are used. The first maintains the constant amplitude of $F(2\omega)$ by adjusting the tip−sample distance. The second adjusts the applied V_{dc} bias so that $F(\omega)$ is zero, as in the Kelvin Probe method.

the polarizability of the materials create attractive electrostatic forces that bend the tip toward the surface. Because electrostatic forces have a long range, they provide a means of imaging at distances of several nanometers. The disadvantage is that the large tip to sample distance results in a lower spatial resolution, on the order of the tip sample distance or the tip radius. On the positive side, the large separation between tip and sample makes it possible to reduce the perturbation of the liquid surface to a negligible value. The vertical resolution of SPFM is not as negatively influenced by the large tip to sample distance and is typically in the angstrom region, comparable to that of other AFM modes. The electrostatic force can be written as follows:

$$F_e(V) = aV^2 + bV + c$$

where a, b, and c are factors that depend on the geometry of the system (tip radius and shape, etc.[167]) and the local dielectric constant at the surface. The first contribution (aV^2) is due to the polarization of the sample and tip (induced charges). The remaining terms contain the interaction between the biased tip and the charges or dipoles that are not induced by the bias voltage on the tip and are located at the surface. If an ac voltage $V = V_{dc} + V_{ac}\sin(\omega t)$ is applied to the tip, the frequency ω can be varied to explore time-dependent phenomena. Using lock-in amplifiers tuned to the second and first harmonic of the modulation signal, respectively, the electrostatic force components $F(2\omega)$ and $F(\omega)$ can be measured separately. $F(2\omega)$ contains information on the polarizability (dielectric constant) and topography. The contact potential contribution to the electrostatic force can be determined from the first harmonic of the lever oscillation (i.e., $F(\omega)$).[168,169]

In the next sections, we concentrate on mica and alkali halide substrates because they have received the most attention due to their easy preparation by cleavage. These surfaces show large, atomically flat terraces and steps and are therefore ideal substrates for fundamental studies of water adsorption.

3.1. Monolayers on Mica

Mica is a layered alumino−silicate mineral commonly found in soils. One of the most common forms is Muscovite mica. The alumino−silicate layers are charged due to excess negative charge on the tetrahedrally coordinated Al^{3+} ions that substitute Si^{4+} in the SiO_2 tetrahedra. Alkali ions are located between the $(Al,Si)O_2$ layers to compensate for this charge. Upon cleavage, these ions become exposed to air. The surface of mica is hydrophilic, and water spreads readily on the freshly prepared surface. Although studies of water adsorption on mica at ambient conditions have been already included in reviews and books published a few years ago,[2,170] and also in the present volume,[171] we review briefly some of them here because they provide unique insights into how experiment and theory combine to provide information about the structure of adsorbed water.

Beaglehole and Christenson used ellipsometry to obtain isotherms of water on mica as a function of relative humidity (RH).[172] They found that a 2 Å thick film is present at a relative humidity of 50%, corresponding roughly to a monolayer. Similar results were obtained by Cantrell and Ewing[173] using IR. Using SPFM at room temperature, Salmeron and co-workers[166,174,175] found that the presence of a water film changes the electrostatic force between tip and surface and modifies the contact potential. A brief contact with the tip induced capillary condensation around the contact point where water accumulated to form a neck. After the tip was retracted, some excess water was left on the surface in the form of molecularly thin islands and droplets that could be imaged by SPFM. These structures are metastable and disappear in a few seconds or minutes, depending on the humidity level, by evaporation. The islands were interpreted as a second layer on the monolayer film. An interesting finding of these studies was that the boundaries of the islands were often polygonal, with angles of 120° as shown in Figure 18.

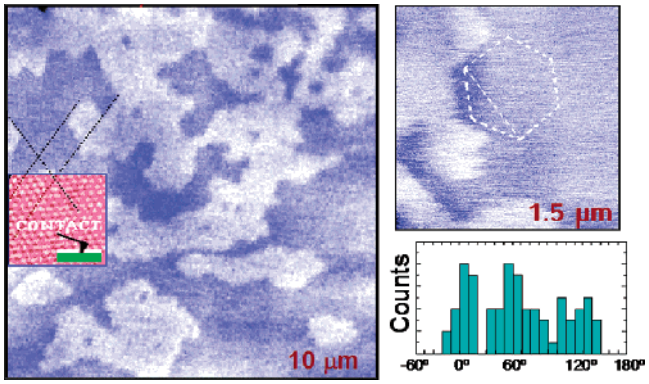

Figure 18. Scanning polarization force microscopy (SPFM) images of structures formed by water on mica. Bright areas correspond to a second water layer, and dark areas are the first water layer. The boundaries tend to have polygonal shapes, as shown in the smaller image where a hexagon is drawn for visual reference. The directions are strongly correlated with the mica lattice. The inset in the large image shows a contact AFM image obtained after the SPFM images, which provides a reference for angle measurements. The histogram shows the angles of the water−film boundaries relative to the mica lattice. (Reproduced by permission of the *MRS Bulletin* (ref 174). Copyright 1997 Materials Research Society. And reprinted with permission from *Science* (http://www.aaas.org), ref 166. Copyright 1995 AAAS.)

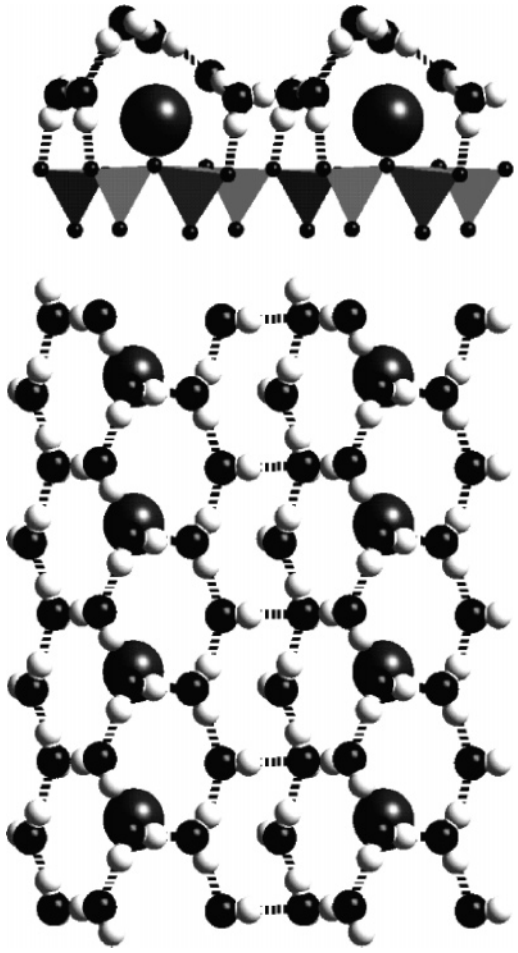

Figure 19. Side and top view of the optimized structure of a water monolayer on mica obtained from molecular dynamics simulations. The water molecules and the first layer of the silica−alumina tetrahedra of the mica substrate are shown. Oxygen atoms are dark, hydrogen atoms are light, and K ions are large dark balls. Notice the ordered ice-like structure and the absence of free OH groups. All H-atoms in the water are involved in a hydrogen bond to another water molecule or to the mica substrate. (Each part of Figure 19 is reprinted with permission from ref 176 (http://link.aps.org/abstract/PRL/v78/p2855). Copyright 1997 by the American Physical Society.)

By comparing SPFM images with contact images of the mica lattice, it was found that the directions of the boundaries are related to the mica crystallographic directions. On the basis of this observation, the authors suggested that the molecularly thin water film has a solid, ice-like structure, in epitaxial relationship with the substrate.

Using MD simulations, Odelius et al.[176] found that at the monolayer coverage, water forms a 2-D H-bonded network in an epitaxial relationship with the mica lattice, as shown in Figure 19, in line with the experimental findings. The simulations predicted also that no free OH bonds stick out from the surface (i.e., each H atom in the film is part of a H-bond with another water molecule or with oxygen atoms of the substrate). These predictions were confirmed by subsequent SFG experiments by Miranda et al.[177] Using D_2O, the authors found that little or no signal was present in the free OD stretch region near 2740 cm^{-1} when the humidity was below 90%. Between 20 and 90% RH, the spectrum was very similar to that of fully H-bonded water. The free OD stretch signal of non-hydrogen-bonded D_2O appears only when the humidity increased above 90%, which was interpreted as due to the growth of water multilayers. The absence of free H-bonds at the surface of the water monolayer on mica implies that there is a net dipole moment with the positive end pointing toward the mica surface. This prediction was confirmed by SPFM experiments by Bluhm et al.[178] where the surface potential of mica was measured as a function of humidity. It was found that the contact potential of the mica substrate decreases by about 400 mV from its value under dry conditions (<10% RH) when the humidity increases to 30%. After this, the potential remains nearly constant up to 80% RH. Above 80% RH, the surface potential increased and became positive, as shown in Figure 20. This is in line with all previous results and models where the first water layer has no free OH pointing out and should therefore have a negative surface potential relative to dry mica. It agrees also with the formation of multilayers at the higher humidity where free OH groups with the H pointing out are present.

3.2. Thin Films on Mica

We have seen that at room temperature, the growth of multilayers produces an increase of surface potential (more positive) as compared to the surface potential of the monolayer, as measured by SPFM. Interestingly, at temperatures below 0 °C, the surface potential changes in the opposite direction (i.e., it becomes more negative above 80% RH, as shown in Figure 20). This suggests that below 0 °C, the water layers on top of the first layer grow with the positive end of the net dipole moment on average oriented toward the mica substrate, implying the growth of a ferroelectric water layer. We have already seen that ferroelectric ordering induced by the substrate was observed on Pt(111) between 120 and 137 K. In that case, the dipole moment pointed up (i.e., opposite of the case of the mica surface). The electrostatic energy accumulated in such dipole-oriented films makes them metastable, and they revert to a dipole-disordered structure as the thickness increases beyond a few layers.

The growth of ice films on mica was studied by Bluhm et al.[179,180] using contact-mode AFM and SPFM. The authors observed the formation of nanometer thin ice films in coexistence with a liquid phase at temperatures below −30 °C. The noncontact (SPFM) images revealed the presence of supercooled water in the form of droplets on top of thin (two to three monolayers) ice islands that could be imaged in contact mode. This Stranski−Krastanov type growth mode might be due to structure of the first ice layer, which is different from that of bulk ice (see Figure 19) and to the difficulty in accommodating the mismatch of about 10% between the mica substrate lattice and that of ice. In subsequent layers, the ice structure reverts to that of the bulk and forms 3-D clusters. Annealing the ice films to −17 °C led to coalescence of the ice islands into a percolating ice film covered by a liquid layer. The coexistence of a liquid film on the thin ice islands is akin to the premelting phenomenon that is observed for bulk ice surfaces at temperatures close to the melting point.[181] For bulk ice, the existence of a liquidlike layer at the surface can be explained by the theoretical model of Fletcher,[182,183] based on the existence of a positive charge on the ice surface due to the orientational ordering of the water dipole moments at the surface that minimizes the total energy of the ice surface. This charge is then compensated by a mesoscopic screening layer in the subsurface region, which contains a high

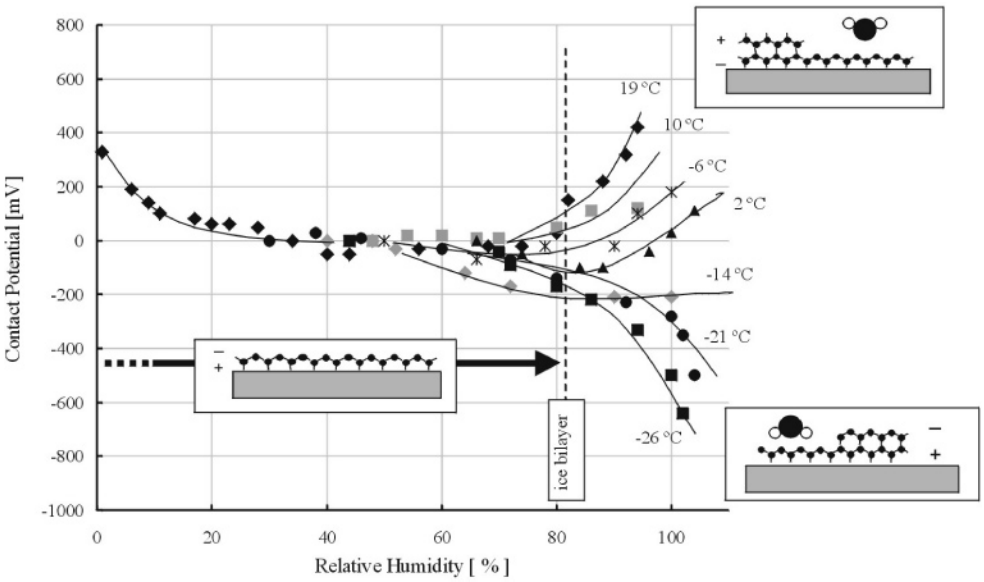

Figure 20. Changes in the contact potential of a mica surface relative to a hydrophobic tip vs relative humidity (RH) and for different temperatures. At room temperature, the potential first decreases by about 400 mV. This change can be explained by the orientation of water in the first monolayer, which has an average dipole moment pointing toward the surface. At ~20−30% RH, it reaches a plateau and remains approximately constant until about 80% RH. At higher humidity, the potential increases again. The observation is explained by a change in orientation of water in the second layer, where H from dangling H-bonds points upward to the vapor phase. Below 0 °C, the change in potential above 80% RH is reversed and becomes negative. This suggests that in that case, the dipole-down orientation of water in the first layer continues in subsequent layers. (Reprinted with permission from ref 178. Copyright 2000 Elsevier Science.)

concentration of Bjerrum[184] defects. This mesoscopic screening layer is therefore structurally weaker than a perfectly ordered ice lattice and will have a lower melting point than bulk ice. Fletcher's model, which is supported by synchrotron-based X-ray diffraction measurements,[185] can be applied to the nanometer thin ice layers, where the net charge is located at the surface of the ice islands due to the dipole ordering in the first bilayers.

Cantrell and Ewing have also studied water films on mica using infrared spectroscopy.[173] They found that water exhibits an infrared spectrum consistent with a bonding network that is more structured and rigid than that of bulk water. The measured changes in enthalpy upon adsorption indicate a strongly bonded first layer. Subsequent layers are less strongly bound with enthalpy values approaching the value for the condensation on bulk water. They also measured differences in entropy between bulk water and adsorbed layer. They found the entropy to be lowest for submonolayer coverage, indicative of a more ordered arrangement of water molecules. When the thickness of the film increased, the entropy difference between bulk water and the film tended toward zero. Wetting is characterized by a coverage that diverges as the RH approaches 100%. In contrast, partial wetting shows isotherms that tend toward a finite water coverage at a relative humidity of 100%. Cantrell and Ewing measured a maximum coverage of only 5 ML close to saturation (95% RH), indicative of an incomplete wetting of the surface.

Although intermittent contact AFM modes are likely to perturb the liquid film, some studies exist where the authors claim to have minimized the perturbation.[186,187] The validity of such intermittent contact modes is predicated on minimization of the contact time, which in tapping mode can be on the order of microseconds per tap. The assumption is that the perturbation of the tip can be negligible because the contact time is small as compared to the relaxation time of capillarity waves. For example, Spagnoli et al.[188] observed structured water layers on mica similar to those observed by Salmeron and co-workers. By changing the force applied to the tip, they could differentiate between a nonstructured water layer, when a low tapping force was used, and an ice-like layer when higher forces were used. They found evidence of a continuous ice-like layer of structured water at ambient temperature and humidity, with a thickness that may correspond to multiple layers under some conditions.

More recent Monte Carlo simulations of the water monolayer on mica by Park and Sposito,[189] based on X-ray reflectivity experiments,[190] proposed a different monolayer structure than the one calculated by Odelius et al.[176] The authors found that water is bound intimately to the hexagonal cavities of the mica surface, followed by a layer of molecules immobilized by hydrogen bonds to the first one and with the potassium ions located between both layers. While the model is still in line with the existence of a strongly bound and highly oriented first layer, no strong orientation is induced to layers above the second layer. It is clear that more experimental and theoretical studies are needed to settle this important point.

3.3. Alkali Halides

The adsorption of water on alkali halides is reviewed in another paper of this issue. We will therefore focus here only on research carried out using SPFM. These studies have examined the role of water in modifying the polarizability and contact potential of the (001) cleavage faces of alkali halides (NaCl, KCl, KBr, KI) as a function of water vapor pressure. They found that there is a characteristic relative humidity value (CRH) that separates two water adsorption regimes.[191,192] Below CRH, the adsorption of water affects primarily the steps, causing preferential solvation of anions or cations, which remain localized in the vicinity of the steps. Humidities larger than CRH produce large scale modifications of the step morphology (see Figure 21). Adsorption

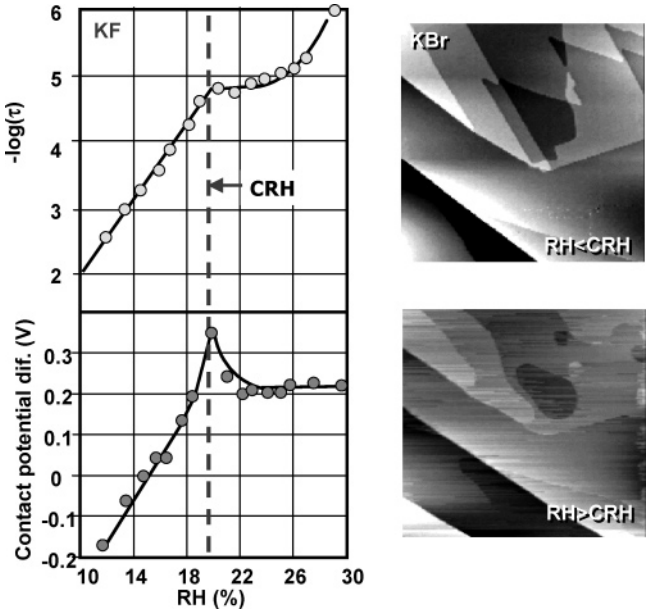

Figure 21. Top left: semilog plot of the time constant τ for solvated ion motion on a potassium fluoride cleaved surface exposed to increased relative humidity (RH). Bottom: simultaneously measured contact potential. This behavior is similar to that found in other alkali halide surfaces. At a critical humidity characteristic of each alkali halide crystal (CHR), there is a break or a change in the slope of these two surface properties. Right side: contact AFM images of KBr at low humidity (top) and high humidity (bottom) relative to the CHR. (Adapted with permission from ref 192. Copyright 1998 American Chemical Society.)

isotherms on NaCl (100) calculated from infrared spectra[193,194] indicate that the first regime (below the CRH) corresponds to a water coverage between zero and one monolayer.

Although many contact and tapping mode AFM experiments have been performed to study the surface modifications and step movements occurring above CRH,[2,195−197] few studies have been performed to study the initial stages of water adsorption (i.e., below CRH). Measurements using SPFM have shown[198−200] that even below the CRH, there is an increase in the electrostatic polarization force near steps as shown in Figure 22. Verdaguer et al.[200] have shown recently that the increase of polarization is related to the mobility of solvated ions. This mobility can be measured by the frequency dependence of the electrostatic force between the tip and the surface, which is in the range of kHz. Luna et al.[192] performed experiments to study the changes in contact potential and response time of the solvated ions as a function of relative humidity. They found a substantial change in the rate of increase of ionic mobility and surface potential when the humidity was increased above CRH (Figure 21). Below the CRH, the contact potential was found to be different on the steps as compared to the terraces. This was explained by the formation of dipoles at the steps resulting from the preferential solvation of one type of ion. As the RH increases, the contact potential difference between steps and terraces decreases and disappeares completely at the CRH, as shown in Figure 22. Goshal et al.[201] have shown that when alkali halide surfaces are exposed to humidities above the CRH, irreversible changes in the ionic distribution take place, so that when the surface is dried, the original distribution is not recovered.

A number of theoretical studies has been performed to investigate the adsorption of water on NaCl(100). DFT[202] and ab initio MD[203] calculations show that for a coverage of one monolayer, water adsorption is favored on top of the Na ions. The most favorable configuration is one with the molecular plane parallel to the surface. Monte Carlo[204] and MD[205] simulations of water on NaCl (100) also show that water molecules bind to the Na ions through the oxygen lone pair, with the molecular plane parallel to the surface or slightly tilted upward. Binding is particularly strong at monatomic step edges.[197] It was also found that below one monolayer coverage, 3-D water clusters can form.[204]

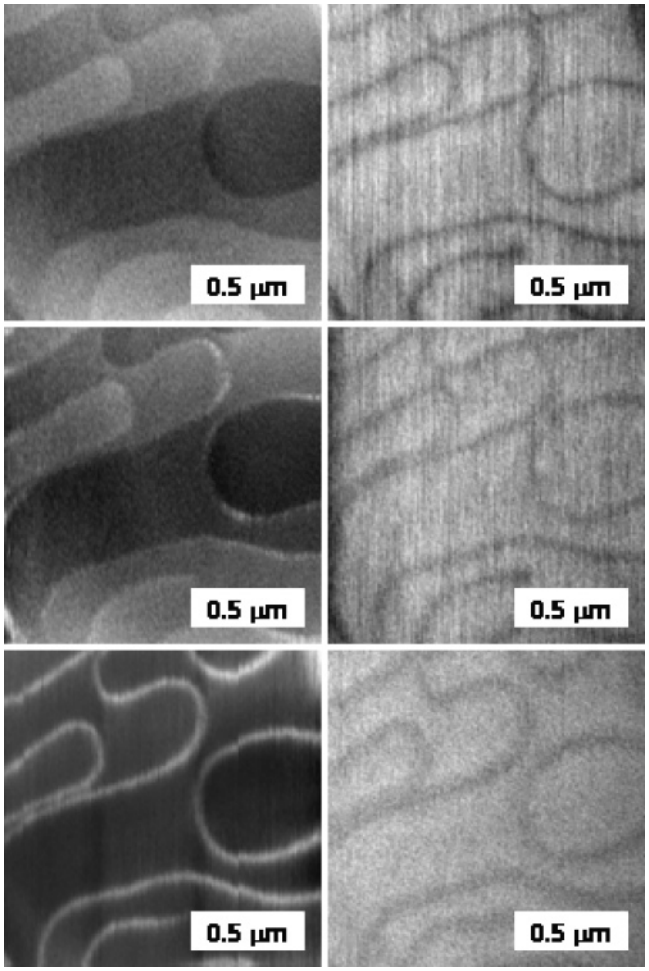

Figure 22. SPFM topographic (left) and contact potential (right) images acquired at different relative humidity (RH) values. The images at the top correspond to RH = 25%. The middle images, at 30% RH, show a moderate enhancement of the step contrast. At 35% RH (bottom images), the step enhancement is large (several nanometers). At the same time, the contrast of the steps in the contact potential images relative to the terraces decreases with humidity. Gray scales are 10 nm for the topographic images and 50 mV for the contact potential images. The enhancement is due to solvated ions, in this case predominantly Cl^-. (Reprinted with permission from ref 200. Copyright 2005 American Institute of Physics.)

On the basis of all these results, we propose the following model for water adsorption on alkali halide surfaces. Below the CRH, water adsorbs preferentially at the step edges, where it solvates ions. Anions appear to solvate preferentially in the case of NaCl[200] and probably other salts although, as mentioned previously, the type of ion that solvates first can depend on the history of water exposure and impurities in the crystal. The solvated anions give rise to a negative potential relative to the surface and are mobile along the steps. The increased ionic mobility gives rise to a stronger

electrostatic force that produces the contrast enhancement observed in the SPFM topographic images (Figure 22). At the CRH and higher humidity, both cations and anions solvate at similar rates. This removes the imbalance in the sign of mobile charges at the steps. This triggers large scale motion of the steps and eliminates the contact potential difference between steps and terraces that is present at low humidity.

3.4. Other Substrates

Water interaction with surfaces at ambient conditions has been studied for many years on a variety of surfaces using different techniques. An example of combined use of different techniques can be found in a recent work of Summer et al.[206] In this work, contact angle, IR, AFM, and XPS measurements were combined to study water uptake on different hydrophilic and hydrophobic surfaces such as glass, Teflon, SAMs, and quartz. As a general trend, suggested also from other studies, up to 60% relative humidity, even for very hydrophilic surfaces, less than five monolayers of water are present on the surface.

SAMs have been used as a model to study water adsorption on hydrophobic surfaces. Rudich et al.[207] used SAMs of methyl terminated silanes on SiO_2 to study the effect of surface corrugation on water adsorption. Using samples with different corrugation values, they measured water adsorption using a quartz crystal microbalance and a field effect transistor-like device. They found that the more corrugated surfaces adsorb also more water. From the experimental results and from molecular dynamics simulations, they suggest that water adsorbs as small droplets mainly on imperfections or structural defects on the organic layer.

The interaction of water with many other oxide surfaces has been also studied in connection with environmental chemical processes.[119] IR spectroscopy has been used extensively to obtain adsorption isotherms at ambient conditions on SiO_2, TiO_2, MgO, CaO, α-Al_2O_3, and γ-F_2O_3,[208] on single crystals of α-Al_2O_3(0001)[209] and MgO(100),[210,211] and on amorphous SiO_2 surfaces.[212] As noted in section 2.2, one important issue is the extent of hydroxylation of the surfaces due to water dissociation.[2,119] The formation of an OH rich surface can induce a highly oriented growth of the adsorbed water layers through H-bonds with surface OH groups and with other water molecules. This has been suggested from IR measurements for coverages up to three to four monolayers on amorphous SiO_2[212] and α-Al_2O_3-(0001).[209] The existence of an ordered water monolayer on hydroxylated α-Al_2O_3(0001) at RH > 40% has been recently suggested from crystal rod truncation diffraction experiments using synchrotron X-rays.[213] In contrast, other studies on MgO(100)[210,211] found liquid-like water growth at all coverages. Although the disordered nature of this film seems to be related to surface defects and to the presence of OH groups at the oxide surface, more work is needed to clarify this system.

There has been a particular interest in the study of water adsorption on surfaces that have crystal structures commensurate with one of the faces of I_h ice because it is thought that those surfaces can readily induce ice nucleation. This idea is behind one of the oldest attempts of mankind to influence weather and to produce substances that, when released in the atmosphere, would trigger condensation of water from clouds (rain seeding). One surface with a close commensurability to the basal plane of ice is the (111) face of BaF_2. Miura et al.[214−216] used noncontact AFM techniques to image water islands on NaF(100), LiF(100), CaF_2(111), and BaF_2 (111). They observed that at 30% RH, structures on the cleaved surfaces grew by island nucleation. They also found that the islands have different heights on each surface, depending on the dielectric properties of the substrate. The apparent height differences were due to experimental artifacts in the noncontact tapping measurements. After correction for these artifacts, a common island height of about 5 Å was found for all substrates, which is indicative of the adsorption of two layers of water. From measurements of the time-dependent evolution of the water film growth, the authors concluded that growth proceeds via island coalescence. For BaF_2(111), they found that at 70% RH, small islands with a height of about 1 nm and diameters of about 20 nm were initially formed, which then coalesced until a uniform water layer was created. In a macroscopic picture, the low aspect ratio of the initial islands would correspond to a small contact angle. The authors suggested that such a small contact angle indicates that droplets grow on top of a film of the same liquid. Below 50% RH, droplets were not observed, suggesting the presence of only a monolayer or submonolayer of water.

Sadtchenko et al.[217,218] studied the adsorption of water and ice films on BaF_2(111) using infrared spectroscopy. The spectra showed a diffuse doublet similar to that theoretically predicted for the surface bilayer of I_h ice, suggesting an ice-like hydrogen-bonded network even at room temperature. At multilayer coverage, the spectra became similar to that of bulk liquid water. Values for the enthalpy and entropy of water adsorption were derived from the adsorption isotherms. The enthalpy of formation of the monolayer was found to be greater than that of condensation to either the liquid or the solid phases. The absolute entropy of the monolayer revealed a high degree of order, with a value near that of ice at room temperature. Both enthalpy and entropy approached values for bulk liquid water at multilayer coverage. According to the authors, the results are consistent with an ice-like hexagonal water layer at temperatures above the ice melting point, if the thickness of the layer does not exceed the monolayer. They found that the formation of thicker ice films was unstable even at −65 °C. After a few minutes, these thicker ice films spontaneously reassembled into an array of crystallites. We have seen previously that similar unstable films form on mica below 0 °C.

Monte Carlo simulations[219] of water adsorption on BaF_2-(111) indicate that no ice-like bilayer forms for a coverage of one or more layers. The authors found that monomers adsorb preferentially with the hydrogen atoms pointing toward the surface. The energy penalty required to change this configuration to one more favorable for accommodating additional molecules and forming hexagonal I_h bilayers is less than the energy gained in the formation of the increased hydrogen-bonding of I_h ice. The authors observed instead cross-linked chains as the most favorable structures. Although the calculations were done at 0 K, the authors claim that the results indicate that stable ice films will not form on BaF_2-(111). It appears then that to be an effective ice nucleating substrate, it is not enough to have a lattice constant close to that of ice but that the orientation of the adsorbed water molecules must also be close to that in the tetrahedral ice structure.[220] Recent infrared studies of ice on BaF_2(111) indicate that surface defects (pitting of the crystal) dramati-

cally improve ice formation on the surface, probably by allowing the adsorption of molecules in less restricted configurations.[221]

Gil et al.[222,223] and Luna et al.[224] used noncontact AFM techniques to image thin water films on mica, on Au(111) and on graphite. On mica, they observed water islands with two different apparent heights of 0.7 and 4 nm at 90%RH. They also observed the formation of water films on gold for RH above 30%, whereas on graphite, a RH of 90% was necessary. On gold, islands of 0.2 nm height were observed to grow from the steps at 35% RH, and a full coverage was observed at 65% RH. On graphite, two different heights for the water islands were observed with 2 and 5 nm. These observations are surprising in view of the high hydrophobicity of graphite. Both on gold and on graphite they observed water structures aligned with the crystallographic directions of the substrate. Clearly, these systems should be reexamined with other techniques to confirm and to understand the nature and structure of the condensed films.

4. Water/Vapor Interface

Until now, we have considered water in the form of thin films and the effects of the substrate on the structure of the film. The first layer can be strongly influenced by the substrate, and this influence can propagate into the subsequently adsorbed multilayers, until the water film reverts to its bulk structure. The top layer of water at the interface with the gas environment is also special. The missing bonds with other layers of water modify the structure of this layer and of those underneath with diminishing strength, as is commonly seen in surface science studies. For solid surfaces, this is manifested by reconstructions and relaxations to minimize the energy of the system, where the surface atomic positions differ from those of the extrapolated bulk termination. In the case of water, we have shown previously an example of enhanced vibrational amplitudes detected by LEED that affect the terminating layer of water molecules on ice films (>3 nm thickness) on Pt(111) at 140 K. Orientational disorder of the dangling OH bonds near 200 K was observed by SFG by Wei et al.[225,226] and is discussed in a different paper in this issue.[159] Another manifestation of surface restructuring is the premelting phenomena, where a disordered, liquidlike film is formed at the surface with a thickness that increases when the temperature approaches the melting point.[181] The presence of a liquidlike layer at a surface close to the melting point of a material is not a special feature of ice surfaces but has been shown to be a rather general phenomenon.[227] The driving force for surface melting of ice might be, however, unique in that it is electrostatic in nature, as described in the previous chapter, while for most other materials, increased atomic vibrations at the surface are thought to be the reason for premelting at the solid−vapor interface. The measurement of the thickness of the liquidlike layer at the ice surface has yielded a great variety of results (for a compilation of the results before 1993, see Elbaum et al.[228]), where the thickness at a given temperature varied by a factor of up to 100 depending on the experimental technique.[228] The sensitivity of the different techniques that were used to measure surface melting (e.g., NMR,[229] surface conductivity,[230] X-ray diffraction,[185,231] ellipsometry,[232] and proton channeling[233]) to different properties of the liquidlike layer likely accounts for part of the discrepancy of the results. Another reason might be the presence of small amounts of contamination on the surface. This effect was calculated for the case of NaCl doped ice samples by Wettlaufer,[234] where small amounts of impurities were found to have a strong effect on premelting. It is therefore necessary to measure simultaneously the thickness of the liquidlike layer and the amount of contaminants at the surface. This has been recently accomplished in combined ambient pressure XPS and NEXAFS experiments,[53] where at least part of the extent of premelting was found to correlate with the concentration of hydrocarbon contamination at the surface.

5. Confined Water

Water confined in narrow pores or cavities can give rise to large capillary forces that are visible on the mesoscopic scale (>micrometers). These forces are important in micro-electro-mechanical systems, magnetic hard drives, nanolithography, and tribology. At the nanometer scale, the presence of solid walls can have a profound effect because the modifications of the molecular structure of water near each wall can overlap. In STM, water influences electron transport through the gap and is thought to be responsible for the conductivity of otherwise poorly conducting biomolecules such as DNA on insulating substrates.[235,236]

Interesting effects take place when two solid surfaces confining a liquid approach each other such that the separation is comparable to the decay length of the molecular layering imposed by the rigid walls. How far this layering extends is one of the important questions in interface science, with a large impact in areas such as biology and colloidal chemistry. The layers of more or less ordered water can be thought of as solvation shells,[237] causing oscillatory forces (solvation forces) on the approaching surfaces. Oscillatory solvation forces can be measured directly using the surface forces apparatus (SFA) and the AFM. In the SFA, the confining walls are atomically smooth and parallel over a lateral extension of several tens of micrometers. Their separation can be controlled with subnanometer precision, at the same time that the confinement pressure, in the megapascal range, can be measured. The walls are usually mica sheets shaped into cylindrical lenses and arranged with their axis rotated by 90°. Studies using SFA focus on force and distance measurements as well as on viscosity, which is accomplished by lateral displacement of the mica surfaces. The use of AFM to study confined liquids and water in particular is more recent. It has the advantage of high lateral resolution, which makes it possible, in principle, to conduct the study of many other surfaces that can only be prepared atomically flat over small regions of the surface. Unfortunately, the long time needed to stabilize the tip at a given distance makes the measurements difficult due to the lateral displacements of the tip caused by thermal drift.

5.1. Water Confined between Flat Mica Surfaces

The viscosity of water in confined geometries has been an interesting topic to which several publications have been devoted in the last few years. It is well-established that the viscosity of aqueous electrolytes confined to films with thicknesses greater than 2−3 nm remains close to that in the bulk.[238] The question of what happens when the liquid is confined to gaps narrower than a few nanometers is less understood and remains controversial. Granick et al.[239,240] found that when the thickness of water films between mica surfaces is on the order of one or two molecular layers, the

effective viscosity of the film is orders of magnitude higher than in the bulk liquid for certain relative orientations of the confining walls. The authors interpreted the observed periodic oscillations with a twist angle of the walls as indicative of the existence of spatial correlations of the water structure induced by the substrate. In contrast with these results, Raviv et al.[241,242] found that the effective viscosity of water remains within a factor of at most three from its bulk value when confined to a thickness in the range of 3.5 ± 1 to 0.0 ± 0.4 nm. They interpreted this result as due to the suppression of the highly directional hydrogen-bonded network associated with freezing.[243] Recent molecular dynamics simulations seem to agree with this interpretation,[244] associating the persistent fluidity with rotational dynamics of water molecules, accompanied by fast translational diffusion under this confinement. On the other hand, a significant slow-down of the dynamics of the system as the confining separation was reduced has been found by Jeffrey et al.[245] Using AFM, they found that the dynamics of the system is determined not only by the interfacial pressure but more significantly by solvation effects that depend on the exact separation between the tip and the mica surface.

Although as we have seen, mica can impose a highly structured, nearly epitaxial structure to the water film,[166,177,178] this structure refers to water interacting with only one mica surface. Proximity and misorientation of two nearby mica surfaces confining the water film can give rise to a different structure. Unfortunately, no direct observations have been performed on the molecular structure of confined water films.

To close this section, it is worth commenting on the difficulty of controlling the structure and cleanliness of the surfaces used to confine the liquid films. Even carefully prepared surfaces can have very a small fraction of their surface contaminated with foreign species, or even worse, can contain nanometer size particles as shown by Becker and Mugele.[246] A method of preparation where the mica surfaces are recleaved after mounting in the lenses of the SFA has proven effective in producing surfaces with higher adhesion (i.e., cleaner).[247] Because recleaved surfaces are prepared in situ just before the experiments, they are likely to provide better substrates to revisit some of these important questions. Experiments with AFM where the contact area is of a nanometer dimension can in principle be done on cleaner surfaces because it is always possible to image the surface and select the flatter, cleaner spots. The recent observation of liquid layering effects with AFM is exciting and promising in that regard. We devote the following section to examine results obtained using this local probe technique.

5.2. Studies of the Layering Structure of Water Using AFM

O'Shea et al.[248] observed solvation shells during the approach of an AFM tip to a graphite surface in different liquids. They were able to measure oscillatory force curves with a mean periodicity approximately equal to the dimension of the molecules for dodecanol and octamethylcyclotetrasiloxane (OMCTS). However, in the case of water, the tip was observed to jump into the surface at a nominal distance of 6 nm because of strong attractive forces due to the hydrophobic interaction with the surface, which energetically favors the expulsion of water from the gap between tip and surface (cavitation). Hoh et al.[249] used a similar method to study force curves between a silicon nitride tip and a glass surface (hydrophilic). They measured discrete small adhesive interactions as the tip approached the sample at pH 8. Two different mechanisms were proposed to explain the discrete changes in the force curve. The authors suggested that they could be due to hydrogen bonds forming and breaking between the tip and the surface or because ordered water layers create different force minima near the surface.

Cleveland et al.[250] studied the thermal noise of an AFM tip at different distances from calcite and barite surfaces in water. They observed hopping of the tip between four discrete levels with an average spacing of 0.2 nm for a 20 ms experiment as shown in Figure 23. The thermal noise in each state contains information about the local curvature of the potential well of the tip. An interaction potential can then be extracted from this measurement for each discrete state using the Boltzmann factor. Several minima in the potential with spacings varying between 0.15 and 0.3 nm were observed, a distance that is similar to the size of a water molecule. However, the exact meaning of the spacings was difficult to interpret since it depends on the path followed by the tip. In addition, possible ionic solvation from the crystal surface can also be involved in the layering of water molecules near the crystal surface.

In AFM, detection of the force gradient between tip and sample is generally more sensitive than a measurement of the normal force.[251] The force gradient can be measured by modulating the tip−sample separation. Measuring the frequency dependence of the amplitude and phase of the force gradient provides a way to measure both the stiffness and the damping at the tip−sample junction. The required amplitudes are small, on the order of the distances being measured, which poses difficulties for small molecules such as water. Interesting results have been obtained in liquids of large molecules such as OMCTS and some alcohols.[252] O'Shea et al.[253] used this method to study water layering on mica but could not observe oscillatory forces. However, they found a shift of the resonance peak to higher frequencies as the tip approached the sample, indicative of increased stiffness. This was interpreted as a result of tip−sample mechanical contact, or due to repulsive hydration forces, since both sample and tip are hydrophilic. They also found an increase in damping as the tip approached the surface, which makes it difficult to obtain good measurements when the tip is very close to the surface.

Jarvis et al.[254] used a similar technique to measure water solvation shells on a hydrophilic self-assembled monolayer of $(COOH(CH_2)_2)_{10}$-SH on atomically flat Au(111). To avoid hydrodynamic damping, they used carbon nanotubes attached to an AFM tip as a probe. The measurements were performed by approaching the sample to the tip while recording changes in the voltage applied to the modulation of the tip to keep its oscillation amplitude constant. This is a direct measurement of the dissipation. The approach curves were found to be oscillatory, with a period corresponding approximately to the diameter of the water molecule and with a dissipation that increased as the separation decreased. The authors attributed the oscillations to layering of the water. Higher dissipation was found to occur when the tip was closer to the sample, indicating a stiffer arrangement of the water molecules. One important finding was that nanoscale forces in this experiment appeared to scale with the surface dimension to macroscopic measurements using SFA.

Jeffery et al.[255] measured the stiffness and damping of confined aqueous solutions of 0.01 M KCl between a silicon tip and mica. Stiffness and damping oscillations were

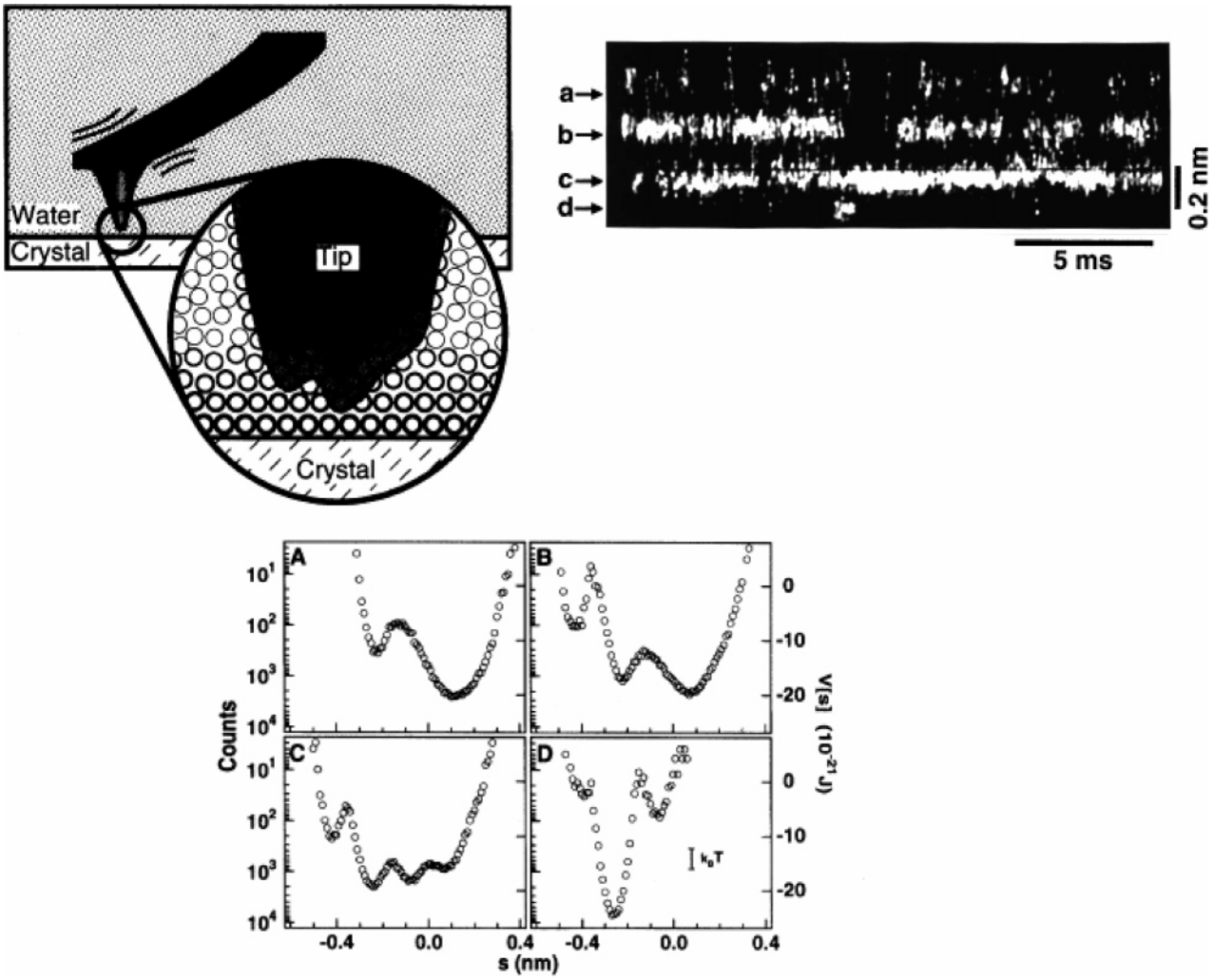

Figure 23. Top left: schematic representation showing an AFM tip penetrating through layers of water near a surface. Top right: photograph of the oscilloscope trace showing the cantilever deflection as a function of time. Position a is the farthest from the surface while position d is closest. The tip hopped between four distinct states visiting a− d in the course of the measurement. Bottom: inverted histograms of the data shown in the oscilloscope photographs. The local curvature of the potential well is extracted from the noise measurement for each state. (Each part of Figure 23 is reprinted with permission from ref 250 (http://link.aps.org/abstract/PRB/v52/pR8692). Copyright 1995 by the American Physical Society.)

observed for up to seven molecular layers, separated by 2.5 ± 0.5 Å each. They also calculated relaxation times and found a significant slow-down of the dynamics of the system as the tip−sample separation was reduced. By assuming that the relaxation time depends linearly on the film stiffness, they reproduced all the important features of the experiments. One finding of these experiments was that the relaxation time increased gradually with pressure and that the increase was larger when the tip−surface spacing was an integral multiple of the size of the molecules.

Uchihashi et al.[256] recently compared water layering on a COOH terminated self-assembled monolayer and OMCTS on HOPG. They used a method proposed by Sader and Jarvis[257] to convert the frequency shift into quantitative force values. An oscillation of the phase shift was observed when the tip was closer than 2 nm of the sample. Six oscillations were observed corresponding to six water layers, as shown in Figure 24. Histograms of the spacing between layers showed an average spacing of 0.23 ± 0.3 nm. This layer spacing decreased in the vicinity of the surface, suggesting a strong attractive interaction between the water molecules nearest to the surface and the carboxyl end groups of the SAM, due to hydrogen bonding with the water molecules.

Other instruments have been developed to study water layering between surfaces. Transverse dynamic force microscopy (TDFM) has been used by Antognozzi et al.[258] to study water layering on mica. A tapered optical fiber was mounted perpendicularly to the sample surface and oscillated horizontally. The oscillation amplitude and phase were then measured using an optical detection system. The authors found that the oscillation amplitude and phase-lag exhibited a steplike behavior at different tip−sample separations. The measured periodicity ranged from 2.4 to 2.9 Å. The authors calculated values of the shear viscosity and ridigity in the water film. An increasing value for both properties was found as the confinement of the water between the tip and the sample increased.

Very recently, Choi et al.[259] used STM to study water confined between the tip and a gold surface in an electrochemical cell. By measuring the difference between the tip advance (driven by piezo actuator) and the actual gap distance between the gold surface and the tip, they observed a mechanical resistance at a gap distance of about 7 Å when a voltage of −100 mV was applied. No such resistance was observed at lower voltages. According to the authors, this suggests a solid behavior of the interfacial water at this

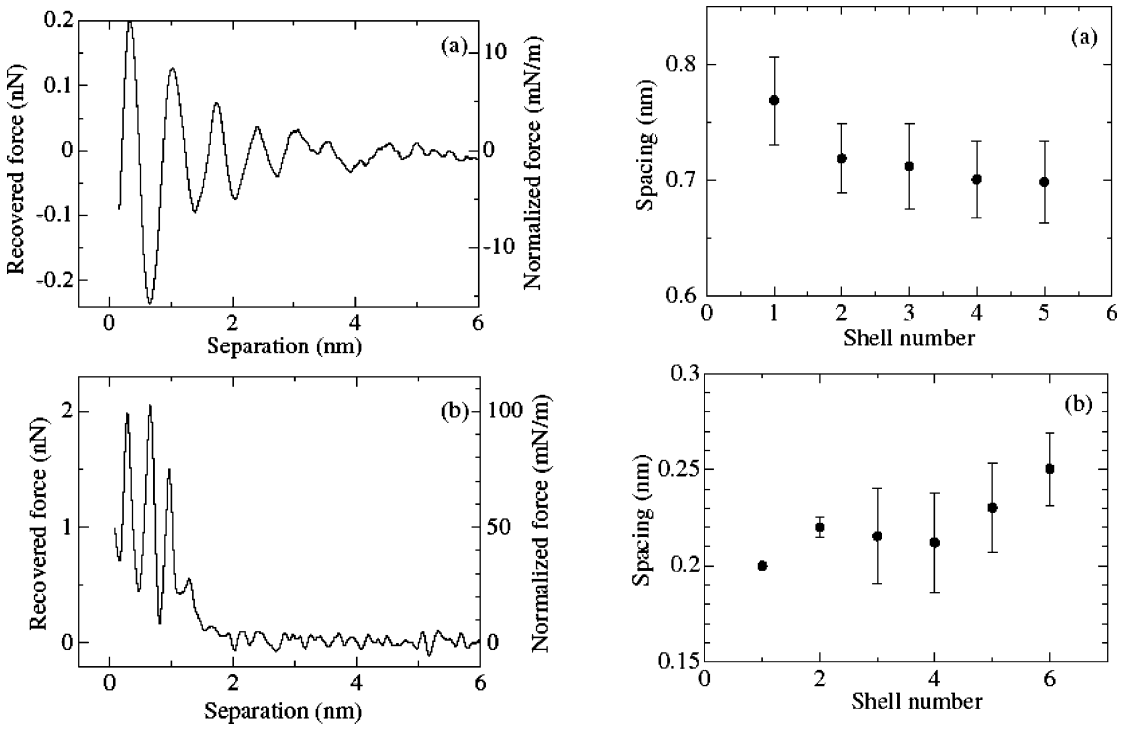

Figure 24. Left: layering of OMCTS on graphite (top) and of water on a -COOH terminated self-assembled monolayer (bottom) as sensed by the tip when approaching to the surface. Right: graphs showing the dependence of the layer spacing on the proximity to the surface for OMCTS on graphite (top) and water on the -COOH terminated self-assembled monolayer (bottom). The bars indicate the average scatter for each measured shell. (Each part of Figure 24 is reprinted with permission from ref 256. Copyright 2005 IOP Publishing Ltd.)

distance, frozen by the electric field. The electric field, on the order of 10^6 V m^{-1}, was much smaller than theoretically predicted for the alignment of water dipoles and crystallization into polar cubic ice ($>10^9$ V m^{-1}). We will discuss more effects of the electric field on the wetting phenomena scale in the next section.

6. Capillarity Phenomena: Water Bridges and Necks

Even if the AFM tip is not immersed in water, condensation due to the ambient relative humidity can produce water bridges around the tip. The driving force behind this phenomenon is capillarity, due to the negative curvature of the water necks, which decreases the pressure of the water vapor necessary to maintain equilibrium.[237] The necks formed around sharp asperities have been shown to be important in modifying and even controlling sliding friction and adhesion forces at the nanoscale. Riedo et al.[260] found that for partially hydrophilic, nanometer-scale rough surfaces, friction decreases logarithmically with the scan velocity, whereas for partially hydrophobic surfaces, friction increases with velocity, a result that was explained by the finite time needed to condense water to form the bridges.

Several experimental groups have studied capillary-induced water bridges on the nanometer scale.[261−263] New applications in imaging and nanofabrication have driven efforts to understand nanometer-size capillarity.[160,264−266] Capillary transport of molecules from the AFM tip to the solid substrate has been used by Piner et al.[267] to write patterns of molecules of submicrometer dimensions. This technique, called dip pen nanolithography, has been also used by Lee et al.[268] to generate protein nanoarrays over different surfaces.

Theoretical work has been done to cover many aspects of capillarity menisci formation between a tip and a surface,[269] structured pores,[270] capillary forces between spherical particles and substrates,[271] forces between surfaces,[272] and kinetics of capillary condensation.[273] This topic is, however, outside the scope of this review.

6.1. Effect of Electric Fields in the Formation of Water Necks

In this last section, we examine the effect of electric fields on the formation of water films and necks. That the presence of electric fields has a strong influence on the condensation of water has been known for a long time, for example, in the formation of ice layers on electrified wires. The presence of electric fields changes the free energy of condensation as can be expected from the high dielectric constant of water. The field of electrochemistry deals with the topic of electric fields, water, and ions. Oriented layers of water molecules give rise to electric fields, and vice versa, charged surfaces help orient the water dipoles in adjacent layers to give rise to ferroelectricity. We have already discussed how, at the molecular level, electric fields and water are intertwined, for example, in the growth of oriented water layers on mica, where the average dipole points down toward the negative mica surface, and in the orientation induced by pH changes on the layers adjacent to quartz in electrolyte solutions.[274]

Calleja and García[275] observed the formation of water necks when a voltage was applied to the AFM tip above a threshold value in humid environments. The formation and rupture of the neck produced changes in the amplitude of oscillation of the lever, as shown in Figure 25. As can be seen in the figure, the amplitude is reduced after the application of a small voltage pulse. The electrostatic interaction changes the resonance frequency, which leads to a reduction of the oscillation amplitude (region II). Once the pulse is off, the tip recovers its initial oscillation

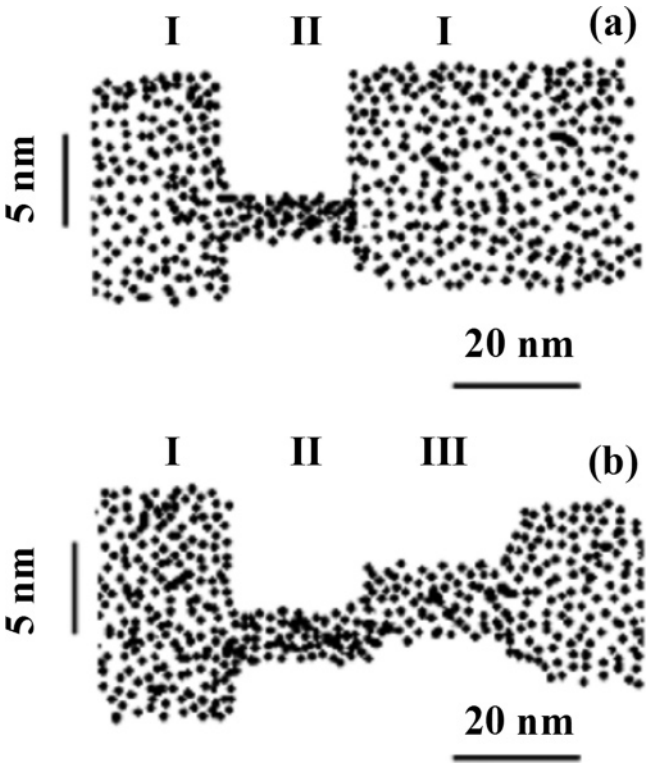

Figure 25. Points in the graph correspond to the instantaneous amplitude of the tip as a function of time as it oscillates over a Si wafer surface in an environment containing water at 37% RH. Top: during application of a 10.2 V voltage pulse for 20 ms (II), the tip is deflected toward the sample, and the amplitude is reduced. In panel b, a pulse of 11 V is applied in II and is off in III. Some deflection and amplitude damping remains after the pulse is off (III). This is indicative of the formation of a water meniscus. (Reprinted with permission from ref 278 (http://link.aps.org/abstract/PRL/v91/p56101). Copyright 2003 by the American Physical Society.)

amplitude. A different behavior is observed in a humid environment after a suitably high voltage pulse. A liquid bridge has been formed, and its capillary force reduces the oscillation. However, the meniscus is not in equilibrium, and the oscillation slowly returns to its initial amplitude. This effect has been used to induce local and controlled electrochemical modifications of the surface for nanopatterning applications.[276,277]

In the following, we review the effects of electric fields in promoting the formation of water films and necks from a theoretical perspective because new and interesting advances in the area have appeared recently that help to understand these phenomena.[276,278]

In the models, the tip−sample system consists of a metallic tip positioned over a metallic sample. The tip is described by a truncated cone or pyramid of length L and semi-angle θ, terminated with a spherical cap of radius R. The surfaces of tip and sample are assumed to be covered by a thin water layer, which in the absence of an electric field conforms to the surface geometry. The profile of this film on the surface is represented by the function $z(r)$, where z is the distance to the metallic surface and r is the lateral distance to the tip apex (see Figure 26). Although a similar film presumably exists also on the tip, it is neglected for simplicity.

Because of its high dielectric constant, the water film is assumed to act as a perfect conductor and can be considered to be at the same potential as the metallic sample. The system is in an environment with relative humidity H. Under these

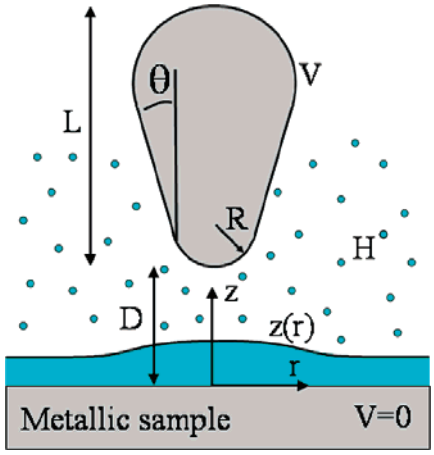

Figure 26. Tip−sample configuration with a water film (in gray) used in the theoretical treatment. The relative humidity H induces water condensation over the substrate with a surface profile characterized by the function $z(r)$.

conditions, the condensation energy of the water film is given by

$$U_c = 2\pi KT\frac{\rho}{m}\ln(1/\mathrm{H})\int_0^\infty z(r)r\,dr \qquad (1)$$

where ρ and m are the molecular density and molecular mass of the water, respectively. Without the tip influence, $z(r)$ should be a plane, but under an applied potential, this simple geometry deforms into a different shape. We describe now how to calculate this shape based on continuum media, which should still be appropriate for nanoscale phenomena at room temperature.

In the presence of a field E, the electrostatic energy of the system ΔU_e can be expressed as[279]

$$U_e = -\frac{\epsilon_0}{2}\int_V {E_0}^2 dV \qquad (2)$$

where V is the volume of condensed water and E_0 the original electric field before the water film was condensed. It has been shown[280] that to model the electrostatic fields in the case of metallic samples, the tip can be substituted by a sphere of radius R and a voltage V. In this simple case, the field is given by a set of point charges inside the tip[281]

$$E_0 = -2RV\sum_{i=1}^{\infty}\frac{\tilde{q}_i}{\tilde{r}_i^{\,2}} \qquad (3)$$

where the values of q_i and r_i are obtained from the standard series for a charged sphere versus a flat metallic plate.[282] Combining these equations, one obtains the electrostatic energy for a generic function $z(r)$

$$U_e = -4\pi\epsilon_0 R^2V^2\int_0^\infty z(r)r\left(\sum_{i=1}^{\infty}\frac{\tilde{q}_i}{\tilde{r}_i^{\,2}}\right)^2 dr \qquad (4)$$

When water is condensed, U_e decreases while U_c increases. The water film profile will therefore be determined by the minimization of the total energy $U_{tot} = U_e + U_c$. Since along the vertical axis through the tip apex the field E is a minimum at the water surface, the electrostatic energy should decrease when the thickness under the apex h increases. Also, due to

its proximity, this field is a maximum relative to the rest of the water surface. This implies that the best position for water to start condensing is just under the tip apex. When the electric field reaches a threshold value at a voltage V_{th}, condensation will accelerate until the water surface touches the tip because E will be increasing when h increases. In this simple approximation, the field $E_0 = E(z = 0, r = 0)$ is the key parameter to obtain V_{th}. Assuming that E_0 is a constant value over the whole water volume, the electrostatic energy would be

$$U_e = -4\pi\epsilon_0 R^2 V^2 \left(\sum_{i=1}^{\infty} \frac{\tilde{q}_i}{\tilde{z}_i^2}\right)^2 \int_0^{\infty} z(r) r dr \qquad (5)$$

The total energy $U_{tot} = U_e + U_c$ must be negative to induce the formation of a water bridge (i.e., the electrostatic energy must be stronger than the condensation energy). V_{th} can be obtained from $U_{tot} = 0$

$$V_{th}^2 = \frac{KT\rho_m}{2R^2 m_m} \left(\sum_{i=1}^{\infty} \frac{\tilde{q}_i}{\tilde{z}_i^2}\right)^{-2} \ln(1/H) \qquad (6)$$

From this, the threshold electric field E_{th}, the induction of the formation of the water bridge can be calculated

$$E_{th} = \sqrt{\frac{2KT\rho_m \ln(1/H)}{m_m \epsilon_0}} \qquad (7)$$

For water, this equation takes the form $E_{th} = (3.5 \ln(1/H))^{1/2}$ V/nm. For H = 30%, $E_{th} \approx 2.05$ V/nm, in good agreement with previous results.[283]

Although the assumption that a flat film is sufficient to predict a reasonable value for V_{th}, it cannot explain the effects that result from the real shape of the water film before the water bridge is formed. The fact that U_e and U_c have the same dependence with $z(r)$ (both are proportional to the volume) implies that the water surface has only two shapes: a planar geometry and a bridge filling the gap. To analyze the changes of $z(r)$, two additional contributions to the energy need to be included.[284] One is the van der Waals energy U_{VdW}, and the other is the surface tension U_s. Since the van der Waals force is a short-range force, it will be a key contribution only when the distance between the water film and the metallic sample is a few angstroms. Assuming that the two surfaces are almost planar, U_{VdW} can be written as

$$U_{VdW} = \int_0^{\infty} \frac{|A| r}{6\pi (r)^2} dr \qquad (8)$$

where A is the Hamaker constant. The capillarity term U_s appears due to the increase of the water surface area when the initially flat layer bulges up under the tip. The increase of the surface tension contribution will be

$$U_s = \int_0^{\infty} 2\pi\alpha r \sqrt{1 + z'^2} dr \qquad (9)$$

where $\alpha = 73$ mN/m is the surface tension of water. Using all these contributions, together with the electrostatic energy U_e, the profile $z(r)$ is then obtained by minimization of the total energy U.

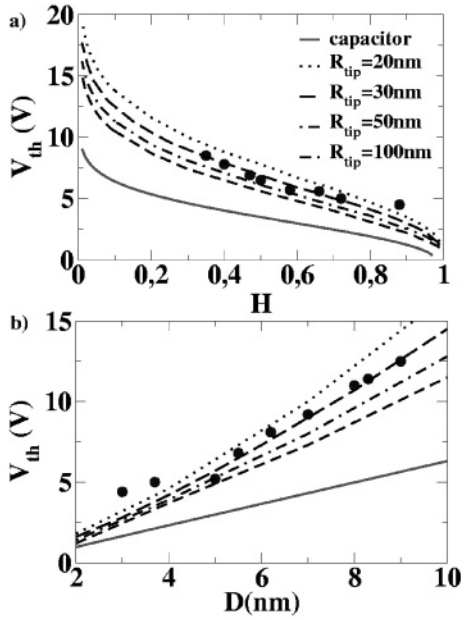

Figure 27. Calculated threshold voltage for the formation of a water bridge as a function of relative humidity H (a) and tip−sample distance (b) for several radii R_{tip}. D = 7 nm in panel a and H = 30% in panel b. The agreement with the experimental points is quite good. (Reprinted with permission from ref 278 (http://link.aps.org/abstract/PRL/v91/p56101). Copyright 2003 by the American Physical Society.)

The functional dependence of the electrostatic field is not easy to calculate because the local electrostatic energy per unit area is not known and depends on the entire function $z(r)$. Different approximations have been developed to calculate the electric field in the tip−sample region. Gil et al.[285−287] assumed that the tip is a sphere of radius R and the sample surface a flat plane and that the field lines are approximated by segments of circles connecting the tip and surface and is perpendicular to them, with the potential decaying linearly along the circular segments. Another and simpler approximation is the radial field approximation (RFA), which assumes that the fields are the same as those existing inside a spherical capacitor, with the spherical tip being the center electrode. Threshold voltages for the formation of water necks calculated using the RFA approximation are shown in Figure 27 as a function of humidity and tip−sample separation. As can be seen, the fit with the experimental data is excellent.[278] In the same paper, the authors discuss in detail the conditions for the stability of the necks and show the existence of bistable solutions leading to hysteresis in the formation and breaking of the neck, as observed experimentally.

7. Conclusions

Our understanding of the structure of water films in the nanometer range of thickness has advanced considerably in the past few years due to the intensive application of new experimental and theoretical techniques, in particular, electron and photon spectroscopies, STM, and DFT calculations. Together, they provide a detailed molecular view of the structure of water monolayers. The current model of the structure of the monolayer on metals is a hexagonal film of H-bonded molecules, close to a flattened version of the bilayer in the basal plane of ice I_h. It is still not completely

solved as to whether this layer is made of intact molecules or of partially dissociated water and OH species. While DFT calculations support the partially dissociated layer on the most reactive surfaces (Ru, Rh), on other more noble surfaces, the layer is formed by nondissociated water molecules. In this intact molecular layer, half the water molecules have their plane parallel to the surface with the two H-atoms bonding to neighboring molecules. They alternate with molecules with their plane perpendicular (or nearly so) to the surface, with the H that does not participate in H-bonding to a neighboring molecule pointing down to the metal substrate. Examples where the H points up have not yet been found for monolayers but could be formed on some metal surfaces. The difference in the stability of the different layers is based on the variation of the strength of the O lone pair orbital bonding with the metal, rather than on the H-bonding contribution to the energy balance of the monolayer. Interestingly, DFT values of the total energy differ very little in many cases for the possible models of alternating partially dissociated, intact H-up, or intact H-down molecules. On the experimental side, a controversy exists regarding the possibility that electrons or X-ray photons assist in the dissociation of water. Aware of these problems, many experimental groups are revisiting this topic, and we believe that soon the situation will be clarified.

A relevant point to keep in mind is that most of the experiments are carried out under cryogenic temperatures, a condition that might preclude the film to reach the thermodynamic equilibrium. This is due to the fact that the activation energy to reach the stable state is quite high (>0.5 eV), and similar to that to evaporate the film, indicating that to form equilibrated films, a high vapor pressure needs to be maintained to produce a thin layer of water on the surface. We have seen how new experimental tools are now being applied for in situ studies under higher temperatures.

As important as the first layer, or perhaps even more, is the structure of the subsequent layers. Questions as to whether and how far the layers beyond the first carry on the information or structure imposed by the substrate remain open. These questions are extremely important since the structure of the layers beyond the first few determines the interactions between objects immersed in water, for example, in biological material (proteins, membranes, etc.). We have seen how in some cases the orientation imposed by the surface to the first layers carries out for several more layers, giving rise to ferroelectric ice films. These studies are being pursued by many researchers at present.

Nonmetallic substrates are the most relevant in environmental, atmospheric, and soil science. We have reviewed some studies of water adsorption on oxides and other nonmetallic substrates. The application of tools such as STM and AFM, spectroscopies such as IR and SFG, and electron spectroscopies such as XPS, XES, and XAS to study the atomic structure of the water films have not yet produced the same amount and quality of data as for the metal cases. This is of course due to experimental difficulties due to the insulating nature of the materials. It is hoped that with more advanced tools, such as noncontact dynamic force microscopy and environmental XPS, this situation will change soon.

We have seen also how new studies provide novel and fundamental insights into the interaction of water with coadsorbed species, a topic of great relevance to understand the phenomena of hydrophillicity and hydrophobicity.

The final topic reviewed involves the structure of water under confinement, again of great importance for biology and material science in general. We have seen, for example, how AFM and the surface force apparatus can provide information on the layering of water near surfaces. Studies where the nature of the interfaces changes from weak to strong water bonding should be very interesting and will help to advance the field of biological interactions, electrochemistry, etc.

Finally, we have shown how important it is to study the structure on water films under ambient conditions of pressure and temperature. Such studies should overcome some of the current difficulties related to the formation of nonequilibrium structures. We have shown how new instrumentation has been developed that will make such studies possible.

We concluded our review by examining studies on the effect of electric fields in favoring the formation of water films. Although no molecular scale details are provided by the experiments so far, we have seen that the electric field produces strong effects at nanoscale film thickness favoring the production of water bridges by virtue of providing a high dielectric constant medium that concentrates the electric field and thus minimizes the energy of the system.

8. Acknowledgments

This work was supported by the Director, Office of Energy Research, Office of Basic Energy Sciences, Materials, and Chemical Sciences Division, of the U.S. Department of Energy under Contract DE-AC02-05CH11231. A.V. acknowledges financial support from AGAUR, Generalitat de Catalunya. G.M.S. acknowledges financial support from the Spanish Ministry of Education.

9. References

(1) Thiel, P. A.; Madey, T. E. *Surf. Sci. Rep.* **1987**, *7*, 211.
(2) Henderson, M. A. *Surf. Sci. Rep.* **2002**, *46*, 1.
(3) Michaelides, A.; Ranea, V. A.; de Andres, P. L.; King, D. A. *Phys. Rev. Lett.* **2003**, *90* (21), 216102.
(4) Meng, S.; Wang, E. G.; Gao, S. *Phys. Rev. B* **2004**, *69*, 195404.
(5) Morgenstern, K.; Rieder, K.-H. *J. Chem. Phys.* **2002**, *116* (13), 5746.
(6) Morgenstern, K.; Rieder, K.-H. *Chem. Phys. Lett.* **2002**, *358*, 250.
(7) Morgenstern, K.; Gawronski, H.; Mehlhorn, M.; Rieder, K.-H. *J. Mod. Opt.* **2004**, *51* (16−18), 2813.
(8) Mitsui, T.; Rose, M. K.; Formin, E., Ogletree, D. F.; Salmeron, M. *Science* **2002**, *297*, 1850.
(9) Fomin, E.; Tatarkhanov1, M.; Mitsui, T.; Rose, M.; Frank Ogletree, D. F.; Salmeron, M. *Surf. Sci.* **2006**, *600*, 542.
(10) Nakamura, M.; Shingaya, Y.; Ito, M. *Chem. Phys. Lett.* **1999**, *309*, 123.
(11) Nakamura, M.; Ito, M. *Chem. Phys. Lett.* **2000**, *325*, 293.
(12) Nakamura, M.; Ito, M. *Chem. Phys. Lett.* **2001**, *335*, 170.
(13) Nakamura, M.; Ito, M. *Chem. Phys. Lett.* **2004**, *384*, 256.
(14) Nakamura, M.; Ito, M. *Chem. Phys. Lett.* **2005**, *404*, 346.
(15) Daschbach, J. L.; Peden, B. M.; Smith, R. S.; Kay, B. D. *J. Chem. Phys.* **2004**, *120* (3), 1516.
(16) Ogasawara, H.; Yoshinobu, J.; Kawai, M. *J. Chem. Phys.* **1999**, *111* (15), 7003.
(17) Yamamoto, S.; Beniya, A.; Mukai, K.; Yamashita, Y.; Yoshinobu, J. *J. Phys. Chem. B* **2005**, *109*, 5816.
(18) Lilach, L.; Buch, V.; Asscher, M. *J. Chem. Phys.* **2003**, *119* (22), 11899.
(19) Ranea, V. A.; Michaelides, A.; Ramirez, R.; de Andres, P. L.; Verges, J. A.; King, D. A. *Phys. Rev. Lett.* **2004**, *92* (13), 136104.
(20) Michaelides, A.; Ranea, V. A.; de Andres, P. L.; King, D. A. *Phys. Rev. B* **2004**, *69*, 075409.
(21) Spitzer, A.; Lüth, H. *Surf. Sci.* **1982**, *120*, 376.
(22) Komeda, T.; Fukimode, H.; Kim, Y.; Kawai, M.; Sainoo, Y.; Shigekawa, H. *Jpn. J. Appl. Phys.* **2002**, *41*, 4932.
(23) He, J.-W.; Norton, P. R. *Surf. Sci.* **1990**, *238*, 95.
(24) Brosseau, R.; Brustein, R.; Ellis, T. H. *Surf. Sci.* **1993**, *280*, 23.
(25) Morgenstern, K.; Nieminen, J. *Phys. Rev. Lett.* **2002**, *88* (6), 066102.

(26) Morgenstern, K. *Surf. Sci*. **2002**, *504*, 293.
(27) Morgenstern, K.; Nieminen, J. *J. Chem Phys.* **2004**, *120* (22), 10786.
(28) Cerda, J.; Michaelides, A.; Bocquet, M.-L.; Feibelman, P. J.; Mitsui, T.; Rose, M. K.; Fomin, E.; Salmeron, M. *Phys. Rev. Lett.* **2004**, *93* (11), 116101.
(29) Salmeron, M. et al., in preparation.
(30) Morgenstern, M.; Michely, T.; Comsa, G. *Phys. Rev. Lett*. **1996**, *77*, 703.
(31) Morgenstern, M.; Mueller, J.; Michely, T.; Comsa, G. *Z. Phys. Chem.* **1997**, *198*, 43.
(32) Smoluchowski, R. *Phys. Rev.* **1941**, *60*, 661.
(33) Glebov, A.; Grahm, A. P.; Menzel, A.; Toennies, J. P. *J. Chem. Phys.* **1997**, *106*, 9382.
(34) Haq, S.; Harnett, J.; Hodgson, A. *Surf. Sci.* **2002**, *505*, 171.
(35) Held, G.; Menzel, D. *Surf. Sci.* **1994**, *316*, 92.
(36) Doering, D.; Madey, T. E. *Surf. Sci.* **1982**, *123*, 305.
(37) Puisto, S. R.; Lerotholi, T. J.; Held, G.; Monzel, D. *Surf. Rev. Lett.* **2003**, *10*, 487.
(38) Feibelman, P. J. *Science* **2002**, *295*, 99.
(39) Ogasawara, H.; Brena, B.; Nordlund, D.; Nyberg, M.; Pelmenschikov, A.; Petterson, L. G. M.; Nilsson, A. *Phys. Rev Lett.* **2002**, *89*, 276102.
(40) Meng, S. *Suf. Sci.* **2005**, *575*, 300.
(41) Michaelides, A.; Alavi, A.; King, D. A. *Phys. Rev. B* **2004**, *69*, 113404.
(42) Materzanini, G.; Tantardini, G. F.; Lindan, P. J. D.; Saalfrank, P. *Phys. Rev. B* **2005**, *71*, 155414.
(43) Denzler, D. N.; Wagner, S.; Wolf, M.; Ertl, G. *Surf. Sci*. **2003**, *532*, 113.
(44) Weissenrieder, J.; Mikkelsen, A.; Andersen, J. N.; Feibelman, P. J.; Held, G. *Phys. Rev. Lett.* **2004**, *93* (19), 196102.
(45) Feibelman, P. J., in preparation.
(46) Denzler, D. N.; Hess, Ch.; Dudek, R.; Wagner, S.; Frischkorn, Ch.; Wolf, M.; Ertl, G. *Chem. Phys. Lett.* **2003**, *376*, 618.
(47) Anderson, K.; Nikitin, A.; Pettersson, L. G. M.; Nilsson, A.; Ogasawara, H. *Phys. Rev. Lett.* **2004**, *93* (19), 196101.
(48) Clay, C.; Haq, S.; Hodgson, A. *Chem. Phys. Lett.* **2004**, *288*, 80.
(49) Andersson, K.; Gómez, A.; Glover, C.; Nordlund, D.; Öström, H.; Schiros, T.; Takahashi, O.; Ogasawara, H.; Petterson, L. G. M.; Nilsson, A. *Surf. Sci.* **2005**, *585*, L183.
(50) Michaelides, A.; Alavi, A.; King, D. A. *J. Am. Chem. Soc*. **2003**, *125*, 2746.
(51) Ghosal, S.; Hemminger, J. C.; Bluhm, H.; Mun, B. S.; Hebenstreit, E. L. D.; Ketteler, G.; Ogletree, D. F.; Requejo, F. G.; Salmeron, M. *Science* **2005**, *307*, 5709.
(52) Siegbahn, H. *J. Phys. Chem.* **1985**, *89*, 897, and references therein.
(53) Bluhm, H.; Ogletree, D. F.; Fadley, C. S.; Hussain, Z.; Salmeron, M. *J. Phys.: Condens. Matter* **2002**, *14*, L227.
(54) Ogletree, D. F.; Bluhm, H.; Lebedev, G.; Fadley, C. S.; Hussain, Z.; Salmeron, M. *Rev. Sci. Instrum.* **2002**, *73*, 3872.
(55) Starke, U.; Materer, N.; Barbieri, A.; Döll, R.; Heinz, K.; Van Hove, M. A.; Somorjai, G. A. *Surf. Sci*. **1993**, *287*, 432.
(56) Materer, M.; Starke, U.; Barbieri, A.; Van Hove, M. A.; Somorjai, G. A.; Kroes, G.-J.; Minot, C. *J. Phys. Chem*. **1995**, *99*, 6267.
(57) Materer, M.; Starke, U.; Barbieri, A.; Van Hove, M. A.; Somorjai, G. A.; Kroes, G.-J.; Minot, C. *Surf. Sci.* **1997**, *381*, 190.
(58) Su, X.; Lianos, L.; Shen, Y. R.; Somorjai, G. A. *Phys. Rev. Lett.* **1998**, *80* (7), 1533.
(59) Bramwell, S. T. *Nature* **1999**, *397*, 212.
(60) Devlin, J. P.; Joyce, C.; Buch, V. *J. Phys. Chem. A* **2000**, *104*, 1974.
(61) Devlin, J. P.; Buch, V. *Mikrochim. Acta* **1997**, 57.
(62) Iedema, M. J.; Dresser, M. J.; Doering, D. L.; Rowland, J. B.; Hess, W. P.; Tsekouras, A. A.; Cowin, J. P. *J. Phys. Chem. B* **1998**, *102*, 9203.
(63) Surplice, N. A.; D'Arcy, R. J. *J. Phys. E* **1970**, *3*, 477.
(64) Witek, H.; Buch, V. J. *Chem. Phys.* **1999**, *110*, 3168.
(65) Angell, C. A.; Sceats, M. G.; Rice, S. A. *Water: A Comprehensive Treatise Vol. 7*; Franks, F., Ed.; Plenum Press: New York, 1982; pp 1−214.
(66) Stevenson, K. P.; Kimmel, G. A.; Dohnalek, Z.; Smith, R. S.; Kay, B. D. *Science* **1999**, *283*, 1505.
(67) Smith, R. S.; Kay, B. D. *Nature* **1999**, *398*, 788.
(68) Dohnálek, Z.; Ciolli, R. L.; Kimmel, G. A.; Setevenson, K. P.; Smith, R. S.; Kay, B. D. *J. Chem. Phys.* **1999**, *110* (12), 5489.
(69) Smith, R. S.; Huang, C.; Wong, E. K. L.; Kay, B. D. *Surf. Sci. Lett.* **1996**, *367*, L13.
(70) Ikemiya, N.; Gewirth, A. A. *J. Am. Chem. Soc.* **1997**, *119*, 9919.
(71) Löfgren, P.; Ahlström, Chakarov, D. V.; Lausmaa, J.; Kasemo, B. *Surf. Sci. Lett.* **1996**, *367*, L19.
(72) Meng, S.; Wang, E. G.; Gao, E. *J. Chem. Phys.* **2003**, *119* (15), 7617.
(73) Dohnálek, Z.; Kimmel, G. A.; Ciolli, R. L.; Setevenson, K. P.; Smith, R. S.; Kay, B. D. *J. Chem Phys.* **2000**, *112* (13), 5932.
(74) Nakamura, M.; Ito, M. *Surf. Sci*. **2002**, *502*, 144.
(75) Baumann, P.; Pirug, G.; Reuter, D.; Bonzel, H. P. *Surf. Sci.* **1995**, *335*, 186.
(76) Doering, D. L.; Semancik, S; Madey, T. E. *Surf. Sci.* **1983**, *133*, 49.
(77) Kizhakevarian, N.; Villegas, I.; Weaver, M. J. *J. Phys. Chem.* **1995**, *99*, 7677.
(78) Bornemann, T.; Steinrueck, H. P.; Huber, W.; Menzel, D. *Surf. Sci.* **1998**, *224*, 195.
(79) Bonzel, H. P.; Pirug, G.; Ritke, C. *Langmuir* **1991**, *7*, 3006.
(80) Doering, D. L.; Madey, T. E. *Surf. Sci.* **1982**, *123*, 305.
(81) Kretzschmar, K.; Sass, J. K.; Hoffmann, P.; Ortega, A.; Bradshaw, A. M.; Holloway, S. *Chem. Phys. Lett*. **1981**, *78*, 410.
(82) Kretzschmar, K.; Sass, J. K.; Bradshaw, A. M.; Holloway, S. *Surf. Sci.* **1982**, *115*, 183.
(83) Gibson, K. D.; Viste, M.; Sibener, S. J. *J. Chem. Phys.* **2000**, *112*, 9582.
(84) Madey, T. E.; Netzer, F. P. *Surf. Sci.* **1982**, *117*, 549.
(85) Pache, T.; Steinrück, H.-P.; Huber, W.; Menzel, D. *Surf. Sci*. **1989**, *224*, 195.
(86) Netzer, F. P.; Madey, T. E. *Phys. Rev. Lett.* **1981**, *47*, 928.
(87) Nakamura, M.; Song, M. B.; Ito, M. *Chem Phys. Lett.* **2000**, *320*, 381.
(88) Thiel, P. A.; Hoffmann, F. M.; Weinberg, W. H. *J. Chem. Phys.* **1981**, *75*, 5556.
(89) Thiel, P. A.; Hoffmann, F. M.; Weinberg, W. H. *Phys. Rev. Lett.* **1982**, *49*, 501.
(90) Nakamura, M.; Ito, M. *Phys. Rev. Lett.* **2005**, *94*, 035501.
(91) Zhu, X. Y.; White, J. M.; Wolf, M.; Hasselbrink, E.; Ertl, G. *J. Phys. Chem.* **1991**, *95*, 8393.
(92) Ogasawara, H.; Yoshinobu, J.; Kawai, M. *Chem. Phys. Lett*. **1994**, *231*, 188.
(93) Zinck, J. J.; Weinberg, W. H. *J. Vac. Sci. Technol*. **1980**, *17*, 188.
(94) Hinch, B. J.; Dubois, L. H. *J. Chem. Phys.* **1992**, *96*, 3262.
(95) Leung, L. W. H.; Goodman, D. W. *Langmuir* **1991**, *7*, 493.
(96) Peebles, D. E.; White, J. M. *Surf. Sci.* **1984**, *144*, 512.
(97) Löfgren, P.; Kasemo, B. *Catal. Lett.* **1998**, *53*, 33.
(98) Ogasawara, H.; Yoshinobu, J.; Kawai, M. *Surf. Sci*. **1997**, *386*, 73.
(99) Kinne, M.; Fuhrmann, T.; Zhu, J. F.; Tränkenschuh, B.; Denecke, R.; Steinrück, H.-P. *Langmuir* **2004**, *20*, 1819.
(100) Wagner, F. T.; Moylan, T. E.; Schmieg, S. J. *Surf. Sci.* **1988**, *195*, 403.
(101) Sanders, H. E.; Gardner, P.; King, D. A.; Morris, M. A. *Surf. Sci* **1994**, *304*, 159.
(102) Kizhakevariam, N.; Jiang, X.; Weaver, M. J. *J. Chem. Phys.* **1994**, *100*, 6750.
(103) Jacobi, K.; Bertolo, M.; Geng, P.; Hansen, W.; Schreiner, J.; Astaldi, C. *Surf. Sci.* **1991**, *245*, 72.
(104) Ellis, T. H.; Kruus, E. J.; Wang, H. *Surf. Sci*. **1991**, *273*, 73.
(105) Yee, N. C.; Chottiner, G. S.; Scherson, D. A. *Phys. Chem. B* **2005**, *109*, 7610.
(106) Bange, K.; Madey, T. E.; Sass, J. K. *Surf. Sci.* **1985**, *152*−*153*, 550.
(107) Kizhakevariam, N.; Stuve, E. M.; Dohl-Oelze, R. *J. Chem. Phys.* **1991**, *94*, 670.
(108) Krasnopoler, A.; Stuve, E. M. *Surf. Sci.* **1994**, *303*, 355.
(109) Sass, J. K.; Lackey, D.; Schott, J.; Straehler, B. *Surf. Sci.* **1991**, *247*, 239.
(110) Krasnopoler, A.; Johson, A. L.; Stuve, E. M. *Surf. Sci.* **1995**, *328*, 186.
(111) Krasnopoler, A.; Kizhakevariam, N.; Stuve, E. M. *J. Chem. Soc., Faraday Trans.* **1996**, *92*, 2445.
(112) Wagner, F. T.; Moylan, T. E. *Surf. Sci.* **1987**, *182*, 125.
(113) Wagner, F. T.; Moylan, T. E. *Surf. Sci.* **1989**, *216*, 361.
(114) Endo, O.; Kondoh, H.; Yonamoto, Y.; Yokoyama, T.; Otha, T. *Surf. Sci*. **2000**, *463*, 135.
(115) Bange, K.; Grider, D.; Sass, J. K. *Surf. Sci.* **1983**, *126*, 279.
(116) Bange, K.; Doehl, R.; Grider, D.; Sass, J. K. *Vacuum* **1983**, *33*, 757.
(117) Sass, J. K.; Richarson, N. V.; Neff, H.; Roe, D. K. *Chem. Phys. Lett.* **1980**, *73*, 209.
(118) Brown, G. E.; Hendrich, V. E.; Casey, W. H.; Clar, D. L.; Eggleston, C.; Felmy, A.; Goodman, D. W.; Gratzel, M.; Maciel, G.; McCarthy, M. I.; Nealson, K. H.; Sverjensky, D. A.; Toney, M. F.; Zachara, J. M. *Chem. Rev.* **1999**, *99*, 77.
(119) Al-Abadleh, H. A.; Grassian, V. H. *Surf. Sci. Rep*. **2003**, *52*, 63.
(120) Schaumb, R.; Thostrup, P.; Lopez, N.; Lægsgaard, E.; Stensgaard, I.; Nørskov, J. K.; Besenbacher, F. *Phys. Rev. Lett.* **2001**, *87* (26), 266104.
(121) Brookes, I. M.; Muryn, C. A.; Thornton, G. *Phys. Rev. Lett.* **2001**, *87* (26), 266103.
(122) Maksymovych, P.; Mezhenny, S.; Yates, J. T., Jr. *Chem. Phys. Lett.* **2003**, *382*, 270.
(123) Diebold, U.; Lehman, J.; Mahmound, T.; Kuhn, M.; Leonardelli, G.; Hebenstreit, W.; Schmid, M.; Varga, P. *Surf. Sci.* **1998**, *411*, 137.
(124) Andersohn, L.; Köhler, U. *Surf. Sci.* **1993**, *284*, 77.
(125) Lo, R.-L.; Hwang, I.-S.; Tsong, T. T. *Surf. Sci. Lett.* **2003**, *530*, L302.

(126) Avouris, P.; Lyo, I. W. *Surf. Sci.* **1991**, *242*, 1.
(127) Tzvetkov, G.; Zubavichus, Y.; Koller, G.; Schmidt, Th.; Heske, C.; Umbach, E.; Grunze, M.; Ramsey, M. G.; Netzer, F. P. *Surf. Sci.* **2003**, *543*, 131.
(128) Leist, U.; Ranke, W.; Al-Shamery, K. *Phys. Chem. Chem. Phys*. **2003**, *5*, 2435.
(129) Daschbach, J. L.; Dohnalek, Z.; Liu, S. R.; Smith, R. S.; Kay, B. D. *J. Phys. Chem. B* **2005**, *109*, 10362.
(130) Picaud, S.; Girardet, C. *Chem Phys. Lett.* **1993**, *209*, 340.
(131) Picaud, S.; Hoang, P. N. M.; Girardet, C. *Surf. Sci.* **1992**, *278*, 339.
(132) Heidberg, J.; Redlich, B.; Wetter, D. *Ber. Bunsen-Ges. Phys. Chem.* **1995**, *99*, 1333.
(133) Xu, C.; Goodman, D. W. *Chem. Phys. Lett.* **1997**, *265*, 341.
(134) Ferry, D.; Glebov, A.; Senz, V.; Suzanne, J.; Toennies, J. P.; Weiss, H. *J. Chem. Phys.* **1996**, *105*, 1697.
(135) Ferry, D.; Glebov, A.; Senz, V.; Suzanne, J.; Toennies, J. P.; Weiss, H. *Surf. Sci.* **1998**, *419*, 48.
(136) Ferry, D.; Picaud, S.; Hoang, P. N. M.; Girardet, C.; Giordano, L.; Dermirdjian, B.; Suzanne, J. *Surf. Sci.* **1998**, *409*, 101.
(137) Dermirdjian, B.; Suzanne, J.; Ferry, D.; Coulomb, J. P.; Giordano, L. *Surf. Sci.* **2000**, *462*, L581.
(138) Langel, W.; Parrinello, M. *Phys. Rev. Lett.* **1994**, *73*, 504.
(139) Russo, S.; Noguera, C. *Surf. Sci*. **1992**, *262*, 259.
(140) Russo, S.; Noguera, C. *Surf. Sci*. **1992**, *262*, 245.
(141) Scamehorn, C. A.; Harrison, N. M.; McCarthy, M. I. *J. Chem. Phys.* **1994**, *101*, 1547.
(142) Giodano, L.; Goniakowski, J.; Suzanne, J. *Phys. Rev. Lett.* **1998**, *81*, 1271.
(143) Delle Site, L.; Alavi, A.; Lyndeln-Bell, R. M. *J. Chem. Phys.* **2000**, *113*, 3344.
(144) Lynden-Bell, R. R.; Delle Stite, L.; Alavi, A. *Surf. Sci.* **2002**, *496*, L1.
(145) Wang, Y.; Truong, T. N. *J. Phys. Chem. B* **2004**, *108*, 3289.
(146) Kim, Y. D.; Stultz, J.; Goodman, D. W. *J. Phys. Chem. B* **2002**, *106* (7), 1515.
(147) Yu, Y.; Guo, Q.; Liu, S.; Wang, E.; Møller, P. J. *Phys Rev. B* **2003**, *68*, 115414.
(148) Hawkins, S.; Kumi, G.; Malyk, S.; Reisler, H.; Witting, C. *Chem Phys. Lett*. **2005**, *404*, 19.
(149) Heidberg, J.; Häser, W. *J. Electron Spectrosc. Relat. Phenom*. **1990**, *54*, 971.
(150) Bruch, L. W.; Glebov, A.; Toennies, J. P.; Weiss, H. *J. Chem Phys.* **1995**, *103*, 5109.
(151) Fölsch, S.; Stock, A.; Henzler, M. *Surf. Sci.* **1992**, *264*, 65.
(152) Malaske, U.; Pfnür, M.; Bässler, M.; Weiss, M.; Umbach, E. *Phys. Rev. B* **1996**, *53*, 13115.
(153) Toennies, J. P.; Traeger, F.; Vogt, J.; Weiss, H. *J. Chem. Phys*. **2004**, *120* (24), 11347.
(154) Nuzzo, R. G.; Zegarski, B. R.; Korenic, E. M.; Dubois, L. H. *J. Phys. Chem.* **1992**, *96*, 1355.
(155) Dubois, L. H.; Zegarski, B. R.; Nuzzo, R. G. *J. Am. Chem. Soc*. **199**, *112*, 570.
(156) Engquist, I.; Lunstroem, I.; Leidberg, B. *J. Phys. Chem*. **1995**, *99*, 12257.
(157) Engquist, I.; Lestelius, M.; Leidberg, B. *Langmuir* **1997**, *13*, 4003.
(158) Engquist, I.; Lunström, I.; Leidberg, B. *J. Phys. Chem*. **1997**, *106*, 3038.
(159) Shen, Y. R.; Ostroverkhov, V. *Chem. Rev.* **2006**, *106*, 1140.
(160) García, R.; Pérez, R. *Surf. Sci. Rep.* **2002**, *47*, 197, and references therein.
(161) Luna, M.; Colchero, J.; Baró, A. M. *Appl. Phys. Lett.* **1998**, *72* (26), 3461.
(162) Pompe, T.; Fery, A.; Herminghaus, S. *Langmuir* **1998**, *14*, 2586.
(163) Zitzler, L.; Herminghaus, S.; Mugele, F. *Phys. Rev. B* **2002**, *66*, 155436.
(164) Hu, J.; Xiao, X. D.; Salmeron, M. *Appl. Phys. Lett*. **1995**, *67*, 476.
(165) Hu, J.; Xiao, X. D.; Ogletree, D. F.; Salmeron, M. *Surf. Sci.* **1995**, *344*, 221.
(166) Hu, J.; Xiao, X. D.; Ogletree, D. F.; Salmeron, M. *Science* **1995**, *268*, 267.
(167) Gómez-Moñivas, S.; Froufe-Pérez, L. S.; Camaño, A. J.; Saenz, J. J. *Appl. Phys. Lett.* **2001**, *79*, 4048.
(168) Schönenberger, C.; Alvarado, S. F. *Phys. Rev. Lett.* **1990**, *65*, 3162.
(169) Yokohama, U. H.; Inoue, T. *Thin Solid Films* **1994**, *242*, 33.
(170) Xu, L.; Salmeron, M. *Nano-Surface Chemistry*; Rosoff, M., Ed.; Marcel Dekker: New York, 2002.
(171) Ewing, G. E. *Chem. Rev.* **2006**, *106*, 1511.
(172) Beaglehole, D.; Christenson, H. K. *J. Phys. Chem.* **1992**, *96*, 3395.
(173) Cantrell, W.; Ewing G. E. *J. Phys. Chem. B* **2001**, *105*, 5434.
(174) Salmeron, M.; Xu, L.; Hu, J.; Dai, Q. *MRS Bull*. **1997**, *22*, 36.
(175) Xu, L.; Lio, A.; Hu, J.; Ogletree, D. F.; Salmeron, M. *J. Phys. Chem. B* **1998**, *102*, 540.
(176) Odelius, M.; Bernasconi, M.; Parinello, M. *Phys. Rev. Lett* **1997**, *78*, 2855.
(177) Miranda, P. B.; Xu, L.; Shen, Y. R.; Salmeron, M. *Phys. Rev. Lett.* **1998**, *81*, 5876.
(178) Bluhm, H.; Inoue, T.; Salmeron, M. *Surf Sci*. **2000**, *462*, L599.
(179) Bluhm, H.; Salmeron, M. *J. Chem. Phys.* **1999**, *111* (15), 6947.
(180) Bluhm, H.; Inoue, T.; Salmeron, M. *Phys. Rev. B* **2000**, *61*, 7760.
(181) Dash, J. G.; Fu, H.; Wettlaufer, J. S. *Rep. Prog. Phys.* **1995**, *58*, 115, and references therein.
(182) Fletcher, N. H. *Philos. Mag. B* **1992**, *66*, 109.
(183) Fletcher, N. H. *Philos. Mag. B* **1968**, *18*, 1287.
(184) Fletcher, N. H. *The Chemical Physics of Ice*; Cambridge University Press: New York, 1970.
(185) Dosch, H.; Lied, A.; Bilgram, J. H. *Surf. Sci.* **1996**, *366*, 43.
(186) Luna, M.; Colchero, J.; Baró, A. M. *Appl. Phys. Lett.* **1998**, *72* (26), 3461.
(187) Pompe, T.; Fery, A.; Herminghaus, S. *Langmuir* **1998**, *14*, 2585.
(188) Spagnoli, C.; Loos, K.; Ulmanand, A.; Cowman, M. K. *J. Am. Chem. Soc*. **2003**, *125*, 7124.
(189) Park, S.-H.; Sposito, G. *Phys. Rev. Lett.* **2002**, *89*, 085501.
(190) Cheng, L.; Fenter, P.; Nagy, K. L.; Schlegel, M. L.; Sturchio, N. C. *Phys. Rev. Lett.* **2001**, *87*, 156103.
(191) Hucher, M.; Oberlin, A.; Hocart, R. *Bull. Soc. Fr. Mineral. Cristallogr*. **1967**, *90*, 320.
(192) Luna, M.; Rieutord, F.; Melman, N. A.; Dai, Q.; Salmeron, M. *J. Phys. Chem. A* **1998**, *102*, 6793.
(193) Foster, M. C.; Ewing, G. E. *J. Chem. Phys*. **2000**, *112* (15), 6817.
(194) Ewing, G. E. *J. Phys. Chem. B* **2004**, *108* (41), 15953.
(195) Shindo, H.; Ohashi, M.; Tateishi, O.; Seo, A. *J. Chem Soc. Faraday Trans*. **1997**, *93*, 1169.
(196) Heidberg, J.; Weisner, S. *Glueckauf* **1999**, *135*, 123.
(197) Garcia-Manyes, S.; Verdaguer, A.; Gorostiza, P.; Sanz, F. *J. Phys. Chem.* **2004**, *120* (6), 2962.
(198) Da, Q.; Hu, J.; Salmeron, M. *J. Phys. Chem. B* **1997**, *101*, 10880.
(199) Xu, L.; Bluhm, H.; Salmeron, M. *Surf. Sci*. **1998**, *407*, 251.
(200) Verdaguer, A.; Sacha, G. M.; Ogledtee, D. F.; Salmeron, M. *J. Chem. Phys*. **2005**, *123* (12), 124703.
(201) Ghosal, S.; Verdaguer, A.; Hemminger, J. C.; Salmeron, M. *J. Phys. Chem. B* **2005**, *109*, 4744.
(202) Park, J. M.; Cho, J.-H.; Kim, K. S. *Phys. Rev. B* **2004**, *69*, 233403.
(203) Hendrik, M.; Entel, P.; Hafner, J. *Surf. Sci.* **2001**, *488*, 177.
(204) Engvist, O.; Stone, A. J. *J. Chem. Phys.* **1999**, *10* (24), 12089.
(205) Stockelmann, E.; Hentschke, R. *J. Phys. Chem*. **1999**, *110* (24), 12097.
(206) Summer, A. L.; Menke, E. J.; Dubowski, Y.; Newberg, J. T.; Penner, R. M.; Hemminger, J. C.; Wingen, L. M.; Brauers, T.; Finlayson-Pitts, B. J. *Phys. Chem. Chem Phys.* **2004**, *6*, 604.
(207) Rudich, Y.; Benjamin, I.; Naaman, R.; Thomas, E.; Trakhtenberg, S.; Ussyshkin, R. *J. Phys. Chem. A* **2000**, *104*, 5238.
(208) Goodman, A. L.; Bernadr, E. T.; Grassian, V. H. *J. Phys. Chem. A* **2001**, *105*, 6443.
(209) Al-Abadleh, H. A.; Grassian, V. H. *Langmuir* **2003**, *19*, 341.
(210) Foster, M.; Furse, M.; Passno, D. *Surf. Sci.* **2002**, *502*−*503*, 102.
(211) Foster, M.; D'Agostino, M.; Passno, D. *Surf. Sci.* **2005**, *590*, 31.
(212) Asay, D. B.; Kim, S. H. *J. Phys. Chem. B* **2005**, *109* (35), 16760.
(213) Eng, P. J.; Trainor, T. P.; Brown, G. E., Jr.; Waychunas, G. A.; Newville, M.; Sutton, S. R.; Rivers, M. L. *Science* **2000**, *288*, 1029.
(214) Miura, K.; Yamada, T.; Ishikawa, M.; Okita, S. *Appl. Surf. Sci*. **1999**, *140*, 415.
(215) Miura, K. *Phys. Rev. B* **1995**, *52* (11), 7872.
(216) Yamada, T.; Miura, K. *Appl. Surf. Sci*. **1998**, *598*, 130.
(217) Sadtchenko, V.; Ewing, G. E. *J. Chem Phys.* **2002,** *116* (11), 4686.
(218) Sadtchenko, V.; Ewing, G. E.; Nutt, D. R.; Stone, A. J. *Langmuir* **2002**, *18*, 4632.
(219) Nutt, D. R.; Stone, A. J. *J. Chem. Phys*. **2002**, *117* (2), 800.
(220) Nutt, D. R.; Stone, A. J. *Langmuir* **2004**, *20*, 8715.
(221) Conrad, P.; Ewing, G. E.; Karlinsey, R. L.; Sadtchenko, V. *J. Chem Phys*. **2005**, *122*, 064709.
(222) Gil, A.; Colchero, J.; Luna, M.; Gomez-Herrero, J.; Baro, A. M. *Langmuir* **2000**, *16*, 5086.
(223) Gil, A.; Colchero, J.; Gomez-Herrero, J.; Baro, A. M. *Ultramicroscopy* **2001**, *86*, 1.
(224) Luna, M.; Colchero, J.; Gil, A.; Gomez-Herrero, J.; Baro, A. M. *Appl. Surf. Sci*. **2000**, *157*, 393.
(225) Wei, X.; Shen, Y. R. *Phys. Rev. Lett*. **2001**, *86*, 4799.
(226) Wei, X.; Miranda, P. B.; Zhang, C.; Shen, Y. R. *Phys. Rev. Lett.* **2002**, *66*, 085401.
(227) Dash, J. G. *Contemp. Phys.* **1989**, *30*, 89.
(228) Elbaum, M.; Lipson, S. G.; Dash, J. G. *J. Cryst. Growth* **1993**, *129*, 491.
(229) Mizuno, Y.; Hanafusa, N. *J. Phys.* **1987**, *48* (Colloque C1), 511.
(230) Maeno, N.; Nishimura, H. *J. Glaciol*. **1978**, *21*, 193.
(231) Lied, A.; Dosch, F.; Bilgram, J. H. *Phys. Rev. Lett*. **1994**, *72*, 3554.
(232) Beaglehole, D.; Nason, D. *Surf. Sci.* **1980**, *96*, 357.

(233) Golecki, I.; Jaccard, C. *J. Phys. C: Solid State Phys.* **1978**, *11*, 4229.
(234) Wettlaufer, J. S. *Phys. Rev. Lett.* **1999**, *82*, 2516.
(235) Heim, M.; Eschrich, R.; Hillebrand, A.; Knapp, H. F.; Cevc, G.; Guckenberger, R. *J. Vac. Sci. Technol., B* **1996**, *14*, 1498.
(236) Guckenberger, R.; Heim, M.; Gevc, C.; Knapp, H.; Wiegräbe, W.; Hillebrand, A. *Science* **1994**, *266*, 1538.
(237) Israelachvili, J. N. *Intermolecular and Surface Forces*, 2nd ed.; Academic: New York, 1991.
(238) Israelachvili, J. N. *J. Colloid Interface Sci.* **1986**, *110*, 263.
(239) Dhinojwala, A.; Granick, S. *J. Am. Chem. Soc.* **1997**, *119*, 241.
(240) Zhu, Y.; Granick, S. *Phys. Rev. Lett.* **2001**, *87*, 096104.
(241) Raviv, U.; Laurat, P.; Klein, J. *Nature* **2001**, *413*, 51.
(242) Raviv, U.; Klein, J. *Science* **2002**, *297*, 1540.
(243) Clifford, J. *Water in Disperse Systems*; Franks, F., Ed.; Plenum: New York and London, 1975; pp 75−132.
(244) Yeng, L.; Cummings, P. T. *Phys. Rev. Lett.* **2005**, *94*, 026101.
(245) Jeffery, S.; Hoffmann, P. M.; Pethica, J. B.; Ramanujan, C.; Özer, H. Ö.; Oral, A. *Phys. Rev. B* **2004**, *70*, 054114.
(246) Becker, T.; Mugele, F. *J. Phys.: Condens. Matter* **2005**, *17*, S319.
(247) Frantz, P.; Salmeron, M. *Tribol. Lett.* **1998**, *5*, 151.
(248) O'Shea, S. J.; Welland, M. E.; Rayment, T. *Appl. Phys. Lett.* **1992**, *60* (19), 2356.
(249) Hoh, J. H.; Cleveland, J. P.; Prater, C. B.; Revel, J.-P.; Hansma, P. K. *J. Am. Chem. Soc.* **1992**, *114*, 4917.
(250) Cleveland, J. P.; Schäffer, T. E.; Hamsa, P. K. *Phys. Rev. B* **1995**, *52* (12), R8692.
(251) During, U.; Zuger, O.; Phol, D. W. *Phys. Rev. Lett.* **1990**, *65*, 349.
(252) O'Shea, S. J.; Welland, M. E. *Langmuir* **1998**, *14*, 4186.
(253) O' Shea, S. J.; Lantz, M. A.; Tokumoto, H. *Langmuir* **1999**, *15*, 922.
(254) Jarvis, S. P.; Uchihashi, T.; Ishida, T.; Tokumoto, H.; Nakayama, Y. *J. Phys. Chem. B* **2000**, *104* (26), 6092.
(255) Jeffery, S.; Hoffman, P. M.; Pethica, J. B.; Ramanujan, C.; Özer, H. Ö.; Oral, A. *Phys. Rev. B* **2004**, *70*, 054114.
(256) Uchihashi, T.; Higgins, M.; Nkayama, Y.; Sader, J. E.; Jarvis, S. P. *Nanotechnology* **2005**, *16*, S49.
(257) Sader, J. E.; Jarvis, S. P. *Appl. Phys. Lett.* **2004**, *84*, 1801.
(258) Antognozzi, M.; Humphris, D. L.; Miled, M. *J. Appl. Phys. Lett.* **2001**, *78* (3), 300.
(259) Choi, E.-M.; Yoon, Y.-H.; Lee, S.; Kang, H. *Phys. Rev. Lett.* **2005**, *95*, 08701.
(260) Riedo, E.; Lèvy, F.; Brune, H. *Phys. Rev. Lett.* **2002**, *88*, 185505.
(261) Fisher, L. R.; Israelachvili, J. N. *J. Colloid Interface Sci.* **1981**, *80*, 528.
(262) Mate, C. M.; Lorenz, M. R.; Novotny, V. J. *J. Chem. Phys.* **1989**, *90*, 7550.
(263) Schenk, M.; Füting, M.; Reichelt, R. *J. Appl. Phys.* **1998**, *84*, 4880.
(264) Piner, R. D.; Zhu, J.; Xu, F.; Hong, S.; Mirkin, C. A. *Science* **1999**, *283*, 661.
(265) Thundat, T.; Zheng, X. Y.; Chen, G. Y.; Warmack, R. J. *Surf. Sci.* **1993**, *294*, L939.
(266) Morimoto, K.; Araki, K.; Yamashita, K.; Morita, K.; Niwa, M. *Appl. Surf. Sci.* **1997**, *117−118*, 652.
(267) Piner, R. D.; Zhu, J.; Xu, F.; Hong, S.; Mirkin, C. A. *Science* **1999**, *283*, 661.
(268) Lee, K.-B.; Park, S.-J.; Mirkin, C. A.; Smith, J. C.; Mrksich, M. *Science* **2002**, *295*, 1702.
(269) Gao, C. *Appl. Phys. Lett.* **1997**, *71*, 1801.
(270) Valencia, A.; Brinkmann, M.; Lipowsky, R. *Langmuir* **2001**, *17*, 3390.
(271) de Lazzer, A.; Dreyer, M.; Rath, H. J. *Langmuir* **1999**, *15*, 4551.
(272) Restagno, F.; Bocquet, L.; Bilben, T. *Phys. Rev. Lett.* **2000**, *84*, 2433.
(273) Kohonen, M.; Maeda, N.; Christenson, H. K. *Phys. Rev. Lett.* **1999**, *82*, 4667.
(274) Ostroverkhov, V.; Waychunas, G. A.; Shen, Y. R. *Phys. Rev. Lett.* **2005**, *94*, 046102.
(275) Calleja, M.; García, R. *Appl. Phys. Lett.* **2000**, *76*, 3427.
(276) Dagata, J. A.; Pérez-Murano, F.; Martín, C.; Kuramochi, H.; Yokoyama, H. *J. Appl. Phys.* **2004**, *96*, 2393.
(277) García, R.; Calleja, M.; Pérez-Murano, F. *Appl. Phys. Lett.* **1998**, *72*, 2295.
(278) Gómez-Moñivas, S.; Sáenz, J. J.; Calleja, M.; García, R. *Phys. Rev. Lett.* **2003**, *91*, 56101.
(279) Gómez-Moñivas, S.; Sáenz, J. J.; Carminati, R.; Greffet, J. J. *Appl. Phys. Lett.* **2000**, *76*, 2955.
(280) Sacha, G. M.; Verdaguer, A.; Martínez, J.; Ogletree, D. F.; Salmeron, M. *Appl. Phys. Lett.* **2005**, *86*, 123101.
(281) Smythe, W. R. *Static and Dynamic Electricity*; McGraw-Hill: New York, 1968.
(282) Jackson, J. D. *Classical Electrodynamics*; Wiley and Sons: New York, 1975.
(283) García, R.; Calleja, M.; Rohrer, H. *J. Appl. Phys.* **1999**, *86*, 1898.
(284) Yuan, J.-Y.; Shao, Z.; Gao, C. *Phys. Rev. Lett.* **1991**, *67*, 863.
(285) Gil, A.; Colchero, J.; Gómez-Herrero, J.; Baró, A. M. *Nanotechnology* **2003**, *14*, 332.
(286) Terris, B. D.; Stern, J. E.; Rugar, D.; Mamin, H. J. *Phys. Rev. Lett.* **1989**, *63*, 2662.
(287) Franz, P.; Agrait, N.; Salmeron, M. *Langmuir* **1996**, *12*, 3289.

CR040376L